C.P. No. 1161

C.P. No. 1161

MINISTRY OF AVIATION SUPPLY

AERONAUTICAL RESEARCH COUNCIL

CURRENT PAPERS

Wind Tunnel Measurements at M = 2.47 of the Mutual Aerodynamic Interference between a Guided Bomb and its Boost Unit During the Seperation Phase

by

J. A. Lang

Aerodynamics Dept., R.A.E., Farnborough

LONDON: HER MAJESTY'S STATIONERY OFFICE

1971

PRICE £1 NET

C.P. No. 1161

C.P. No. 1161

MINISTRY OF AVIATION SUPPLY

AERONAUTICAL RESEARCH COUNCIL

CURRENT PAPERS

Wind Tunnel Measurements at M = 2.47 of the Mutual Aerodynamic Interference between a Guided Bomb and its Boost Unit During the Seperation Phase

by

J. A. Lang

Aerodynamics Dept., R.A.E., Farnborough

LONDON: HER MAJESTY'S STATIONERY OFFICE

1971

PRICE £1 NET

C.P. No. 1161

C.P. No. 1161

MINISTRY OF AVIATION SUPPLY

AERONAUTICAL RESEARCH COUNCIL

CURRENT PAPERS

Wind Tunnel Measurements at M = 2.47 of the Mutual Aerodynamic Interference between a Guided Bomb and its Boost Unit During the Seperation Phase

by

J. A. Lang

Aerodynamics Dept., R.A.E., Farnborough

LONDON: HER MAJESTY'S STATIONERY OFFICE

1971

PRICE £1 NET

C.P. No.1161*
May 1962

WIND TUNNEL MEASUREMENTS AT M = 2.47 OF THE MUTUAL AERODYNAMIC INTERFERENCE BETWEEN A GUIDED BOMB AND ITS BOOST UNIT DURING THE SEPARATION PHASE

by

J. A. Lang

Aerodynamics Department, RAE, Farnborough

SUMMARY

Loads on boost motors in the vicinity of a guided bomb have been measured over a range of positions and incidences likely to occur during separation in order to provide data from which the trajectory may be determined. The loadings and local pressures induced on the bomb by the aerodynamic interference from the boosts have also been measured.

The influence of deflected rear surfaces on the boosts has been investigated as a means of limiting the boost incidence, attained through the angular momentum acquired after release of the forward constraint.

---

* Replaces RAE Technical Note Aero 2822, ARC 25060.

CONTENTS

1 INTRODUCTION

As a development of the stand off bomb, to extend its range and cruising speed, it was proposed to replace the rocket motor by four ramjets; further, to boost the bomb to a speed suitable for the efficient operation of these ramjets, the addition of two solid fuel boost motors was proposed. Ref.1 contains the basic data on the unboosted configuration whereas the present investigation is concerned with the interference forces and moments experienced during the separation of the boost from the bomb. The boost arrangement proposed consisted of twin boost motors mounted above the bomb as shown in Fig.1a.

The purpose of the measurements was to provide aerodynamic data from which the dynamic behaviour of the boost during separation could be calculated. Measurements had therefore been made of the normal force and pitching moment separately on the bomb and its boost over a range of attitudes and positions of the boost.

Further pressure measurements have been made on the body of the bomb to determine the magnitude of the locally increased aerodynamic loading on the structure during the separation phase.

OR 1159 requiring the long range development of Blue Steel was in fact cancelled after the completion of a large proportion of the experimental programme. The results were not therefore analysed to the extent of using them for dynamic response calculations. However, it is hoped that the published results of the aerodynamic forces may prove of general interest.

2 DESCRIPTION OF MODELS

For the sake of expediency the model used was a 1/48 scale model of the early version of Ref.2 modified, as described in Ref.1, with nascelle units at -5^{o} and the upper fin removed (Fig.1a). The boost units constructed of thin walled tubing were mounted on twin internal strain gauge sting supports. These twin stings are joined together at the rear, and the combination is carried on a variable incidence mounting attached to a traverse gear. Three different chord sizes for the aerofoil connecting the rear ends of the two boosts were tested, details of which are given in Table 1.

The small differences between the model tested and the proposed version of Blue Steel are listed in Table 2.

The distribution of pressure plotting holes drilled in the body is shown in Fig.3, these holes were plugged, and the tubing removed, prior to making force measurements.

3 TEST ARRANGEMENT AND PROCEDURE

The tests were made in the RAE No.8 supersonic wind tunnel, a continuous flow non-return circuit tunnel with a 9 in. square working section, at a Mach number of 2.47. The stagnation pressure was atmospheric, and the stagnation temperature was approximately 40°C, which gave a Reynolds number in the working section of 0.26×10^{6} per in. The humidity was kept at less than 0.00015 lb of water per lb of dry air.

For the pressure plotting tests, made before the force measurements, the pipe connections from the bomb were carried aft over the windshield and out to a multitube mercury manometer.

Normal forces and pitching moments on the bomb were measured using the sting balance described in Ref.3. For the majority of the force measurements the bomb was at zero incidence with zero fore plane control angle setting, η; however, a few tests were made at $+7.3^{\circ}$ incidence with the fore plane set at $\eta = +8^{\circ}$, as being representative of the expected trim state of the full scale vehicle at the moment of release of the twin boost unit.

The twin boost unit was mounted on its separate twin sting support on the tunnel traverse gear projecting down from the top of the working section as shown in Fig.2. The incidence could be varied from -1° to $+20^{\circ}$, and the boost unit traversed vertically at any required fore and aft position relative to the bomb, whilst the tunnel was in operation. A twin boost unit incidence greater than $+20^{\circ}$ was precluded from tunnel blockage considerations, and the proximity of the upper liner.

3.1 Accuracy

Prior calibration of the wind tunnel had shown the Mach number to be 2.47 ± 0.015, with flow angle variations of $\pm 0.2^{\circ}$ maximum. No corrections were made for these variations.

The twin boost unit was set optically at each required incidence whilst the tunnel was running. The angular deflection of the bomb from its initial (wind off) setting under the induced loads due to the proximity of the twin sting unit was less than 0.1°. The spatial position of the twin boost unit relative to the bomb could be set by the traverse gear, to an accuracy of ± 0.1 mm. The estimated accuracy of the measurements is given below

Bomb model		Twin boost unit model	
C_z	±0.0025	C_{z_b}	±0.0009
C_m	±0.0012	C_{m_b}	±0.0003
C_p	±0.005	α_b	±0.2°
α	±0.1°		
η	±0.05°		

4 PRESENTATION OF RESULTS

The forces and moments measured on the bomb and the boosts were each referred to their respective body-fixed axes but were reduced to coefficient form using, for convenience of comparison, the same reference area and length. These were respectively the gross wing area of the bomb S (5.757 in^2), and the corresponding mean aerodynamic chord, $\bar{c}$ (2.182 in). The moments on the bomb have been quoted about the apex of the gross wing, whereas those for the twin boost have been in general quoted about a point 2.500 in aft of the base of the nose cone. The recorded data were reduced to coefficient form by Mathematical Services Department using a DEUCE electronic computer.

The orientation of the twin boost unit model to the bomb has been specified with respect to the wind-fixed x'0'z' axes shown in Fig.1b. The x' axis is streamwise and the origin 0' was chosen 0.634 in above the body centre line and in the plane of the rear of the bomb. The position of the boost is then specified by a rotation of α_b about 0' together with translations x' and z' of the point 0_b. At $\alpha = \alpha_b$ with x' = z' = 0 the boost position approximates to the full scale position prior to the release of the boosts. x' and z' were measured on a traverse gear calibrated in metric units, so for convenience, these distances in these units have been retained.

5 SCOPE OF TESTS

5.1 Pressure plotting tests

Tests were made first of all with the bomb in isolation, at zero incidence and with a foreplane setting of zero, and then with the twin boost unit at the datum reference position (x' = z' = 0) with each of the three aerofoils fitted in turn. The twin boost unit incidence was varied up to $\alpha_b = 10°$; this was the highest obtainable at this datum position of the unit without fouling its sting support on the pressure plotting tubes issuing from the rear of the

bomb model. The tests were then repeated with the largest chord rear aerofoil (0.70 in chord) at $+12^{\circ}$ incidence to the boost unit axis. Additional measurements were made with solid blockage added between the boosts, as shown in Fig.20, to simulate the effects of possible attachment and release mechanism.

5.2 Force measurements with the models in isolation

Force and moment measurements were initially made at $M = 2.47$ with the bomb model alone in the tunnel, at $\alpha = \eta = 0^{\circ}$, and at $\alpha = +7.3^{\circ}$, $\eta = +8^{\circ}$, to determine the reference values of C_m and C_z at these two basic configurations, uninfluenced by the proximity of the twin boost unit.

Similarly, force and moment measurements were made with the twin boost unit alone in the tunnel at $M = 2.47$, first with each of the three different chord sizes of rear aerofoil at zero inclination to the boosts, and then with the two larger sizes (0.50 in and 0.70 in chord) at $+12^{\circ}$ to the boosts. Tests were also made with no rear aerofoil fitted. All these tests were made over the incidence range $\alpha_b = 0^{\circ}$ to 20°.

5.3 Measurements of mutual interference loads

Normal force and pitching moment measurements were recorded concurrently on both the bomb and the twin boost unit, as the latter was varied through the incidence range $\alpha_b = 0^{\circ}$ to 20°, and with a spatial coverage from $x' = 0$ to 2 cm and $z' = 0$ to 5 cm in 1 cm incremental steps. The tests were repeated with each of the three aerofoils fitted over the same range of α_b and z', but at $x' = 0$. They were also limited to $x' = 0$ for the 0.70 in chord rear aerofoil at 12° setting. With the bomb at an incidence of 7.3° and a control setting of $\eta = +8^{\circ}$, only the boost arrangement with the largest chord (0.70 in) was tested.

6 RESULTS AND DISCUSSION

6.1 Twin boost unit in isolation

For the various arrangements of rear aerofoil the C_{z_b} and C_{m_b} are given in Figs.4 and 5, and the corresponding CP positions are shown in Fig.6. For comparison, estimates for an isolated boost are included in Figs.4 and 6 using the method given in Ref.4. Estimates have also been made of the mutual interference at small incidences applying the method given in Ref.6. Using the complex velocity potential derived in Ref.5, we find for the two boosts that

$$\frac{\partial C_{z_b}}{\partial \alpha_b} = \frac{4\pi r^2}{S}\left[1 + 2\frac{r^2}{b^2} + 2\frac{r^4}{b^4\left(1 - \frac{r^2}{b^2}\right)^2} + O\left(\frac{r}{b^6}\right)^6\right]$$

where b is the distance separating the axes of the boosts and r is radius of their base.

The term in brackets can be recognized as an interference factor which, as suggested in Ref.7 using a more intuitive approach, can be regarded as arising from equal contributions from the buoyancy and upwash field produced by one body at the location of the other. It would therefore seem logical to apply a factor of

$$\left[1 + \frac{r^2}{b^2} + O\frac{r^4}{b^4}\right]^2$$

to the cross flow velocity when estimating the viscous contribution to the lift. So that we have

$$C_{z_b} = \frac{\alpha}{S}\left\{4\pi r^2\left[1 + 2\frac{r^2}{b^2} + O\left(\frac{r}{b^4}\right)\right] + C_{D_c}\alpha A_p\left[1 + \frac{r^2}{b^2} + O\left(\frac{r^4}{b^4}\right)\right]^2\right\}$$

where A_p is the planform area of the bodies.

C_{D_c} is the cross flow drag coefficient, taken as 1.2. The normal force calculated in this way has been included in Figs.4b and 7, where it is seen clearly to underestimate the experimental values, seemingly a result of the inadequacy of the estimates of the viscous contribution.

6.1.1 Effects of fitting the rear aerofoil to the twin boost unit

The increments in the normal force coefficient $\Delta(-C_z)$ and pitching moment coefficient, ΔC_m, on adding various rear aerofoils are shown in Fig.8. The variation of $\Delta(-C_z)$ with incidence was, for all rear aerofoils tested, markedly non-linear. Estimates based on linearised theory are also included in Fig.8a, for comparison, and it is seen that these exceed the measured values. The pitching moment increment shown in Fig.8b indicates that the point of action of the incremental load due to the aerofoil is ahead of its leading edge.

6.2 Bomb in isolation

The following normal force and pitching moment coefficients were measured at $M = 2.47$ with the bomb alone in the tunnel:

Configuration of the bomb		$-C_z$	C_m
$\alpha = 0^\circ$	$\eta = 0^\circ$	-0.002	+0.0072
$\alpha = 7.3^\circ$	$\eta = 8^\circ$	0.285	-0.0510

6.3 Aerodynamic interference loads on the twin boost unit in the presence of the bomb

6.3.1 Bomb at zero incidence

The $-C_{z_b}$ versus α_b plot of the results obtained at the x' and z' positions covered are shown in Figs.10 to 13, and the corresponding C_{m_b} versus α_b curves, in Figs.15 to 18 inclusive, for the various rear aerofoils tested. It should be noted that at high boost incidences the datum zero vertical positioning could not be obtained at $x' = 1$ and 2 cm aft of the bomb, because of fouling between the two sting supports. In these specific cases the test points were made at the minimum vertical displacements, the actual values of z' being indicated in the figures. The corresponding coefficients for the 'twin boost unit in isolation' tests (labelled $x' = z' = \infty$) are included dotted in Figs.10 to 18, so that the interference effect of the bomb is readily assessed.

(a) Interference loads with rear aerofoils at zero setting to the twin boost unit

With all rear aerofoils tested, the normal forces on the twin boost unit in the presence of the bomb were always greater than the $x' = z' = \infty$ values at all spatial positions tested, up to a boost unit incidence of 15° approximately (Figs.10 to 12). Above this incidence there was a slight relative loss in normal force when the twin boost unit was over 2 cm above the bomb. In addition, it will be noted that the incremental load changes on the twin boost unit, due to increasing the rear aerofoil sizes, were up to $\alpha_b = 15^\circ$, not significantly influenced by the proximity of the other model; and comparable to those obtained with the twin boost unit in isolation. At higher incidences the relative effectiveness of the rear aerofoil became less, indicating increasing local interference effect from the bomb at the rear end of the twin boost unit as the α_b incidence was increased above 15°. However, as would be

expected, the largest overall increments of interference load were obtained with the twin boost unit in the closest proximity to the bomb (i.e. $x' = z' = 0$).

The pitching moment characteristics of the twin boost unit, (Figs.15 to 17), relative to the $x' = z' = \infty$ results, were altered by the presence of the bomb so that, in general, there was a marked nose-up increment in pitching moment coefficient at all spatial positions tested, up to $\alpha_b = 12^o$ approximately. At higher incidences, however, a large nose-down increment is seen to exist with the boost unit close to the bomb ($z' = 0$), but this has disappeared when the displacement has increased by 1 cm ($z' = 1$).

The overall effects of the presence of the bomb at zero incidence on the normal force and pitching moment of the twin boost unit have been presented in Fig.37 for the configuration with the 0.70 in chord rear aerofoil both at $x' = z' = 0$ and at $x' = z' = \infty$. These results have been adjusted to a reference datum point 51.2% of the boost length aft of the nose, this being representative of the likely CG of the full scale unit with both front and rear attachment points released. These curves show that there was not only a nose-up trim change imposed on the twin boost unit by the close proximity of the bomb, but that the CP moved increasingly aft with incidence above $\alpha_b = 6^o$. Similar curves could be drawn for other selected x' and z' combinations, but have been omitted for clarity; however, the general effect would be for these intermediate curves to indicate a reasonably smooth transition to the $x' = z' = \infty$ results also shown on this figure.

(b) Interference airloads with the largest rear aerofoils (0.7 in chord) set at +12°

Because of the initial nose-up pitching moment increment, it seemed reasonable to assume that a positive incidence setting of the rear surface connecting the boosts, would be advantageous in producing an extra restoring moment and parting force when the rear attachment point was released. Additional measurements were therefore made with the largest aerofoil set at 12^o. These measurements, made only at $x' = 0$, are shown plotted in Figs.13 and 18. The results at $z = 0$ have also been shown in Fig.37, on the $-C_{z_b}$ versus C_{m_b} plot, with C_{m_b} corrected to a reference datum of 51.2% of the boost unit length aft of the nose, as explained in (a) above. A large nose-down pitching moment increment due to the 12^o deflection of the rear aerofoil was obtained at low boost incidences (Fig.37), but, as was noted with the twin boost unit in isolation, the increment of normal force fell sharply as incidence was increased above $\alpha_b = 10^o$.

6.3.2 Bomb at cruising incidence

With the bomb set at $+7.3^{\circ}$ incidence, and with a fore plane setting of 8°, to simulate the expected trim condition just prior to jettisoning of the twin boost unit, a limited number of tests were completed with the largest chord (0.70 in) rear aerofoil on the twin boost unit. Tests were terminated at this stage because of the cancellation of the project.

The normal force and moment characteristics for the boosts are included in Figs.14 and 19, again with the corresponding $x' = z' = \infty$ characteristics for comparison.

With the bomb at 7.3° incidence, the twin boost unit forces and moments were measured over the range $\alpha_b = 8^{\circ}$ to 20°, and relative to the $x' = z' = \infty$ results at the same incidence, they showed a marked loss of normal force at all incidences, this loss being substantially independent of x' at $z' = 0$, but diminishing as the vertical displacement was increased up to the maximum tested ($z' = 5$ cm). These losses in normal force were accompanied by a very large nose-up trim change on the twin boost unit, see Fig.19. A comparison of Figs.12 and 14 with 17 and 19 shows that the flow field around the boost is considerably modified as the incidence of the bomb is increased, thereby influencing to a marked extent the forces experienced by the twin boost unit.

6.4 Interference loads on the bomb due to the presence of the twin boost unit

6.4.1 Bomb at zero incidence

(a) Results of pressure plotting tests

Static pressures were measured at the positions indicated in Fig.3 on the upper surface of the bomb model both with and without the twin boost unit in close proximity. The results are given in coefficient form in Table 3.

During the tests the twin boosts were maintained at the datum zero reference position ($x' = z' = 0$), whilst their incidence was varied from $\alpha_b = 0^{\circ}$ to 10°, the highest obtainable at $x' = 0$ without the twin boost unit support system fouling the pressure tubing issuing from the rear of the bomb model.

It was found, by traversing the twin boost unit forward at $\alpha_b = 10^{\circ}$, that for adjacent pressure points the pressures depended only on their relative position to the twin boost unit. This fact was made use of to provide the supplementary points shown flagged in Fig.20. Such traverses were made at

$\alpha_b = 10^o$ with the 0.70 in chord rear aerofoil on, and with the gap between its trailing edge and the twin boosts partially blocked. The degree of this blockage is shown in Fig.20. These results have been plotted in Fig.20 as an increment ΔC_p, of static pressure coefficient above that with the model in isolation. An additional scale, $\Delta p/p_{t2}$, has been included to show the ratio of measured pressure to stagnation pressure behind a normal shock at $M = 2.47$. The corresponding flow pattern for the case with the 0.70 in chord rear aerofoil without blockage has been reproduced in Fig.21 from schlieren photographs taken during these tests. The wing leading edge and nacelle shock systems have been omitted for clarity, since in the original schlieren pictures they tended to obscure the shock at the leading edge of the 0.70 in chord aerofoil.

The marked influence of the rear aerofoil configuration on the local pressures on the top of the bomb is apparent, as is also the undulating nature of the static pressure field ahead of the influence of the rear aerofoil. This latter is undoubtedly caused by the complex threedimensional nature of the shock system emanating from the twin nose cones of the boosts, and subsequently reflected to and fro between the two models.

Measurements at plane 'C' (Fig.3), i.e. at holes 2, 13 and 14, situated below the rear aerofoil showed that the pressure disturbances were a maximum on the top of the fuselage over the range covered. Unfortunately it was not possible with the present model to extend this range sufficiently far forward to include the pressure field from the reflections of the bow shock system from the boosts, where regions of high pressure may also exist.

(b) Measured interference loads

The forces and pitching moments imposed on the bomb at zero incidence by the proximity of the twin boost unit, are shown plotted in Figs.22 to 24 and Figs.27 to 29 respectively, at the various x' and z' positions and boost incidences for the three different sizes of rear aerofoil on the boost unit. Further measurements, at $x' = 0$ only, were made with the largest (0.70 in chord) rear aerofoil at 12^o incidence to the boost unit. These measurements are shown plotted in Figs.25 and 30. It can be seen from Figs.22 to 24 and Figs.27 to 29 that, at $z' = 0$, a downward force and a slight nose-down pitching moment are induced on the bomb by the presence of the boost unit at zero incidence. The sign of this induced force is not affected by incidence of the boosts. The nose-down pitching moment remains until the boost incidence, α_b, exceeds 5^o, then a nose-up pitching moment occurs which increases rapidly

with increasing α_b. It can be inferred from Fig.30 that with the 0.70 in chord rear aerofoil at $+12^{\circ}$ to the boost unit, the increased local download at the rear of the bomb (cf. Fig.20) has apparently been cancelled by some upstream effect.

The normal force and pitching moment on the bomb due to aerodynamic interference varied with vertical displacement (z'), at a given x' position fore and aft. A maximum is reached, for constant twin boost unit incidence α_b, at zome z' value between 0 and 5 cm, for all boost unit incidences up to approximately $\alpha_b = 12^{\circ}$. At higher α_b the maximum value at a given incidence occurred at z' = 0. Examination of schlieren pictures, taken concurrently, showed that this maximum $-C_z$ and C_m value occurred in general when the twin boost unit bow shock enveloped the wing of the bomb. At higher twin boost unit incidences the area of planform of the bomb influenced by the pressure field of the boost unit rapidly diminished as the boost unit was traversed upwards at any given incidence. The attitudes of the boosts when they cease to interfere with the bomb were deduced from schlieren photographs and are indicated in Fig.32. The $-C_z$ versus α_b curves at varying z' therefore formed an envelope curve giving the maximum possible interference loading on the bomb for any given twin boost unit x' and z' position over the range of α_b tested. This envelope curve was governed by low boost unit incidence settings, at large vertical displacements, and high boost unit incidences, (generally of the order of $\alpha_b = 20^{\circ}$) at the datum zero reference position. These envelope curves for the normal force imposed by interference on the bomb, due to the proximity of the various twin boost unit configurations, have been reproduced in Fig.33. Very similar characteristics were obtained with the pitching moments induced on the bomb by the presence of the twin boost unit, as shown in Fig.35.

There was little systematic variation of the envelope values with rear aerofoil chord size, although in the majority of cases the largest chord rear aerofoil did give slightly larger normal force and pitching moment increments at small vertical displacements between the models.

6.4.2 The bomb at the cruising incidence

As mentioned in section 6.3.2 the bomb cruise condition considered corresponded to an incidence of 7.3° with a foreplane setting of 8°. The only boost configurations considered was that with the 0.70 in chord rear aerofoil. The normal force and pitching moments induced on the bomb by the boosts are shown in Figs.26 and 31 for a range of α_b from 8° to 20°. By comparing

Fig.24 with 26, and Fig.29 with 31, it appears that, in the pre-release position (i.e. $\alpha \approx \alpha_b$, $x' = z' = 0$), there is only a very small influence of the bomb incidence α on the forces induced on the bomb by the boosts. The comparison also shows that the trends in these forces with boost displacement, and incidence, are very similar at both the bomb incidences considered. Envelope curves are shown in Figs.34 and 36.

7 CONCLUSIONS

7.1 Static aerodynamic characteristics were measured to provide the information necessary to calculate the trajectory of the separating boost unit from a guided bomb.

7.2 The measured normal force variation with incidence, at $M = 2.47$, produced by the twin boost was very non-linear. Estimates were made, including the effects of mutual interference between the boost and viscous cross flow, but these were significantly less than the measured values.

7.3 The maximum force and moment coefficients induced on the bomb by the twin boosts up to a boost incidence of 20° were 0.21 and 0.28 respectively, these coefficients being based on the bomb wing area and mean aerodynamic chord.

7.4 Without any inclination of the rear aerofoil on the boost unit the aerodynamic force on the boost was small when the bomb was at zero incidence. The force was greater, in the sense that it tended to part the boost from the bomb, when the bomb was at its cruising incidence. It was demonstrated that this parting force could be increased by suitably inclining the rear aerofoil.

7.5 Pressure distributions, measured on the bomb with the blockage presented by the boost attachment crudely simulated, showed that relatively large local loading could be experienced.

Table 1

MODEL DETAILS

BLUE STEEL

As detailed in Technical Note Aero 2566 but with the top fin removed and twin ramjet units added at each tip at -5° to body axis.

TWIN BOOST UNIT

Bodies	Parallel portion	6 in by 0.375 in diameter.
	Nose cone	40° apex angle, 0.375 in diameter base; 0.52 in long.
Disposition		Axes parallel and 0.57 in apart.
Rear aerofoils		
	Planform	Rectangular.
	Span	0.8 in.
	Chord(s)	0.35 in, 0.50 in and 0.7 in.
	Section	Flat plate 0.035 in thick with 20° wedge at LE.
	Location	Trailing edge 0.375 in forward of rear of boost unit.

Table 2

FULL SCALE COMPARISON OF TWIN BOOST MODEL AND PROPOSED UNITS

	Item	Model	Proposed unit
Nose	Cone angle	40°	40°
	Length	2 ft 0.73 in	1 ft 11.36 in
Body	Diameter	1 ft 6 in	1 ft 4.5 in
	Length	24 ft 0 in	21 ft 0 in
	Distance apart between centres	2 ft 3.36 in	2 ft 5.52 in
	Distance above Blue Steel C_L	2 ft 6.42 in	2 ft 6.42 in
Rear aerofoils			
	Section	Flat plate with 20° LE wedge angle	Same section
	Thickness	1.68 in	1.5 in
	Span	3 ft 2.4 in	3 ft 4.52 in
	Chord(s)	2 ft 9.6 in	2 ft 6 in
		2 ft 0 in	
		1 ft 4.8 in	
	Location of TE		
	Forward of rear end of unit	1 ft 6 in	1 ft 6 in

Table 3

RESULTS OF PRESSURE PLOTTING TESTS AT M = 2.47

Bomb configuration	Twin boost unit configuration				C_p at pressure point numbers as shown in Fig.3													
	Rear aerofoil	α_b	'X' dist.	'Z' dist.	1	2	3	4	5	6	7	8	9	10	11	12	13	14
$\alpha = \eta = 0^o$	Not fitted				+0.0425	-0.0027	-0.0079	-0.0040	-0.0066	-0.0131	-0.015	-0.010	-0.010	0	-0.005	-0.020	+0.015	+0.045
$\alpha = \eta = 0^o$	0.35 in chord	0^o	0	0	+0.0013	+0.0820	-0.0302	-0.0147	-0.0018	+0.0124	-0.030	-0.075	-0.005	-0.010	-0.015	-0.025	+0.075	+0.030
		1^o			+0.0885	-0.0238	-0.0018	+0.0072	-0.0212	-0.0483	-0.060	-0.095	-0.045	-0.030	0	-0.035	+0.010	+0.030
		2^o			+0.0949	-0.0199	-0.0005	-0.0018	-0.0274	-0.0431	-0.070	-0.090	-0.040	-0.035	-0.010	-0.040	0	+0.030
		3^o			+0.1144	-0.0185	+0.0034	-0.0018	-0.0263	-0.0392	-0.080	-0.070	-0.040	-0.035	-0.015	-0.040	0	+0.035
		4^o			+0.1493	-0.0082	+0.0124	-0.0082	-0.0405	-0.0341	-0.070	-0.035	-0.060	-0.030	-0.015	-0.040	+0.020	+0.040
		5^o			+0.1854	-0.0005	+0.0085	-0.0122	-0.0043	-0.0702	-0.045	-0.030	-0.060	-0.010	-0.020	-0.035	+0.025	+0.040
		6^o			+0.1791	+0.0048	+0.0009	-0.0043	-0.0223	-0.0559	-0.020	-0.055	-0.050	0	-0.020	-0.040	+0.025	+0.040
		7^o			+0.2153	+0.0009	-0.0004	-0.0199	-0.0223	-0.0133	-0.055	-0.030	-0.015	0	-0.035	-0.035	+0.030	+0.055
		8^o			+0.2372	+0.0061	-0.0068	-0.0352	+0.0242	-0.0017	-0.040	0	-0.020	-0.005	-0.015	-0.015	+0.035	+0.075
		9^o			+0.1739	+0.0280	-0.0120	-0.0017	+0.0500	-0.0249	+0.015	+0.045	-0.025	+0.005	+0.015	+0.005	+0.055	+0.095
		10^o			+0.1262	+0.0664	-0.0094	+0.0306	+0.0181	-0.0146	+0.015	+0.070	-0.015	+0.020	+0.045	+0.015	+0.060	+0.100
		5^o			+0.2114	+0.0087	+0.0035	+0.0022	-0.0199	-0.0533	-0.020	-0.055	-0.045	0	-0.025	-0.040	+0.035	+0.045
		0^o			+0.0242	+0.0094	-0.0210	+0.0048	+0.0183	-0.0017	-0.050	-0.080	-0.015	-0.015	0	-0.015	+0.015	+0.020
$\alpha = \eta = 0^o$	0.50 in chord	0^o	0	0	+0.0113	+0.0759	-0.0199	-0.0081	+0.0010	+0.0126	-0.010	-0.080	0	-0.005	-0.015	-0.020	+0.085	+0.050
		2^o			+0.0345	+0.0303	-0.0004	+0.0190	-0.0093	-0.0391	-0.055	-0.090	-0.035	-0.020	+0.005	-0.020	+0.035	+0.035
		4^o			+0.0397	-0.0055	+0.0177	+0.0061	-0.0275	-0.0262	-0.075	-0.045	-0.045	-0.025	-0.005	-0.030	+0.020	+0.040
		6^o			+0.0681	+0.0113	+0.0074	-0.0068	-0.0430	-0.0417	+0.005	-0.040	-0.040	-0.005	-0.010	-0.040	+0.035	+0.045
		8^o			+0.1107	+0.0047	+0.0177	-0.0532	+0.0177	+0.035	-0.035	0	+0.005	0	-0.015	-0.015	+0.030	+0.075
		10^o			+0.1890	+0.0568	-0.0081	+0.0268	+0.0438	-0.0081	+0.010	+0.070	-0.010	+0.025	+0.045	+0.020	+0.065	+0.135
$\alpha = \eta = 0^o$	0.70 in chord	0^o	0	0	+0.0152	+0.0319	+0.0114	-0.0054	-0.0003	-0.0029	-0.010	-0.075	-0.010	0	-0.010	-0.020	-0.005	-0.005
		1^o	0		+0.0023	+0.0437	-0.0326	-0.0029	+0.0140	-0.0145	-0.075	-0.090	-0.020	-0.020	-0.010	-0.020	+0.075	+0.065
		2^o	0		+0.0307	+0.1121	-0.0067	+0.0075	-0.0171	-0.040	-0.060	-0.095	-0.035	-0.025	-0.005	-0.030	+0.130	+0.050
		3^o	0		+0.0631	+0.1806	+0.0036	+0.0101	-0.0197	-0.045	-0.075	-0.080	-0.045	-0.035	0	-0.030	+0.095	+0.040
		4^o	0		+0.0992	+0.2747	+0.0152	+0.0088	-0.0339	-0.020	-0.075	-0.040	-0.050	-0.030	-0.005	-0.035	+0.085	+0.050
		5^o	0		+0.1225	+0.1612	+0.0152	-0.0132	-0.0119	-0.070	-0.040	+0.015	-0.065	-0.015	-0.010	-0.035	+0.060	+0.045
		6^o	0		+0.1289	+0.1432	+0.0204	-0.0184	-0.0158	-0.065	-0.025	-0.035	-0.055	-0.005	-0.010	-0.035	+0.055	+0.040
		7^o	0		+0.1561	+0.1561	+0.0165	-0.0145	-0.0106	-0.050	-0.005	-0.045	-0.045	+0.005	-0.010	-0.035	+0.070	+0.045
		8^o	0		+0.1730	+0.1588	+0.0114	-0.0041	-0.0299	-0.040	+0.020	-0.040	-0.025	+0.010	-0.015	-0.030	+0.075	+0.045
		9^o	0		+0.1859	+0.0218	+0.0023	-0.0041	+0.0515	-0.015	-0.010	+0.055	-0.020	+0.005	+0.015	+0.010	+0.055	+0.120
		10^o	0		+0.2506	+0.0386	-0.0067	+0.0218	+0.0683	-0.005	+0.010	+0.065	-0.010	+0.025	+0.040	+0.020	+0.060	+0.135
		10^o	0.079 in fwd.		+0.3940	+0.0476	+0.0063	+0.0127	+0.0890	-0.005	+0.010	+0.070	-0.020	+0.025	+0.025	+0.025	+0.065	+0.135
		10^o	0.158 in fwd.		+0.2700	+0.1097	+0.0269	+0.0036	+0.0919	0	+0.005	+0.060	-0.010	+0.020	+0.020	+0.020	+0.070	+0.125
		10^o	0.236 in fwd.		+0.2764	+0.2092	+0.0386	-0.0067	+0.0774	+0.020	+0.005	+0.055	0	+0.010	+0.010	+0.020	+0.110	+0.135
		10^o	0.315 in fwd.		+0.2032	+0.2014	+0.0425	-0.0118	+0.0528	+0.030	+0.005	+0.055	+0.025	+0.010	+0.010	+0.015	+0.140	+0.130
		10^o	0.394 in fwd.		-0.0170	+0.1213	+0.0334	-0.0171	+0.0360	+0.050	0	+0.045	+0.015	+0.010	+0.010	+0.010	+0.115	+0.130
		10^o	0.472 in fwd.		+0.0399	+0.1368	+0.0247	-0.0171	+0.0257	+0.070	0	+0.040	+0.025	+0.010	0	0	+0.085	+0.135
		10^o	0.500 in fwd.		+0.1459	+0.1963	+0.0334	-0.0183	+0.0204	+0.065	0	+0.040	+0.025	+0.010	0	0	+0.095	+0.135
		0^o	0		-0.0041	+0.0257	+0.0088	-0.0144	-0.0041	-0.010	-0.020	-0.080	+0.020	-0.005	-0.015	-0.025	+0.050	+0.055

Table 3 (Contd)

Bomb configuration	Twin boost unit configuration				C_p at pressure point numbers as shown in Fig.3													
	Rear aerofoil	α_b	'X' dist.	'Z' dist.	1	2	3	4	5	6	7	8	9	10	11	12	13	14
$\alpha = \eta = 0^o$	0.07 in chord plus 'block-age'	0^o	0	0	-0.0565	+0.2022	+0.1016	+0.0545	+0.0101	-0.0069	-0.0186	-0.0839	-0.0160	-0.0029	+0.0467	+0.0075	-0.0434	+0.0598
		2^o			-0.0826	+0.4634	+0.2309	+0.0075	+0.0180	-0.0251	-0.0709	-0.0905	-0.0265	-0.0186	+0.0010	-0.0134	-0.0500	+0.1055
		4^o			-0.1361	+0.4676	+0.4192	+0.0102	-0.0225	-0.0577	-0.0747	-0.0656	-0.0421	-0.0316	-0.0029	-0.0303	+0.1592	+0.1526
		6^o			-0.1375	+0.4284	+0.4244	-0.0146	-0.0185	-0.0721	-0.0381	-0.0120	-0.0604	-0.0106	-0.0120	-0.0316	+0.1775	+0.1317
		8^o			-0.0983	+0.5616	+0.0286	-0.0420	-0.0016	+0.0063	-0.0420	-0.0093	-0.0069	-0.0016	-0.0289	-0.0225	+0.2337	+0.2076
		10^o	0		-0.0905	+0.4153	+0.0403	-0.0133	+0.0337	-0.0106	-0.0133	+0.0390	-0.0186	+0.0050	+0.0050	+0.0063	+0.1383	+0.2298
		10^o	0		-0.0709	+0.4388	+0.0899	-0.0055	+0.0429	-0.0029	-0.0069	+0.0481	-0.0146	+0.0128	+0.0103	+0.0141	+0.1252	+0.2232
		10^o	0.098 in fwd.		-0.1034	+0.4846	+0.3212	-0.0186	+0.0769	+0.0180	-0.0093	+0.0403	-0.0029	+0.0075	+0.0037	+0.0103	+0.0925	+0.2010
		10^o	0.197 in fwd.		-0.1034	+0.1055	+0.6558	-0.0238	+0.0455	+0.0363	-0.0106	+0.0350	+0.0037	+0.0089	-0.0029	+0.0075	-0.0251	+0.1657
		10^o	0.295 in fwd.		-0.1061	-0.0577	+0.5068	-0.0263	+0.0233	+0.0559	-0.0093	+0.0286	+0.0115	+0.0063	-0.0081	-0.0016	-0.0460	+0.1383
		10^o	0.394 in fwd.		-0.0773	-0.0447	+0.2487	-0.0055	+0.0115	+0.0494	-0.0106	+0.0272	+0.0154	+0.0089	+0.0075	-0.0055	-0.0303	+0.1016
		10^o	0.500 in fwd.		-0.0055	-0.0525	+0.5695	+0.0598	+0.0010	+0.0520	-0.0093	+0.0207	+0.0089	+0.0141	+0.0573	-0.0029	-0.1022	+0.0925
		10^o	0		-0.0695	+0.4663	+0.0769	-0.0055	+0.0416	-0.0029	-0.0069	+0.0481	-0.0172	+0.0115	+0.0103	+0.0141	+0.1526	+0.1696
		0^o	0		-0.0773	+0.5068	+0.1343	+0.0337	-0.0029	-0.0120	-0.0316	-0.1100	-0.0172	-0.0055	+0.0337	+0.0063	-0.0447	+0.0337
$\alpha = \eta = 0^o$	0.70 in chord at 12^o to boost unit centre line	0^o	0	0	+0.0921	+0.2033	+0.1208	+0.0449	-0.0009	-0.0115	-0.0233	-0.0704	-0.0102	-0.0009	+0.0488	-0.0036	+0.0016	+0.0946
		2^o			+0.1405	+0.2950	+0.2610	+0.0173	-0.0128	-0.0403	-0.0599	-0.0888	-0.0403	-0.0259	+0.0042	-0.0206	+0.0776	+0.1392
		4^o			+0.2295	+0.3042	+0.2309	+0.0108	-0.0285	-0.0547	-0.0770	-0.0508	-0.0442	-0.0298	-0.0009	-0.0298	+0.0566	+0.1392
		6^o			+0.2610	+0.4155	+0.0553	-0.0180	-0.0075	-0.0586	-0.0220	-0.0377	-0.0508	-0.0036	-0.0089	-0.0272	+0.1444	+0.1483
		8^o			+0.2990	+0.4274	+0.0279	-0.0180	-0.0180	-0.0069	-0.0350	-0.0075	-0.0049	-0.0135	-0.0140	-0.0232	+0.1851	+0.1837
		10^o			+0.2859	+0.4536	+0.0004	+0.0148	+0.0619	-0.0049	+0.0056	+0.0737	-0.0088	+0.0161	+0.0279	+0.0226	+0.1929	+0.1706

SYMBOLS

b	gross span = 3.25 in
$\bar{\bar{c}}$	mean aerodynamic chord = 2.182 in
C_m	$\frac{M}{qS\bar{\bar{c}}}$
C_{m_b}	$\frac{M_b}{qS\bar{\bar{c}}}$
C_z	$\frac{Z}{qS}$
C_{z_b}	$\frac{Z_b}{qS}$
M	pitching moment (on the bomb) see Fig.1b
M_b	pitching moment (on twin boost unit) see Fig.1b
q	kinetic pressure = $\frac{1}{2}\rho V^2$
S	gross wing area = 5.757 in^2
Z	normal force (on the bomb) see Fig.1b
Z_b	normal force (on twin boost unit) see Fig.1b
α	incidence angle (the bomb) see Fig.1b
α_b	incidence angle (twin boost unit) see Fig.1b
η	foreplane setting (the bomb)
x', z'	co-ordinates defining the boost position (in cm) see Fig.1b
C'_{m_b}	pitching moment coefficient on the boost about an axis 51.2% of the boost length from the nose (see 6.3.1(a))

REFERENCES

No.	Author(s)	Title, etc.
1	J.A. Lang	Supersonic wind tunnel measurements of the contribution of the nacelle units to the static stability of Blue Steel. RAE Technical Note Aero 2741 (ARC 23088) (1961)
2	P.E. Watts B.E. Pecover	Five component wind tunnel tests on a 1/48th scale model of a guided bomb (Blue Steel) at M = 2.47. RAE Technical Note Aero 2566 (ARC 21750) (1959)
3	P.E. Watts B.E. Pecover	A wind tunnel investigation of the longitudinal and lateral aerodynamic characteristics of a guided bomb test vehicle (A.T.U.2) at M = 2.47. RAE Report Aero 2597 (ARC 20887) (1958)
4	H.J. Allen E.W. Parkin	A study of effects of viscosity on flow over slender inclined bodies of revolution. NACA Report 1048 (1951)
5	L.H. Carpenter	On the motion of two cylinders in an ideal fluid. Research Paper 2889. Nat. Bur. Stnds. Jnl. Vol.61, No.2, pp.83-87 (1958)
6	A.H. Sacks	Aerodynamic forces, moments and stability derivatives for slender bodies of general cross section. NACA TN 3283 (1954)
7	L.E. Moskowitz	Approximate theory for calculation of lift of bodies, afterbodies and combinations of bodies. NACA TN 2669 (1952)

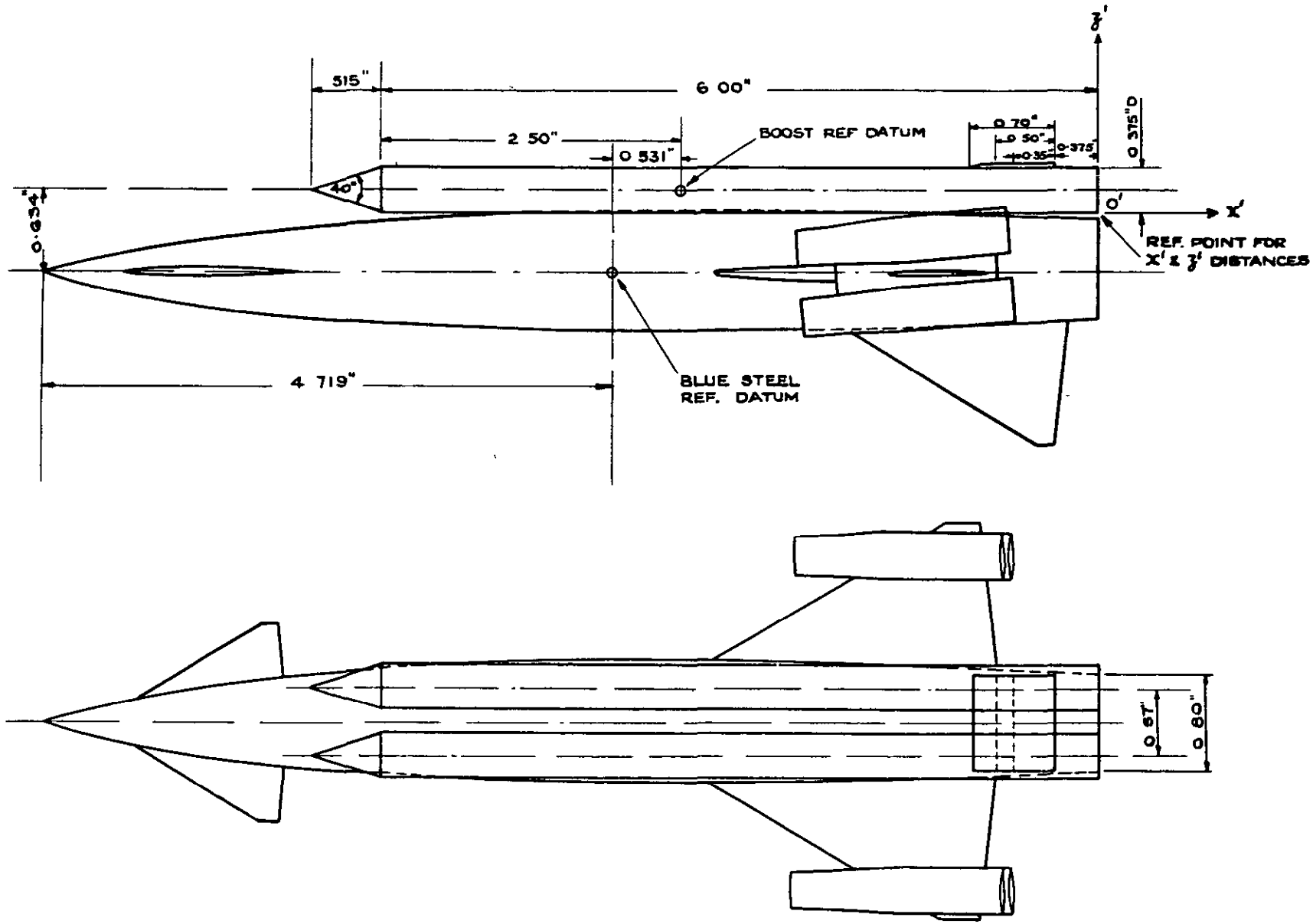

FIG. 1. (a) BLUE STEEL MODEL TOGETHER WITH THE TWIN BOOST UNIT.

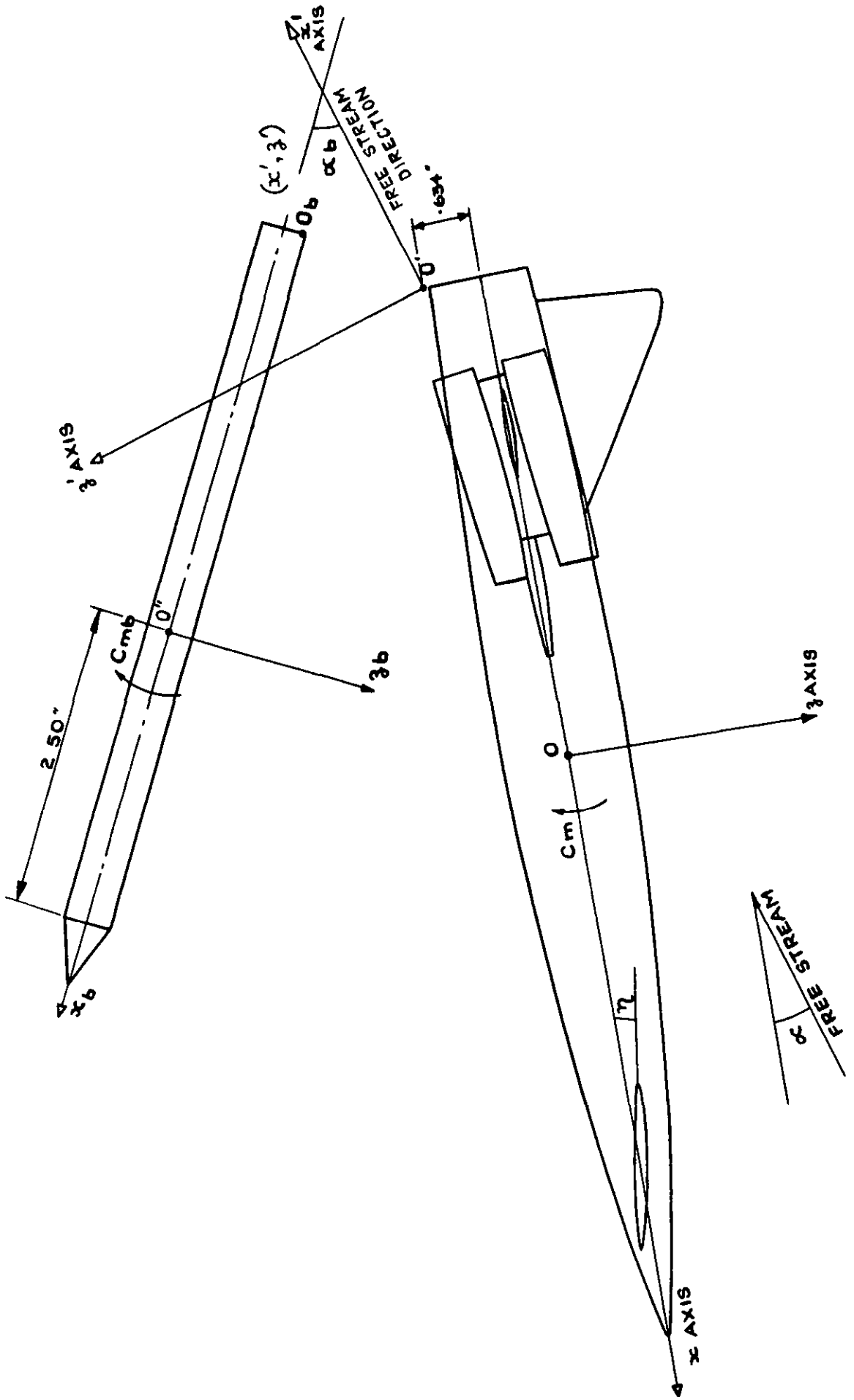

FIG.1(b)SKETCH SHOWING NOTATION USED.

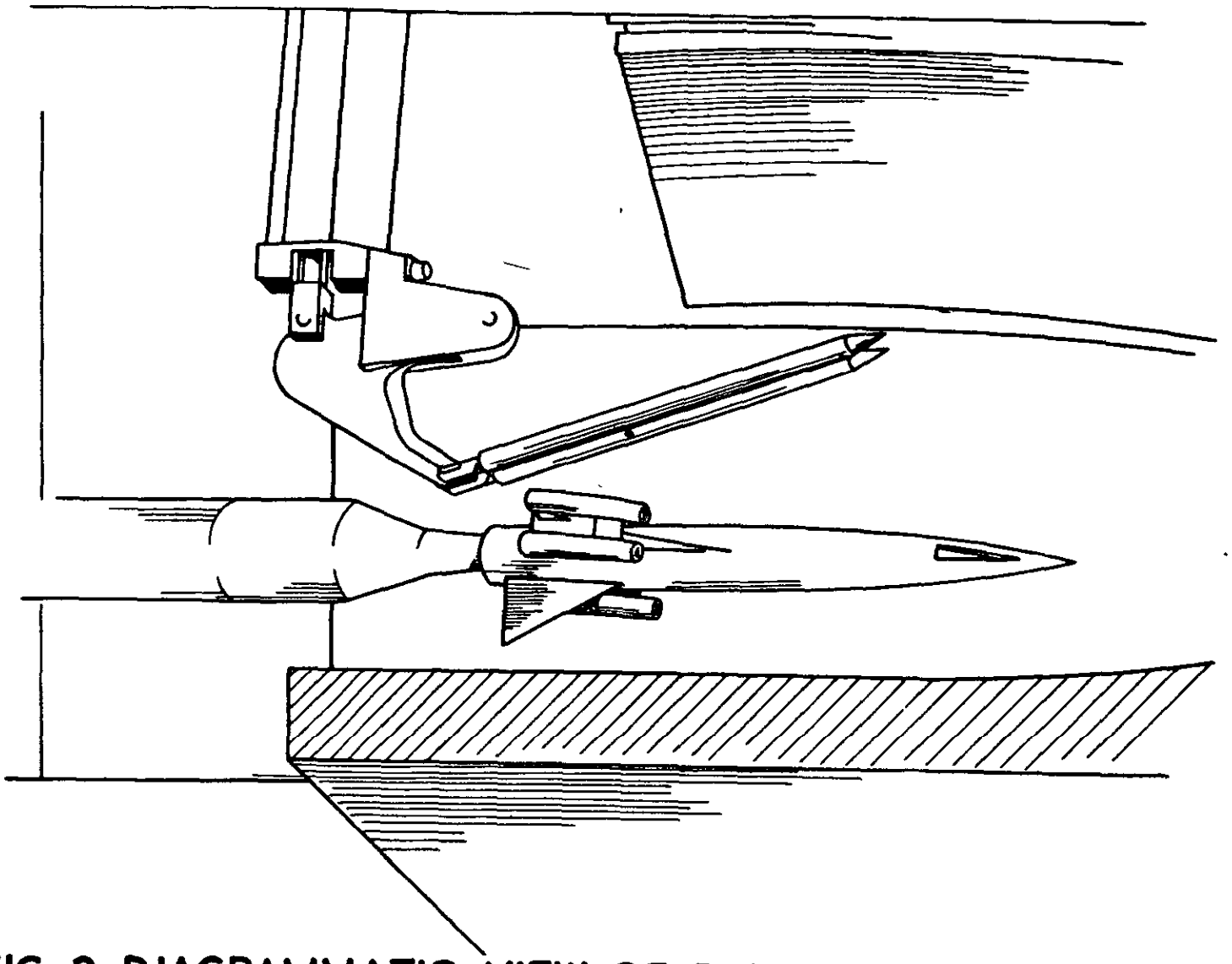

FIG. 2. DIAGRAMMATIC VIEW OF BLUE STEEL MODEL AND OF TWIN BOOST UNIT MOUNTED ON THE TRAVERSE GEAR IN THE R.A.E. Nº8 TUNNEL.

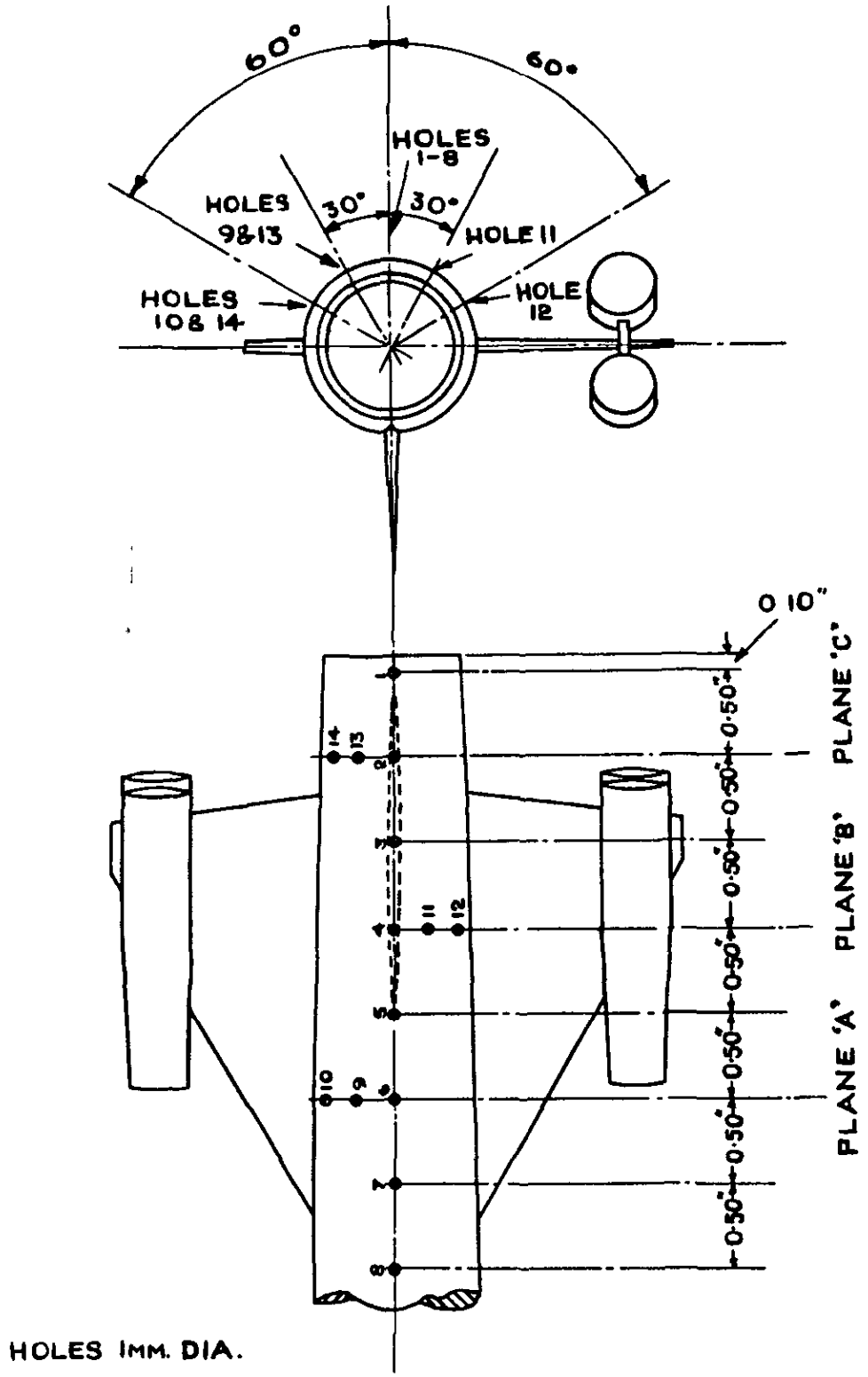

FIG.3. POSITION OF PRESSURE PLOTTING HOLES ON TOP OF BLUE STEEL MODEL.

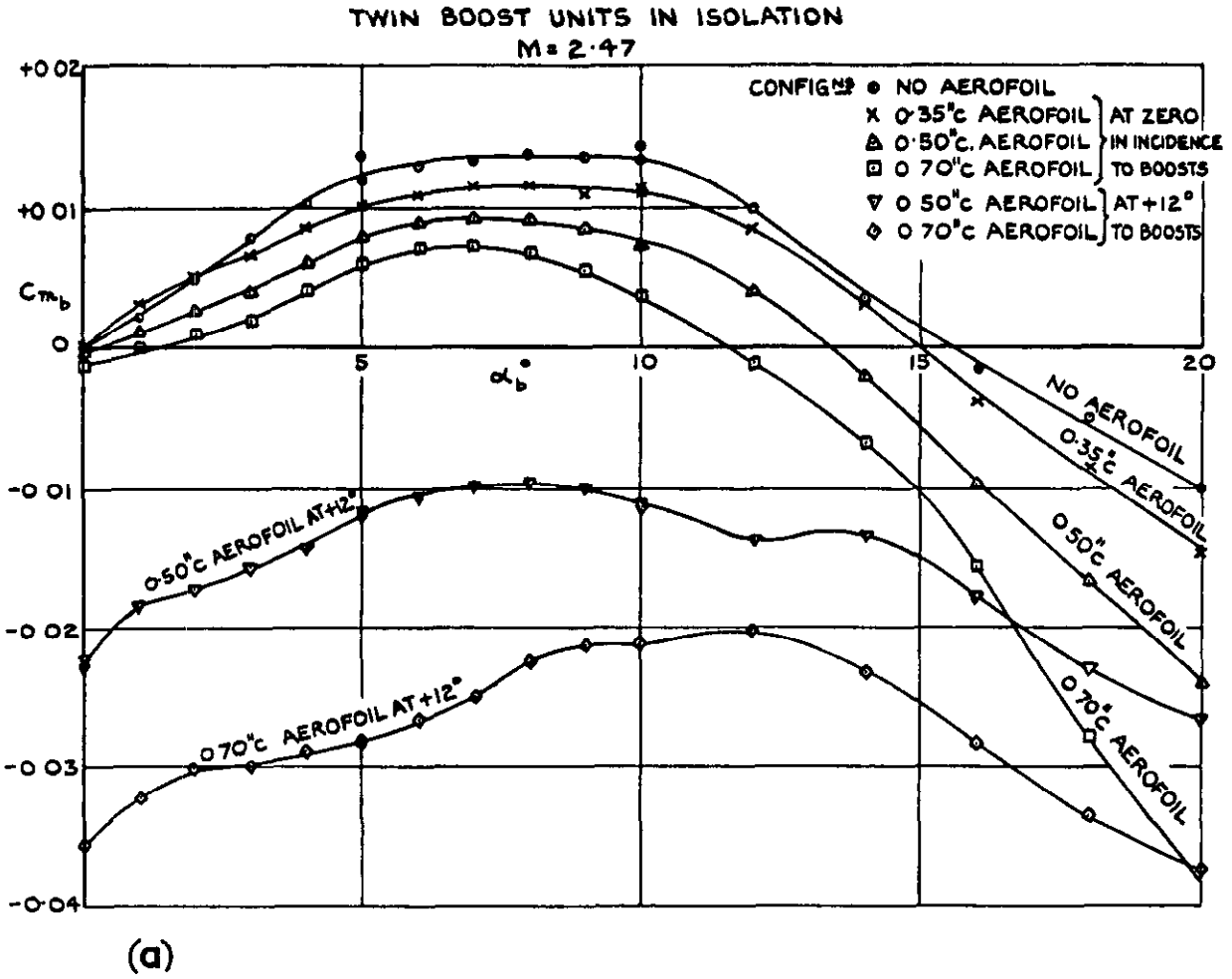

(a)

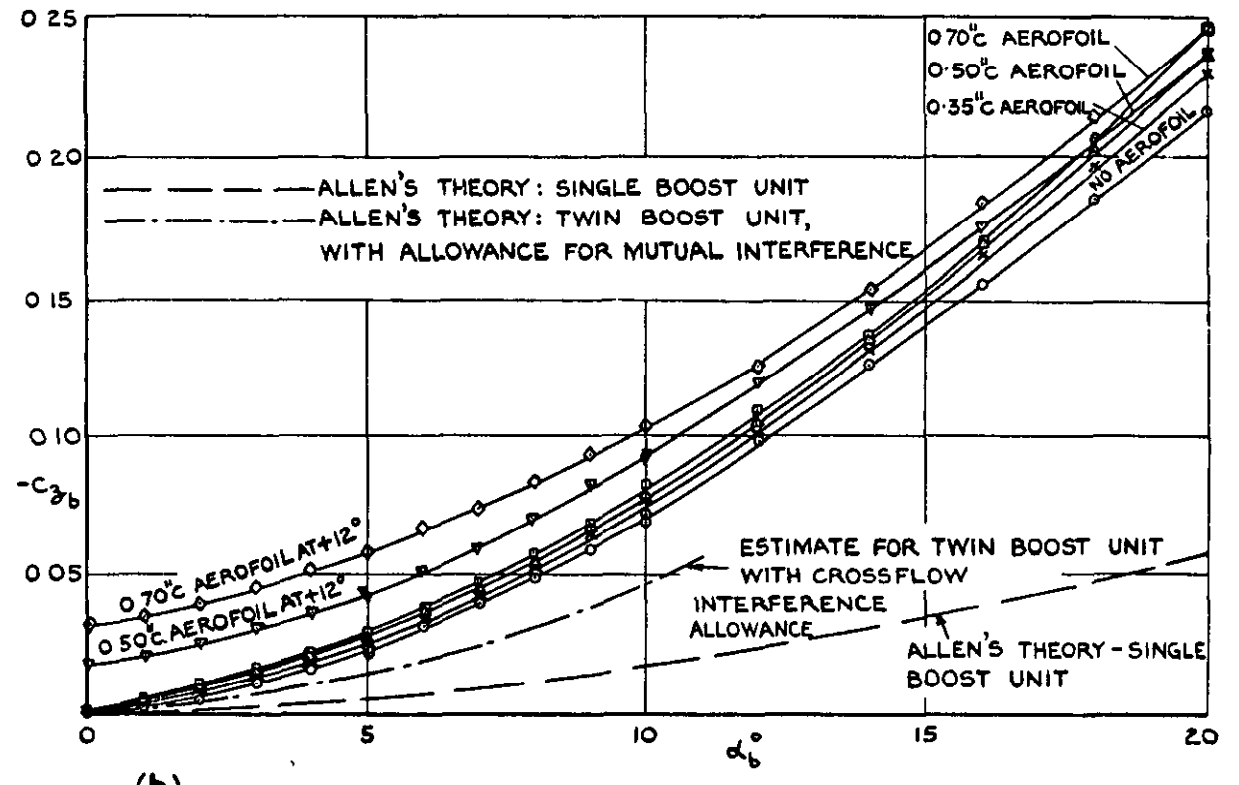

(b)

FIG. 4. VARIATION OF C_{m_b} AND $-C_{z_b}$ WITH α_b OF THE TWIN BOOST UNIT IN ISOLATION M = 2·47, ALL CONFIGURATIONS.

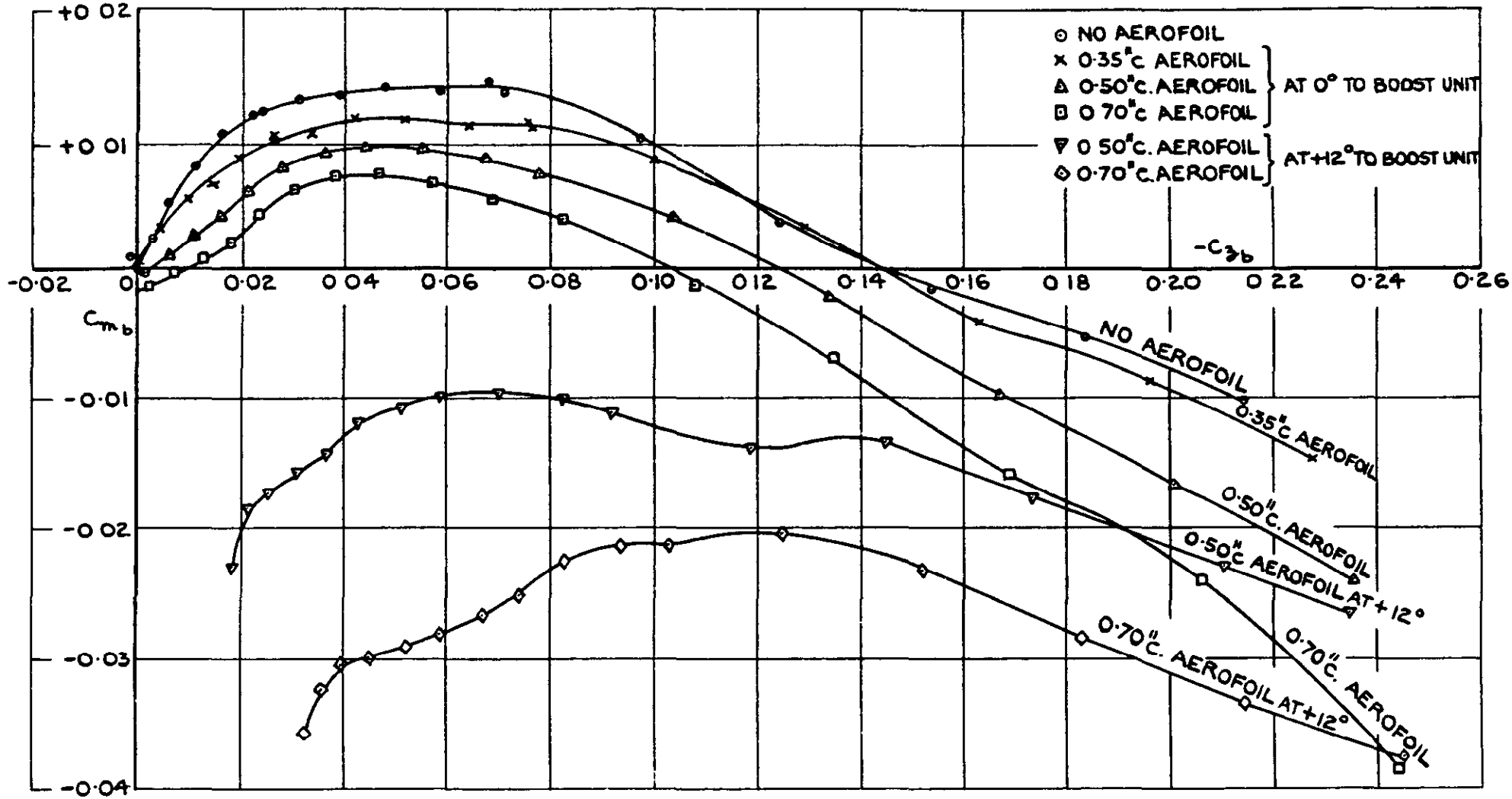

FIG.5. C_{m_b} vs $-C_{z_b}$ FOR ALL CONFIGURATIONS OF THE TWIN BOOST UNITS IN ISOLATION M = 2·47.

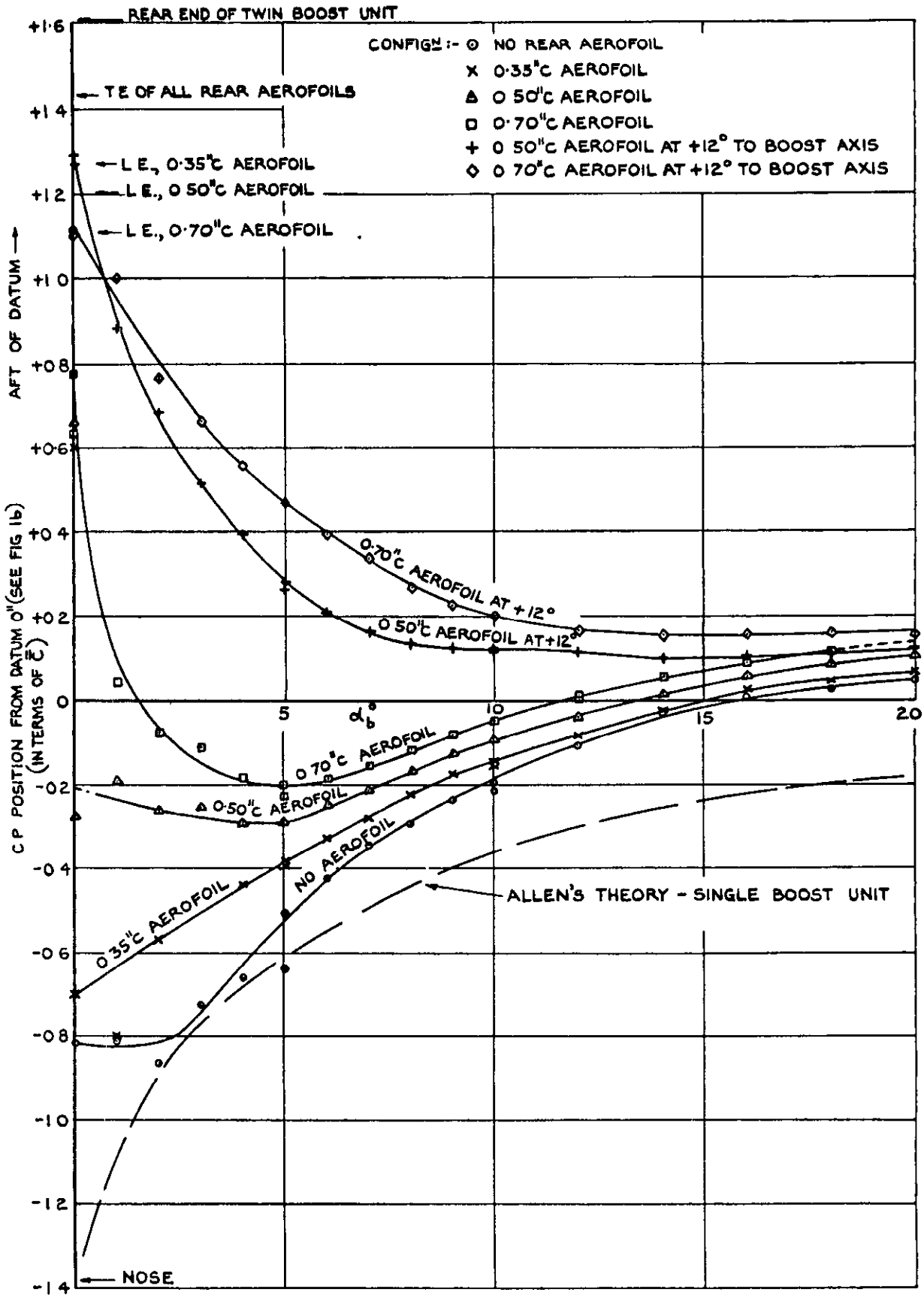

FIG.6. C.P. POSITION FROM DATUM 0", vs. α_b FOR ALL CONFIGURATIONS OF THE TWIN BOOST UNIT IN ISOLATION M=2·47.

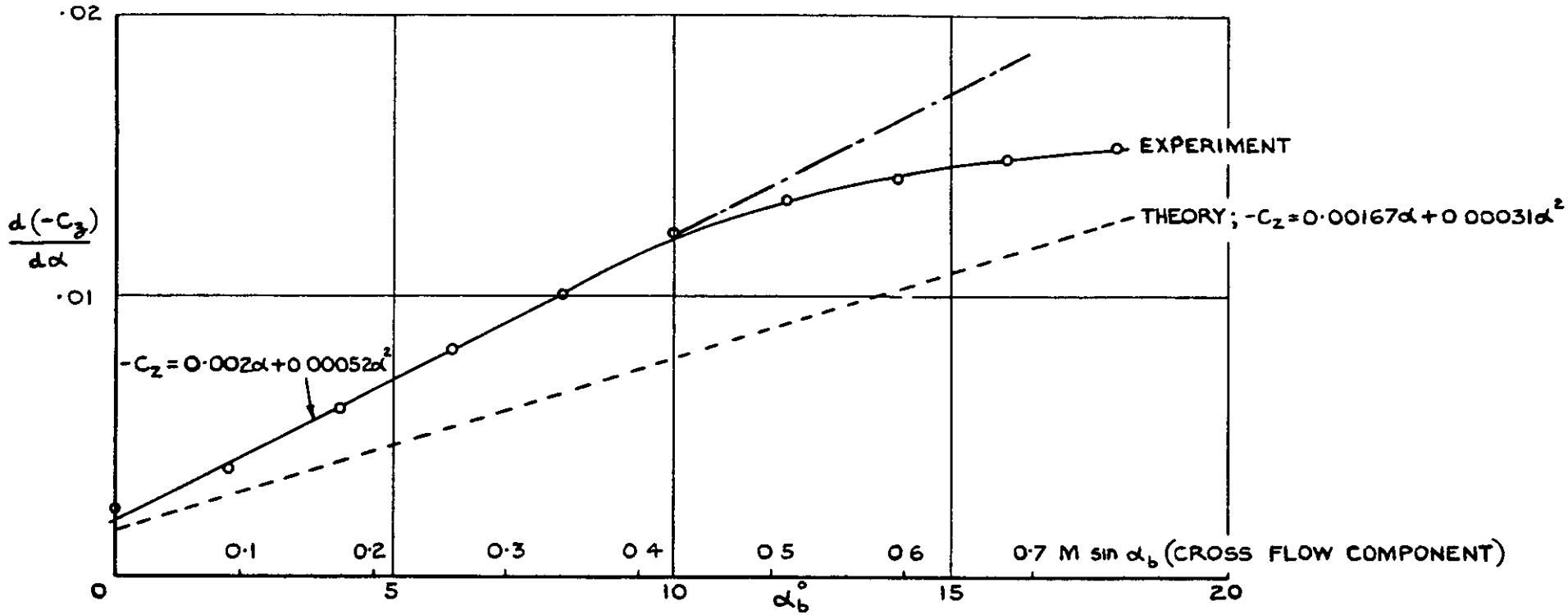

FIG. 7. COMPARISON OF THEORETICAL AND EXPERIMENTAL NORMAL FORCE CURVE SLOPES OF TWIN BOOST UNIT AT M = 2·47.

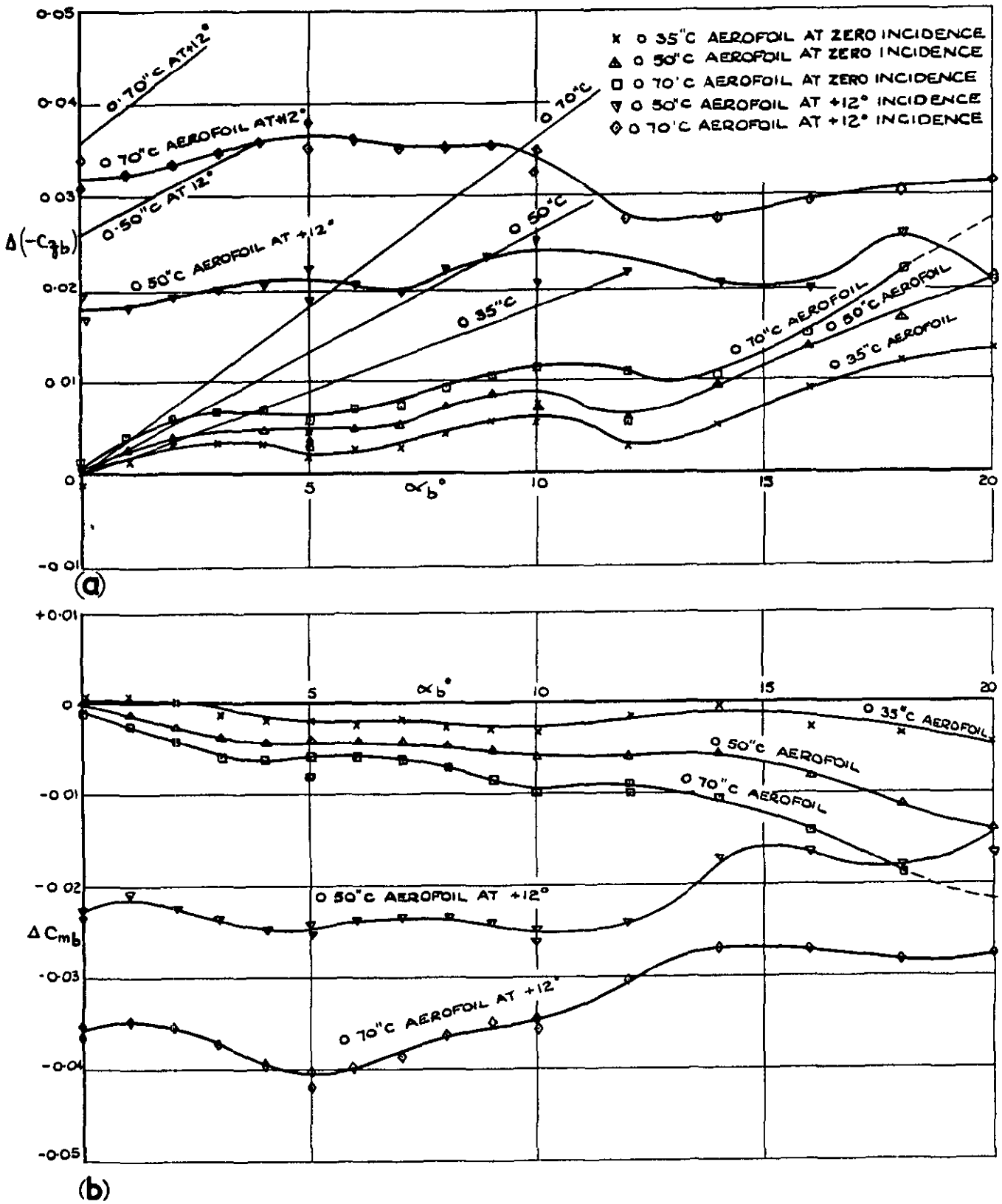

FIG. 8. INCREMENTAL LOADS AND MOMENTS FROM THE REAR AEROFOILS FITTED TO THE TWIN BOOST UNIT, M 2·47.

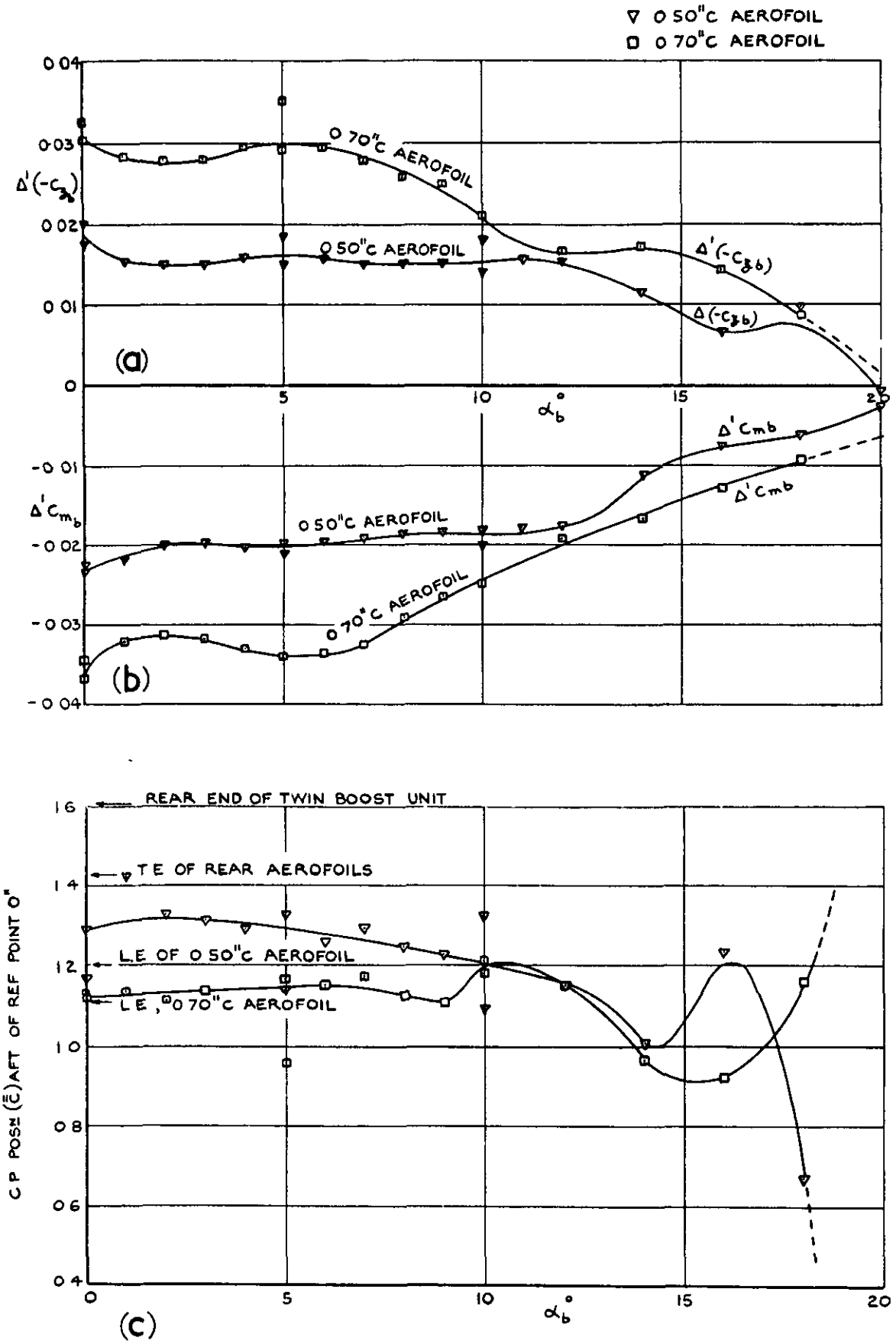

FIG.9. INCREMENTAL LOADS AND MOMENTS PRODUCED BY AN INCREASE OF 12° IN INCIDENCE OF TWO OF THE REAR AEROFOILS ON THE TWIN BOOST UNIT, M = 2·47.

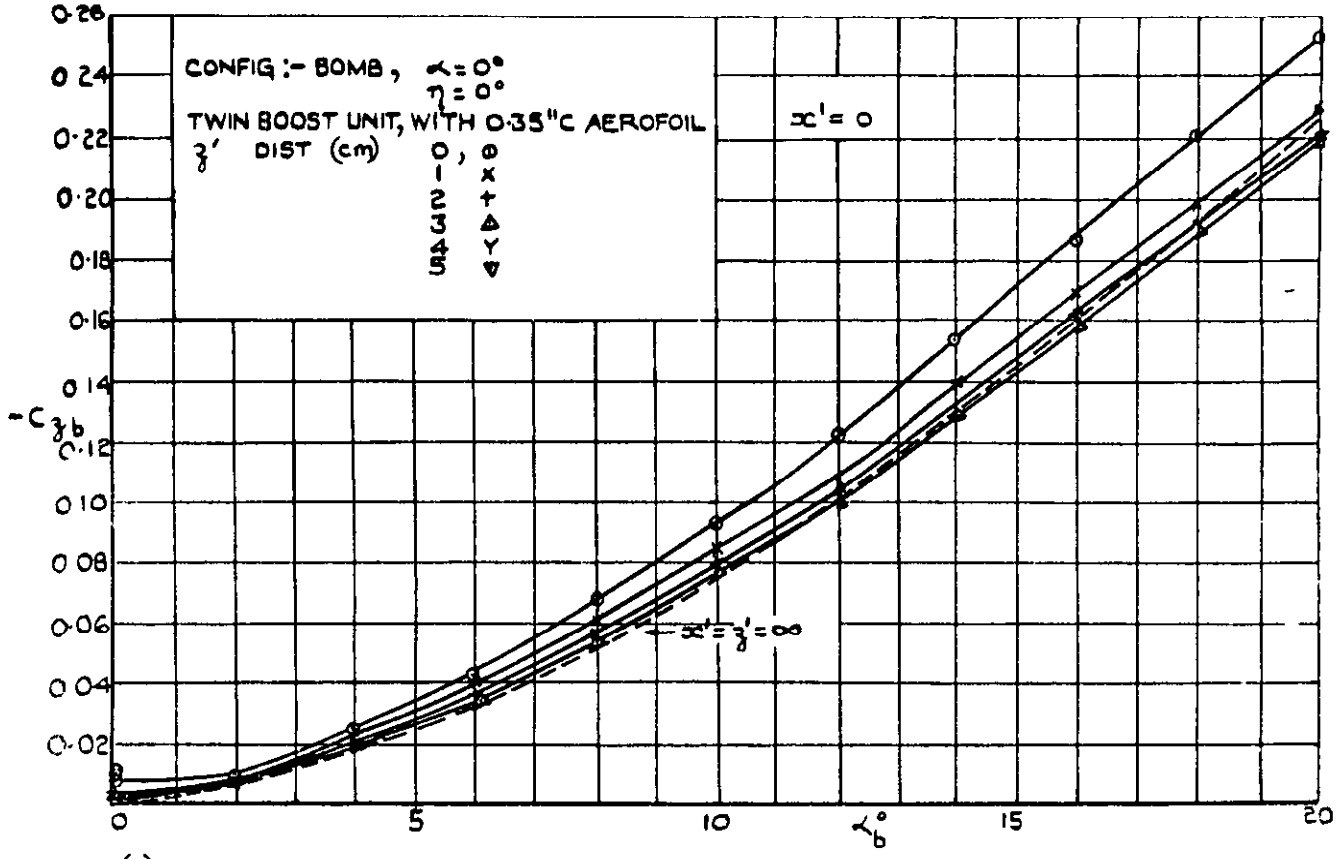

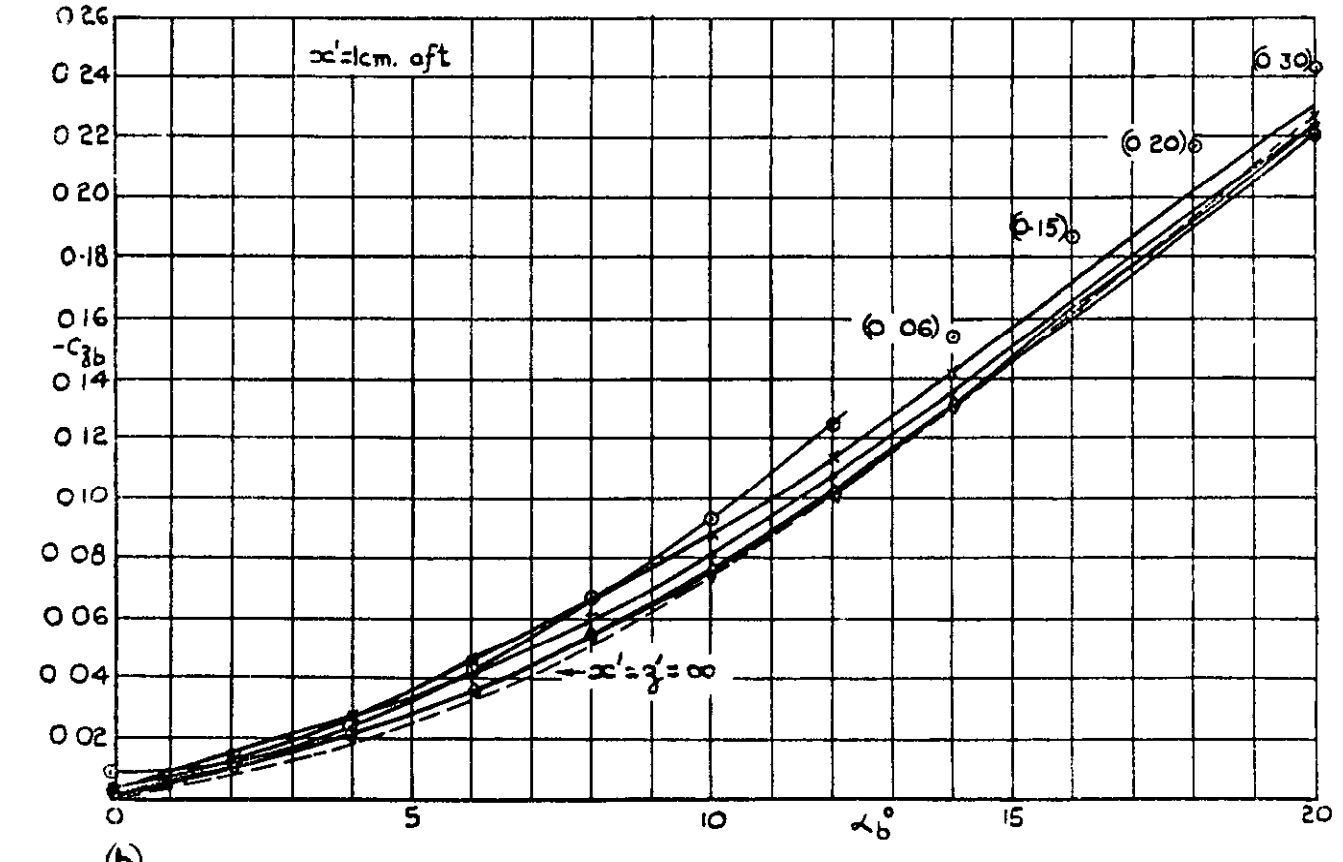

FIG.10.-C_{zb} vs α_b AT VARIOUS x' AND z' STATIONS FOR THE TWIN BOOST UNIT WITH THE 0·35"C REAR AEROFOIL, IN THE PRESENCE OF THE BOMB AT ZERO INCIDENCE, M=2·47.

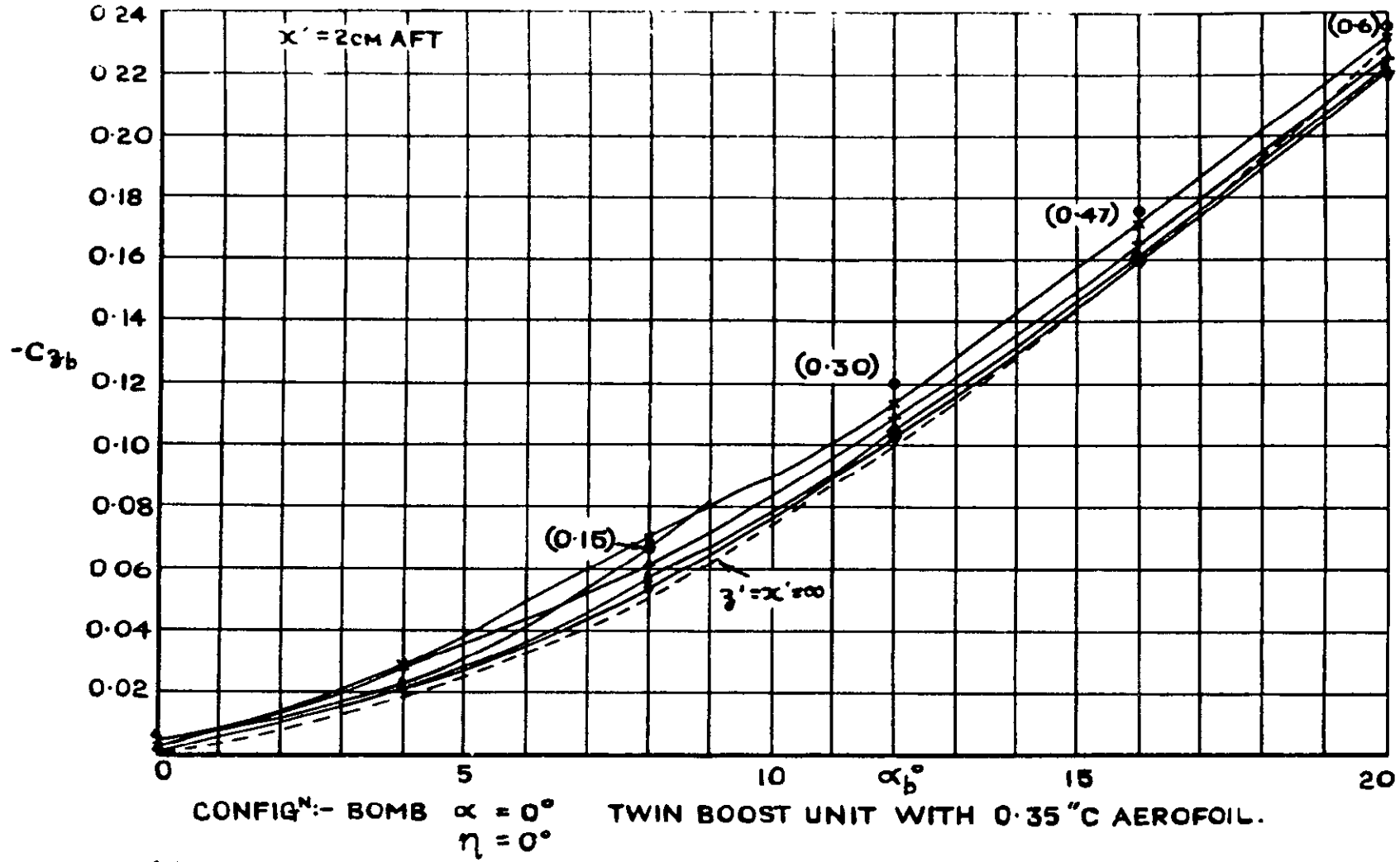

(c)

FIG.10. $-C_{\zeta_b}$ VS α_b AT VARIOUS x' AND ζ' STATIONS FOR THE TWIN BOOST UNIT WITH THE 0·35" C. REAR AEROFOIL, IN THE PRESENCE OF THE BOMB AT ZERO INCIDENCE, M=2·47.

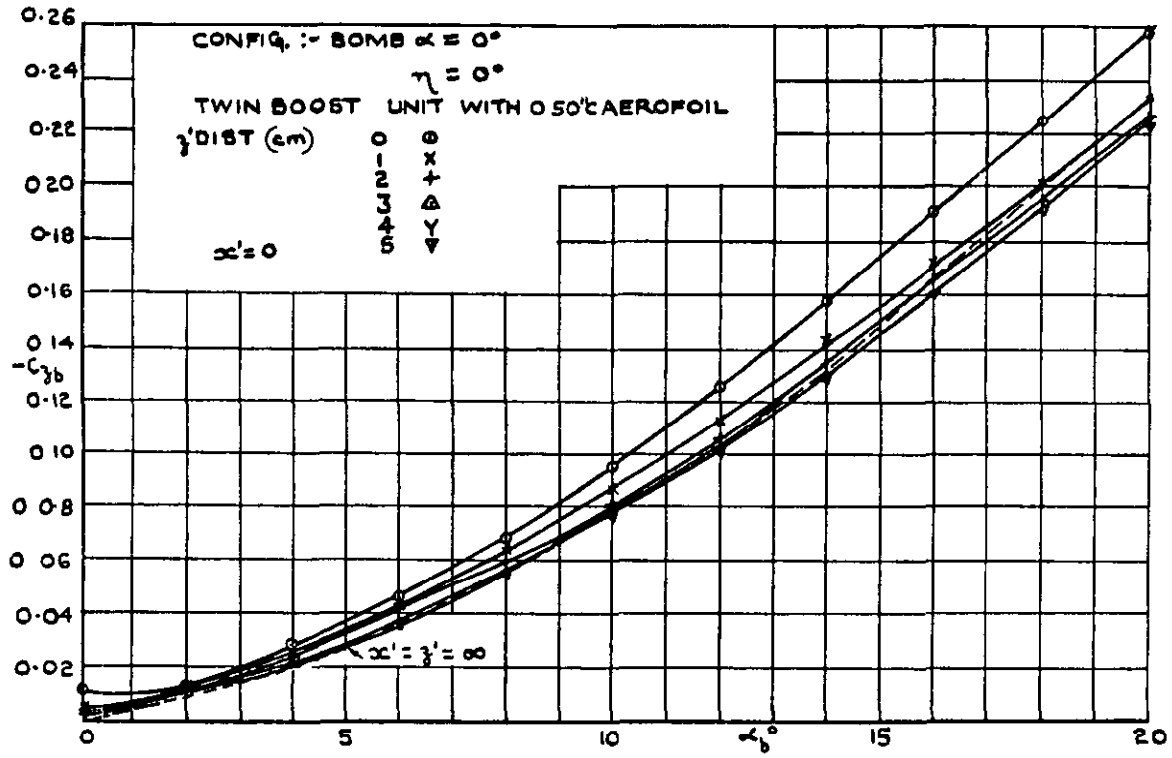

(a)

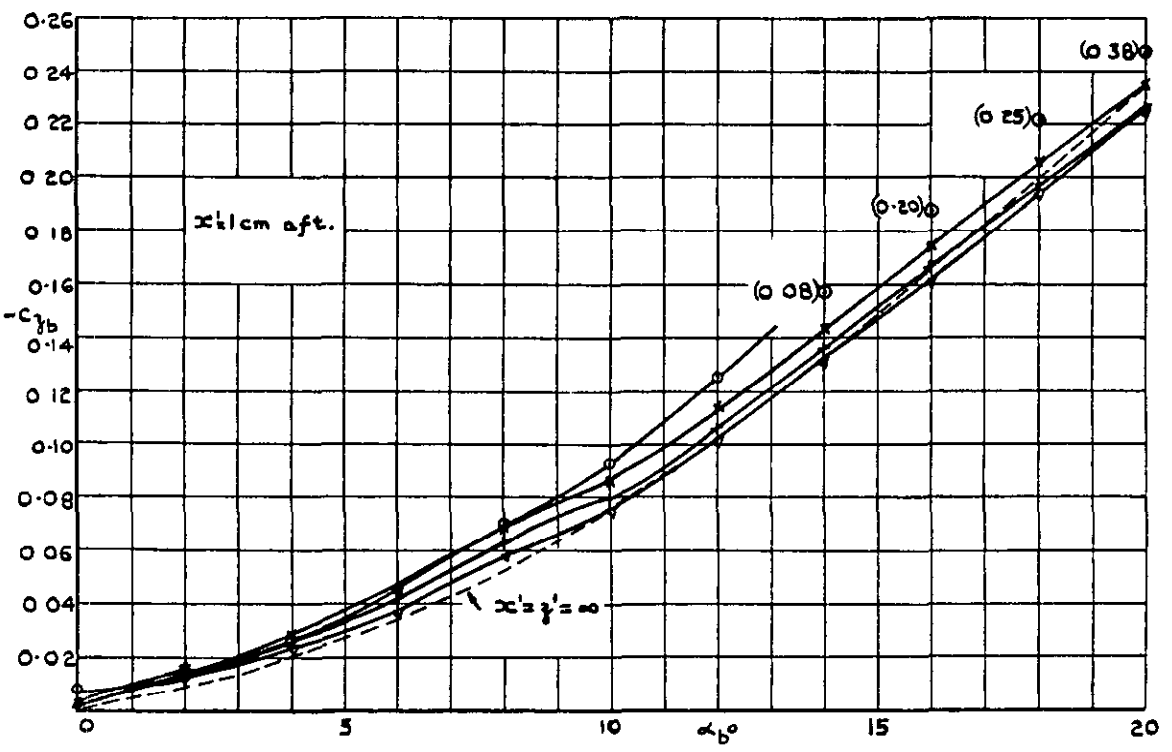

(b)

FIG.11.-C_{zb} vs α_b AT VARIOUS x' & z' STATIONS FOR THE TWIN BOOST UNIT WITH THE 0·50"C. REAR AEROFOIL, IN THE PRESENCE OF THE BOMB AT ZERO INCIDENCE (M= 2·47.)

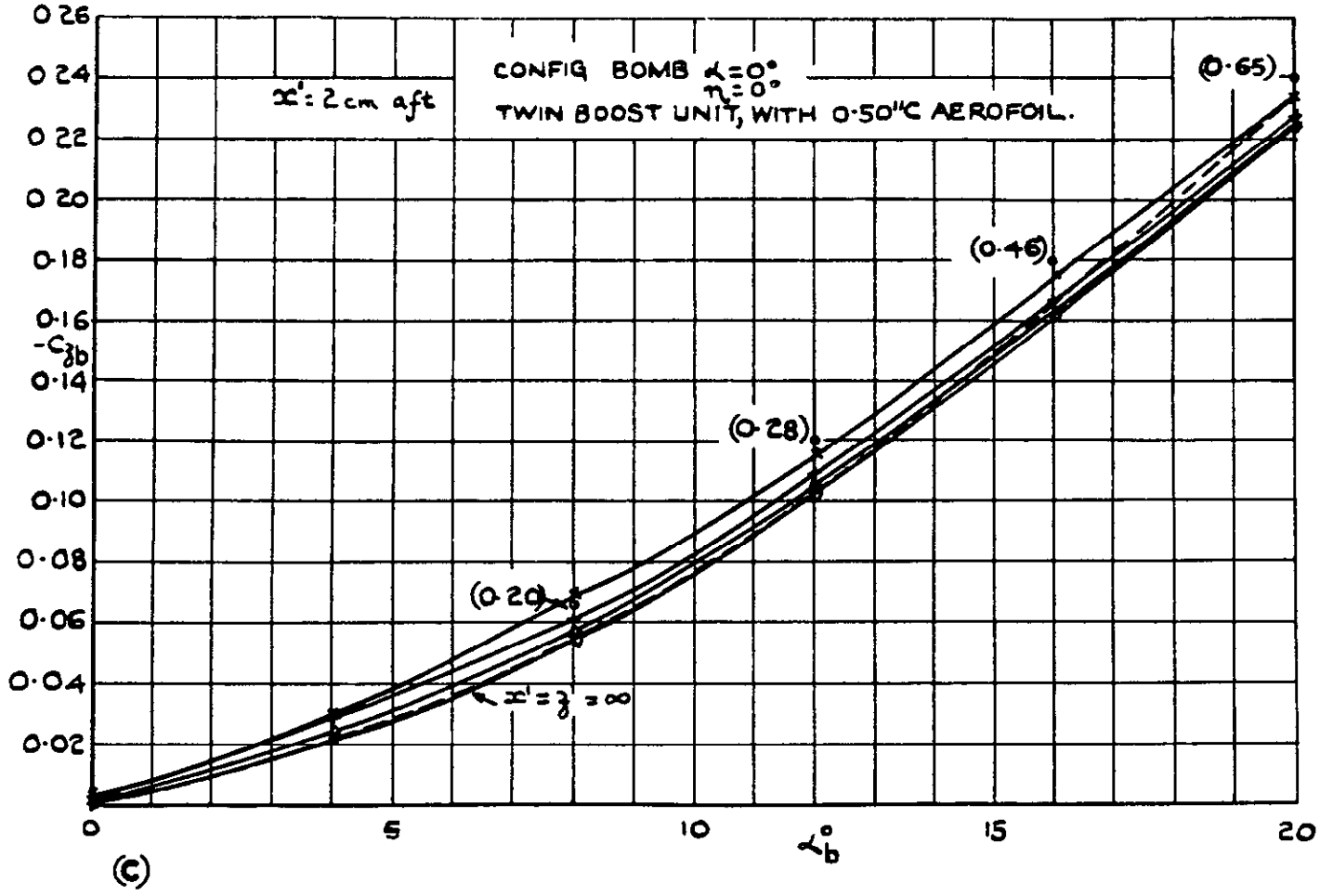

FIG.11.-C_{zb} vs α_b AT VARIOUS x' & z' STATIONS FOR THE TWIN BOOST UNIT WITH THE 0·50"C. REAR AEROFOIL, IN THE PRESENCE OF THE BOMB AT ZERO INCIDENCE M = 2·47

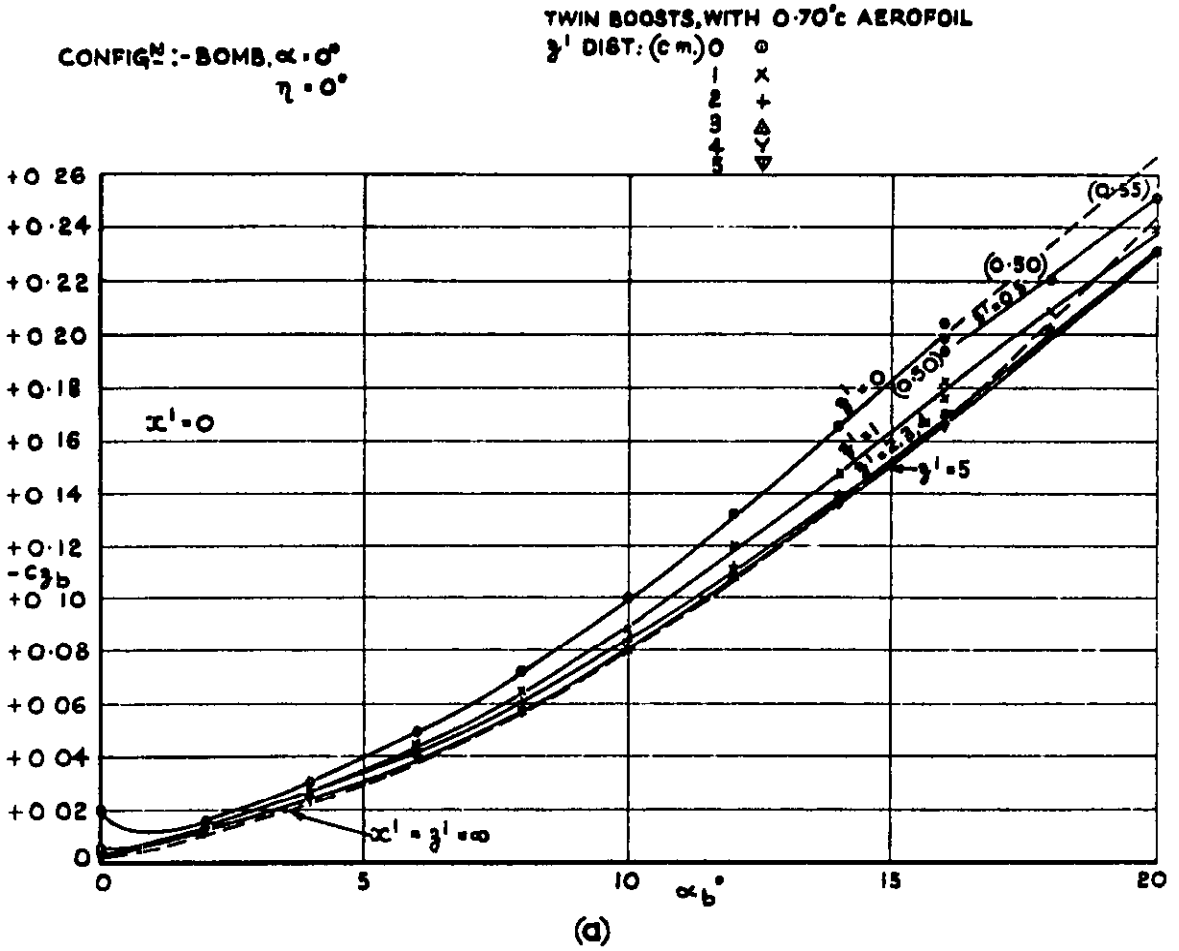

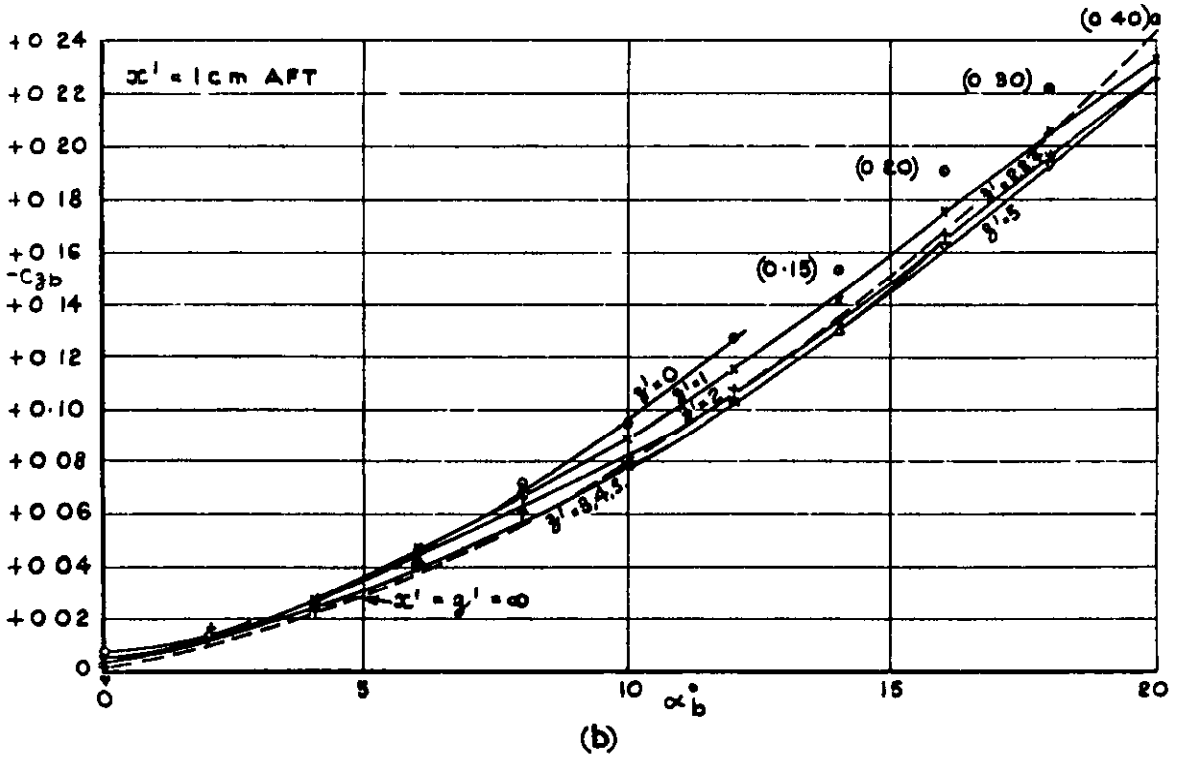

FIG. 12.-C_{z_b} vs. α_b AT VARIOUS x' AND y' STATIONS FOR THE TWIN BOOST UNIT WITH THE 0·70$\bar{c}$. REAR AEROFOIL, IN THE PRESENCE OF THE BOMB AT ZERO INCIDENCE, M=2·47.

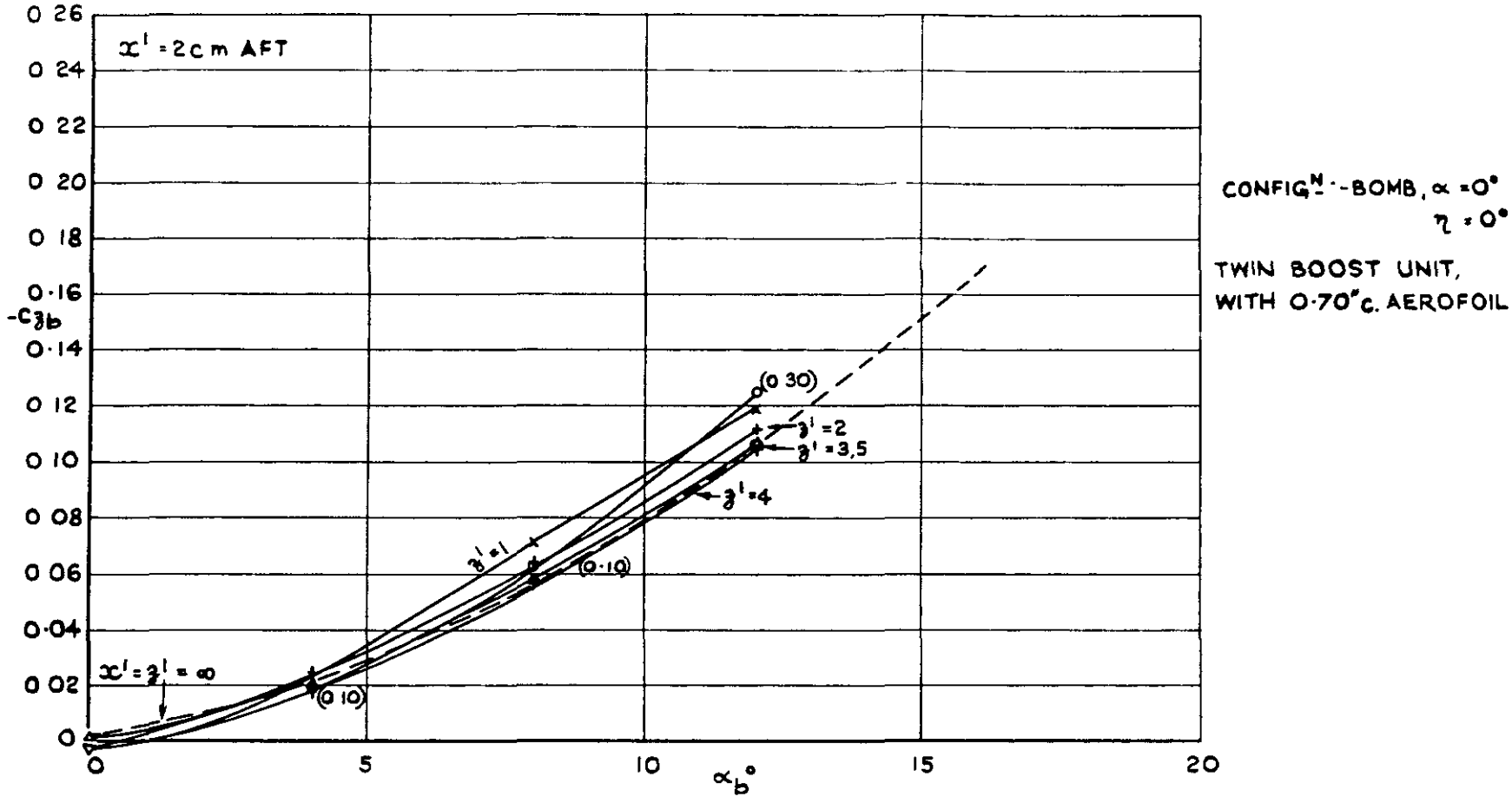

(c)

FIG. 12.-C_{zb} vs. α_b AT VARIOUS x^1 AND z^1 STATIONS FOR THE TWIN BOOST UNIT WITH THE 0·70"c. REAR AEROFOIL, IN THE PRESENCE OF THE BOMB AT ZERO INCIDENCE, M=2·47.

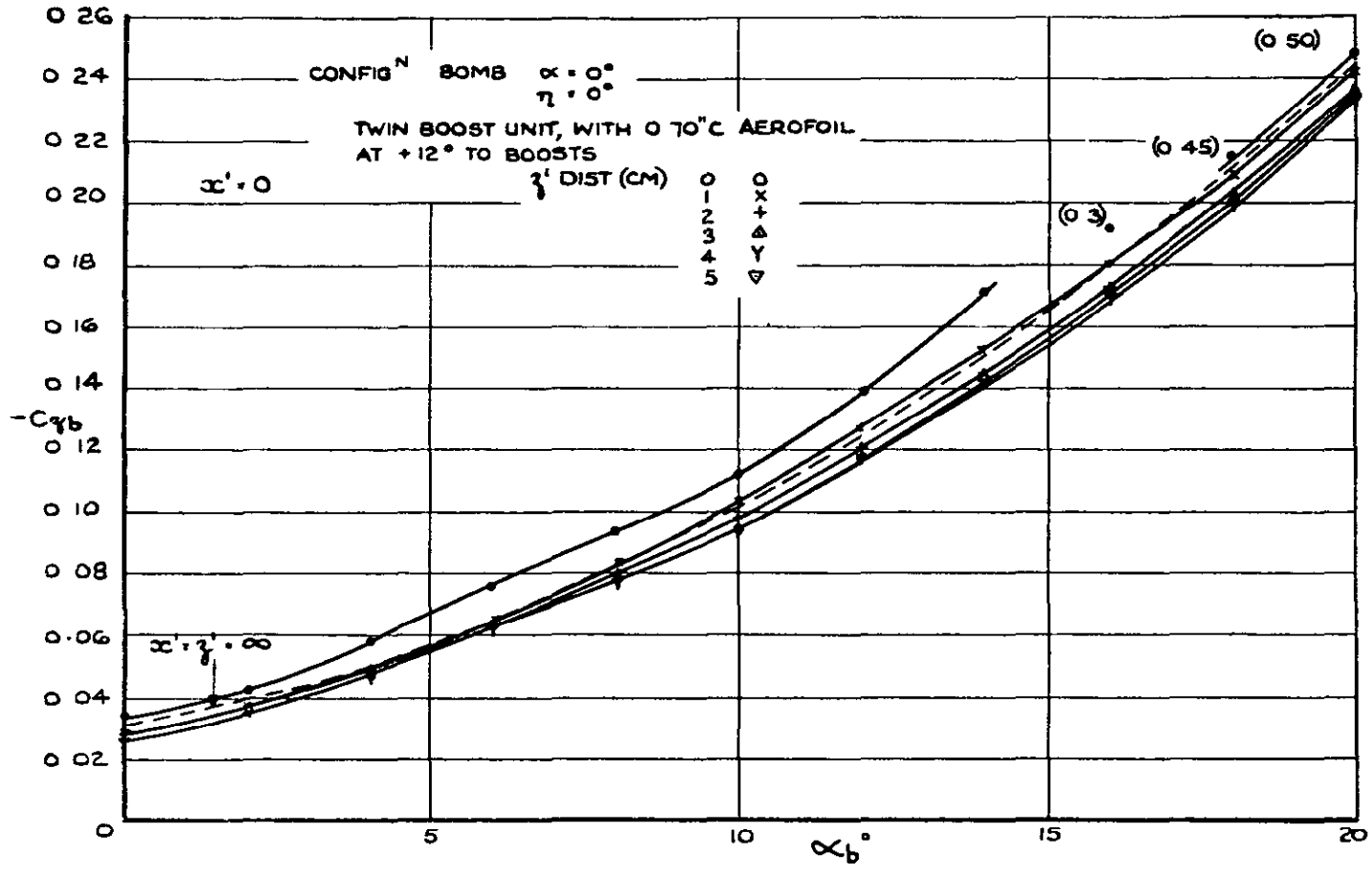

FIG. 13. $-C_{zb}$ vs α_b AT $x'=0$ AND VARIOUS z' STATIONS FOR THE TWIN BOOST UNIT WITH THE 0·70"C REAR AEROFOIL SET AT 12° TO THE BOOSTS, IN THE PRESENCE OF THE BOMB AT ZERO INCIDENCE, M=2·47.

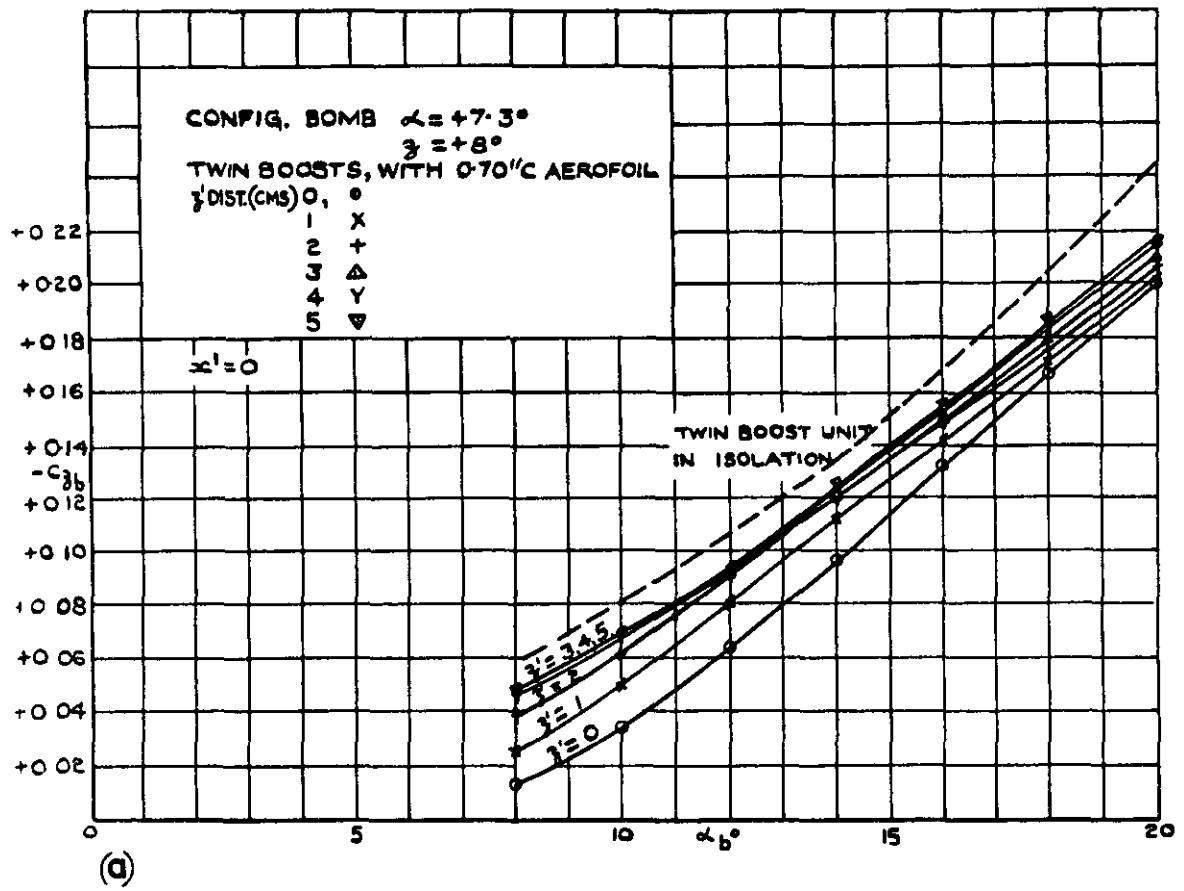

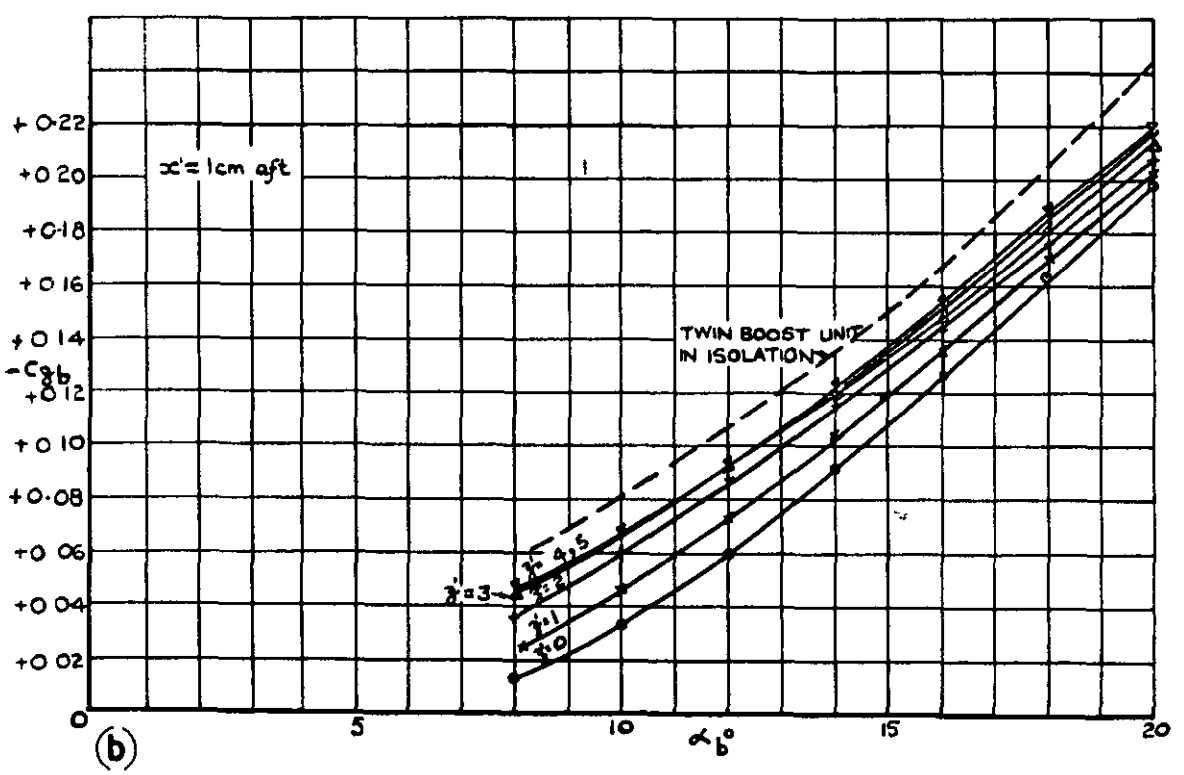

FIG.14. $-C_{\zeta b}$ vs. α_b AT VARIOUS x' AND ȝ' STATIONS FOR THE TWIN BOOST UNIT WITH THE 0·70"C REAR AEROFOIL, IN THE PRESENCE OF THE BOMB AT CRUISING INCIDENCE, M=2·47.

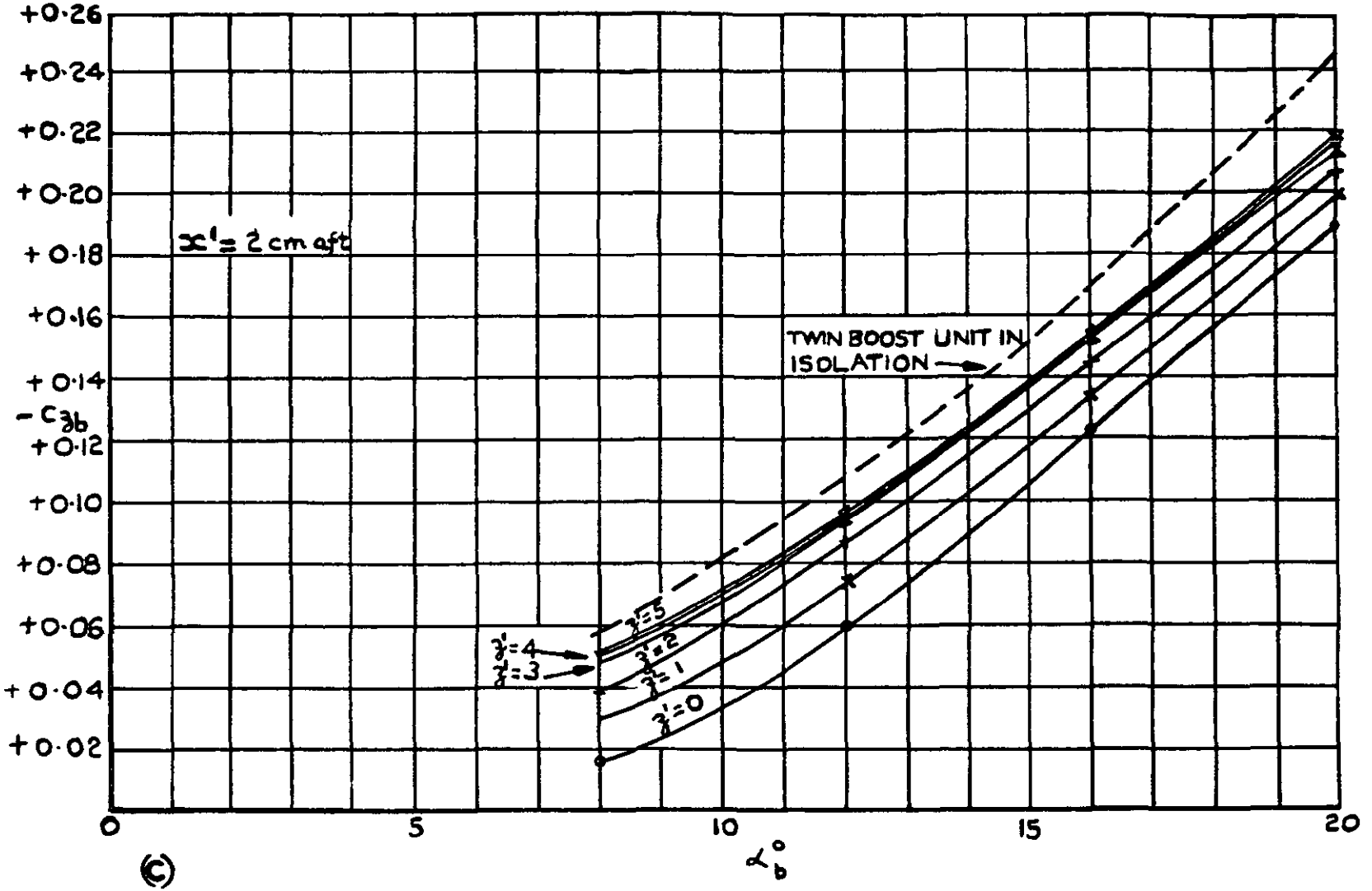

FIG.14.-C_{3b} vs α_b AT VARIOUS x' & z' STATIONS FOR THE TWIN BOOST UNIT WITH THE 0·70"C REAR AEROFOIL, IN THE PRESENCE OF THE BOMB AT CRUISING INCIDENCE, M=2·47.

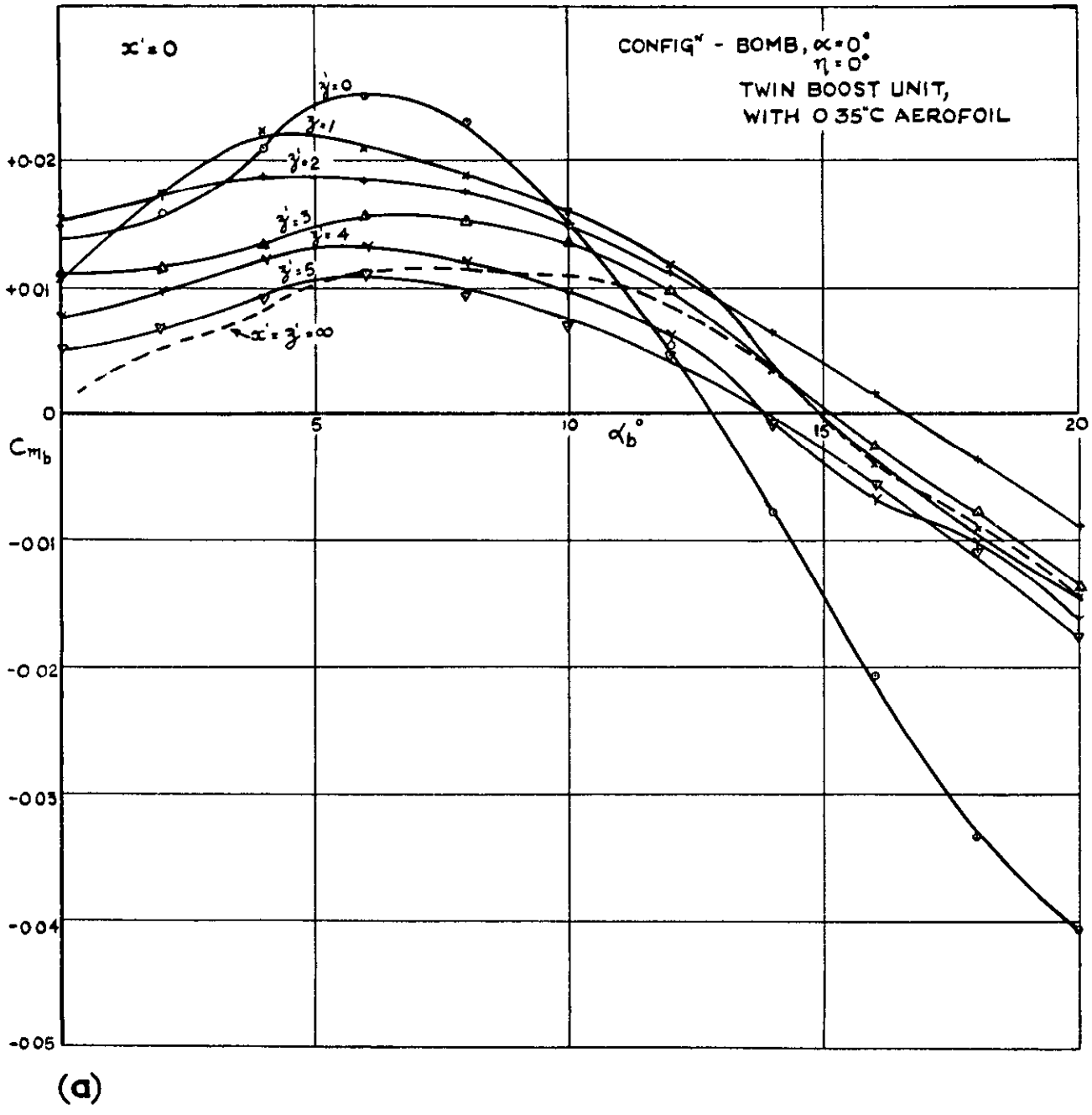

(a)

FIG. 15. C_{m_b} vs α_b AT VARIOUS x' AND y' STATIONS FOR THE TWIN BOOST UNIT WITH THE 0·35C REAR AEROFOIL, IN THE PRESENCE OF THE BOMB AT ZERO INCIDENCE, M=2·47.

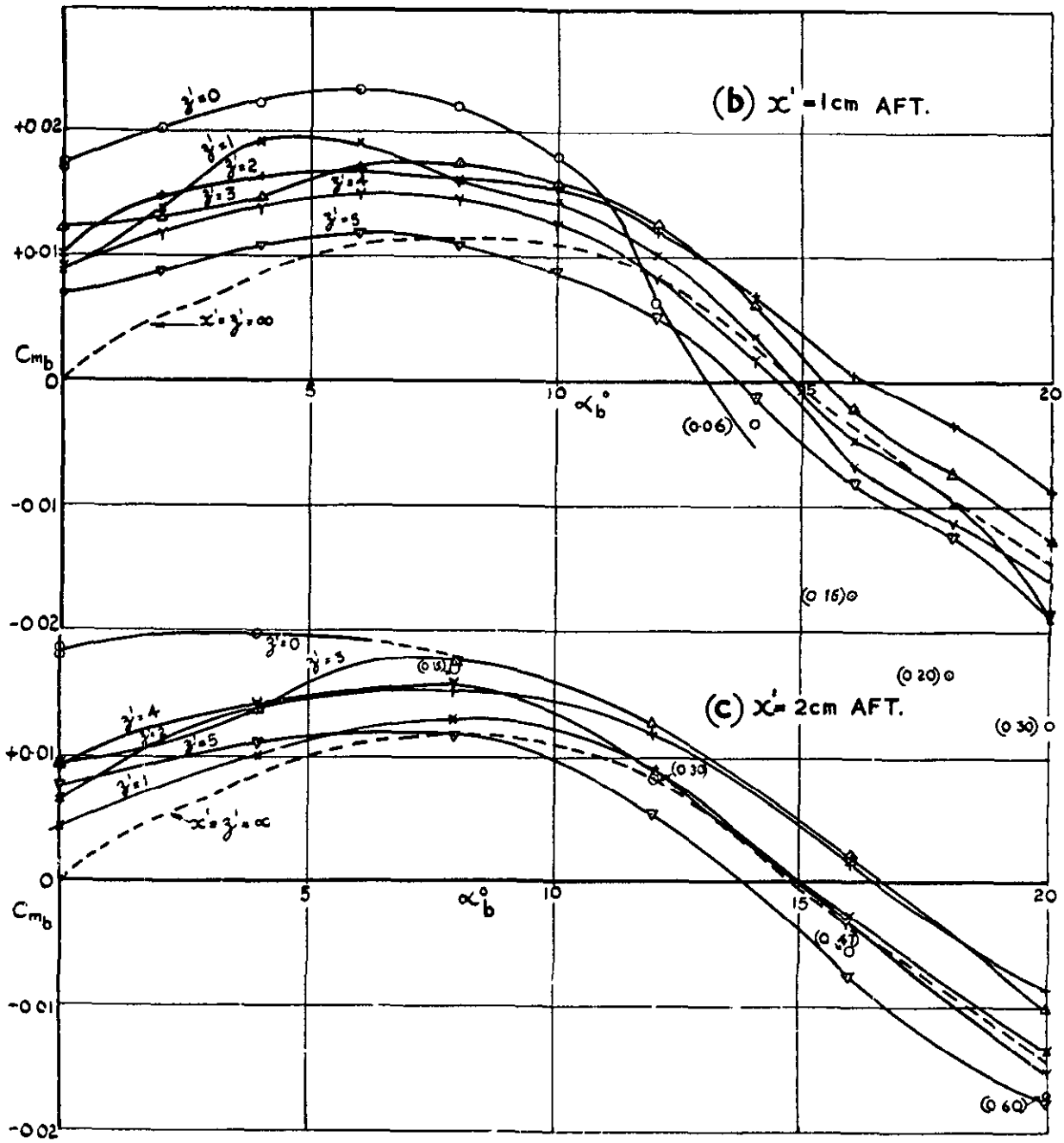

FIG. 15. C_{m_b} vs α_b AT VARIOUS x' AND y' STATIONS FOR THE TWIN BOOST UNIT WITH THE 0·35C REAR AEROFOIL IN THE PRESENCE OF THE BOMB AT ZERO INCIDENCE, M=2·47.

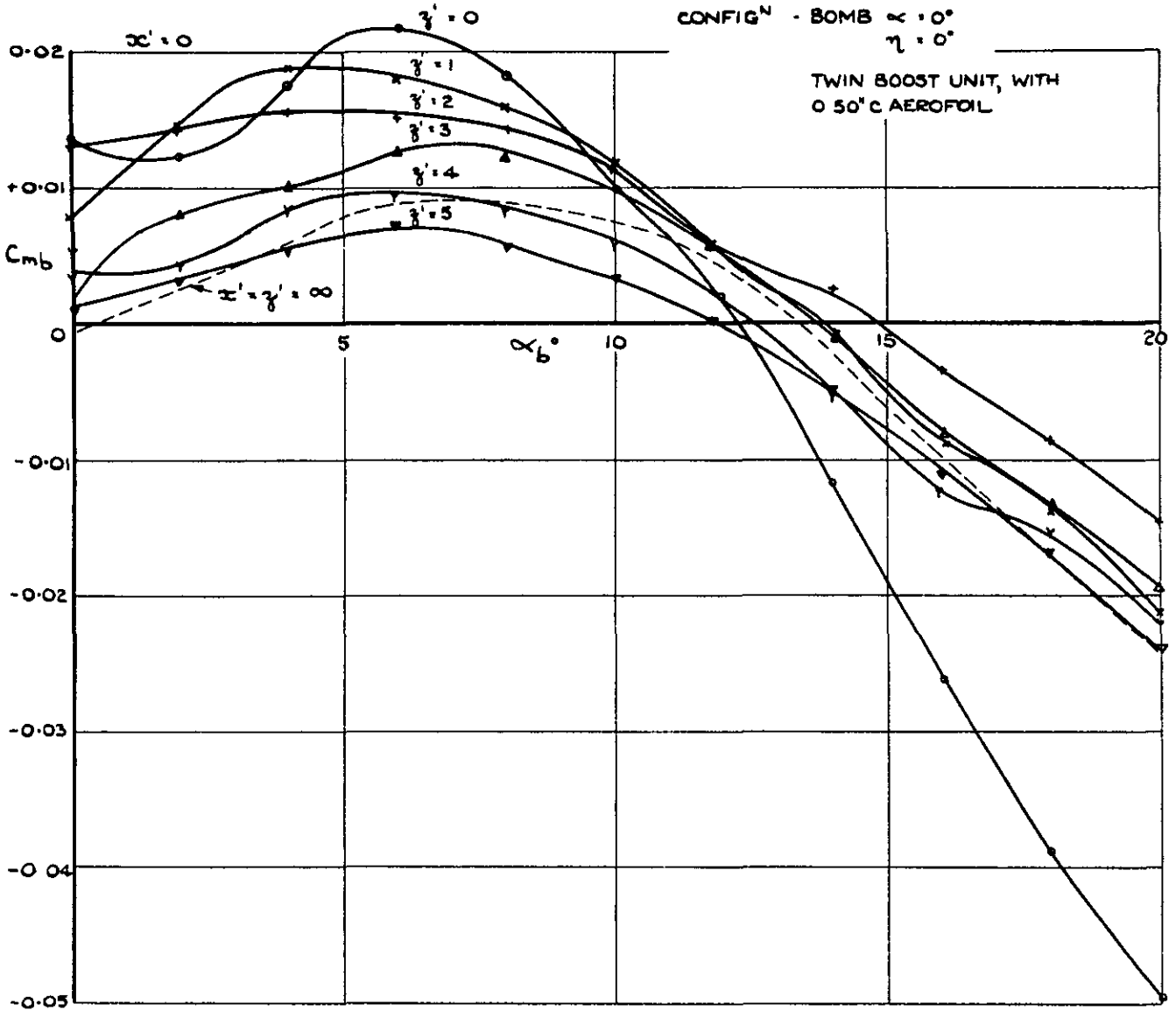

FIG.16. C_{mb} vs α_b AT VARIOUS x' AND ζ' STATIONS FOR THE TWIN BOOST UNIT WITH THE 0·50" C REAR AEROFOIL, IN THE PRESENCE OF THE BOMB AT ZERO INCIDENCE, M=2·47.

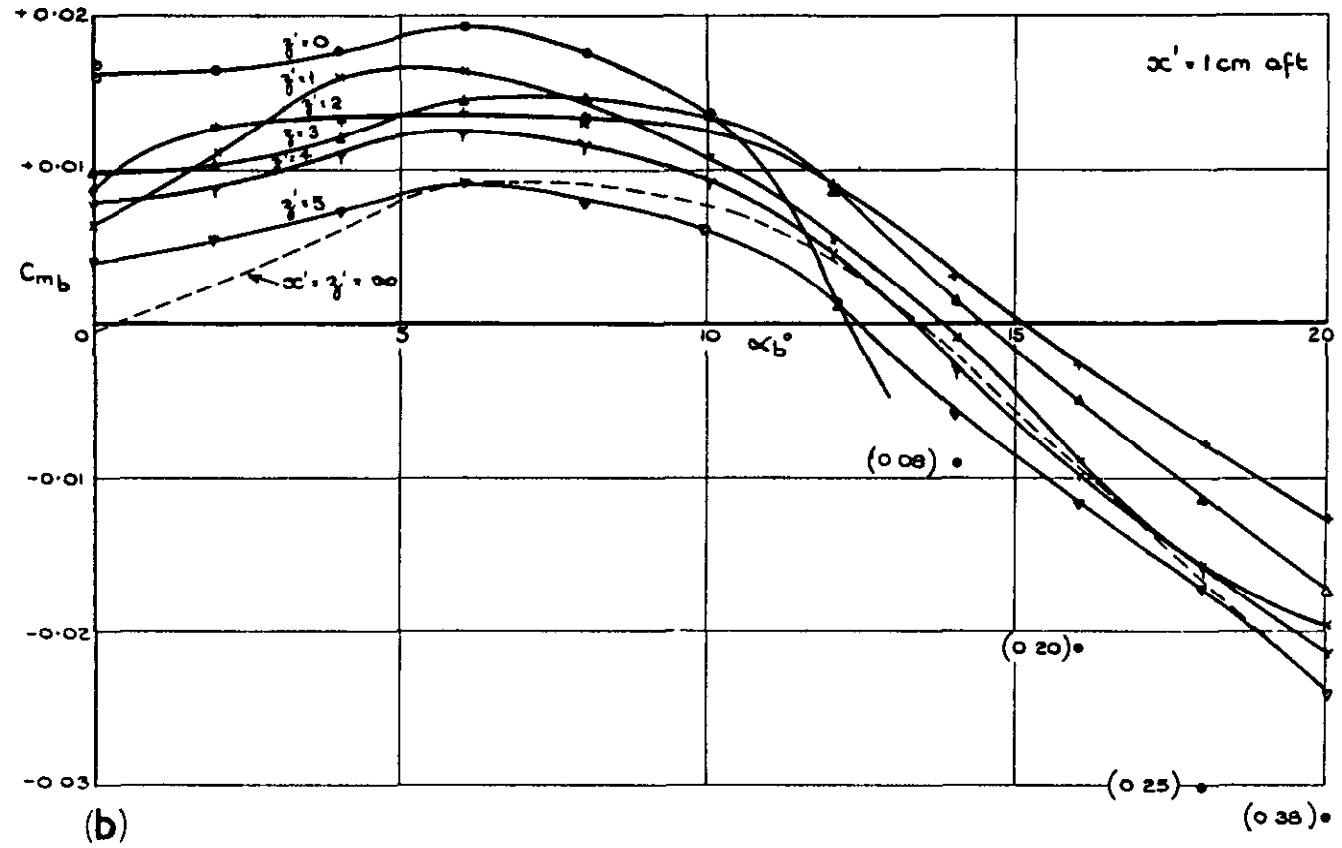

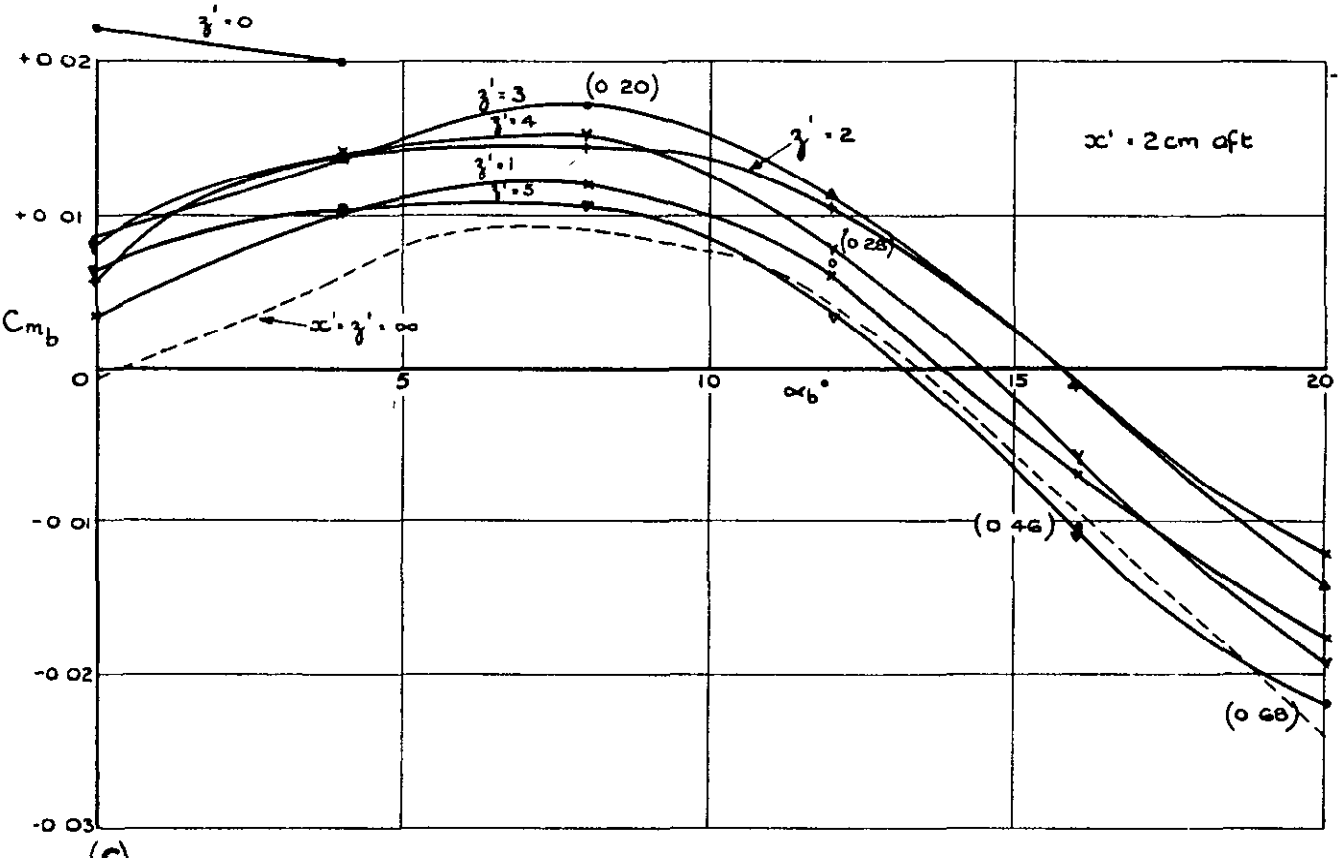

FIG.16. C_{m_b} vs α_b AT VARIOUS x' AND y' STATIONS FOR THE TWIN BOOST UNIT WITH THE 0·50"C REAR AEROFOIL, IN THE PRESENCE OF THE BOMB AT ZERO INCIDENCE, M=2·47.

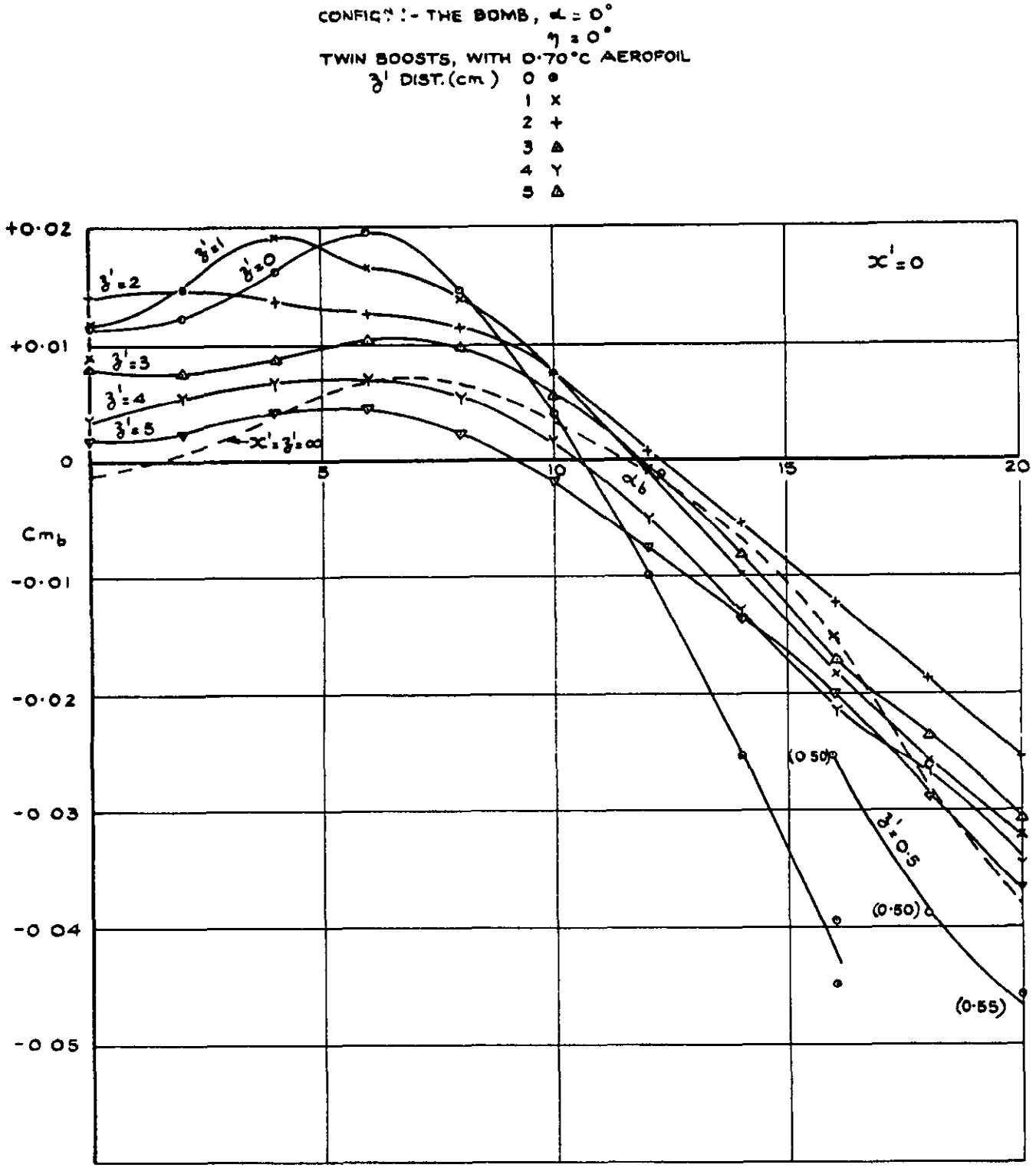

FIG. 17. Cm_b vs. α_b AT VARIOUS x' AND z' STATIONS FOR THE TWIN BOOST UNIT WITH THE 0·70"c REAR AEROFOIL, IN THE PRESENCE OF THE BOMB AT ZERO INCIDENCE, M= 2·47.

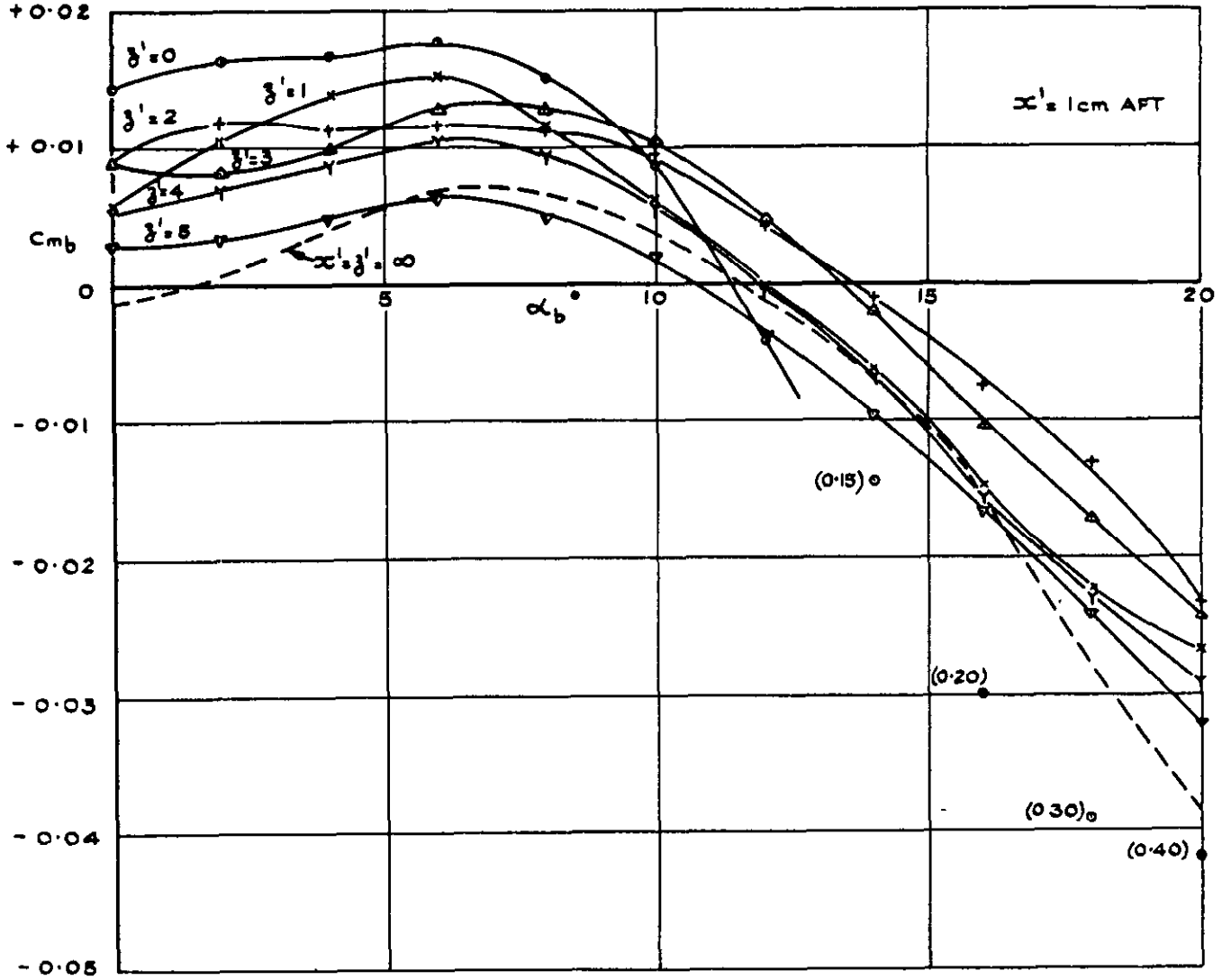

(b)

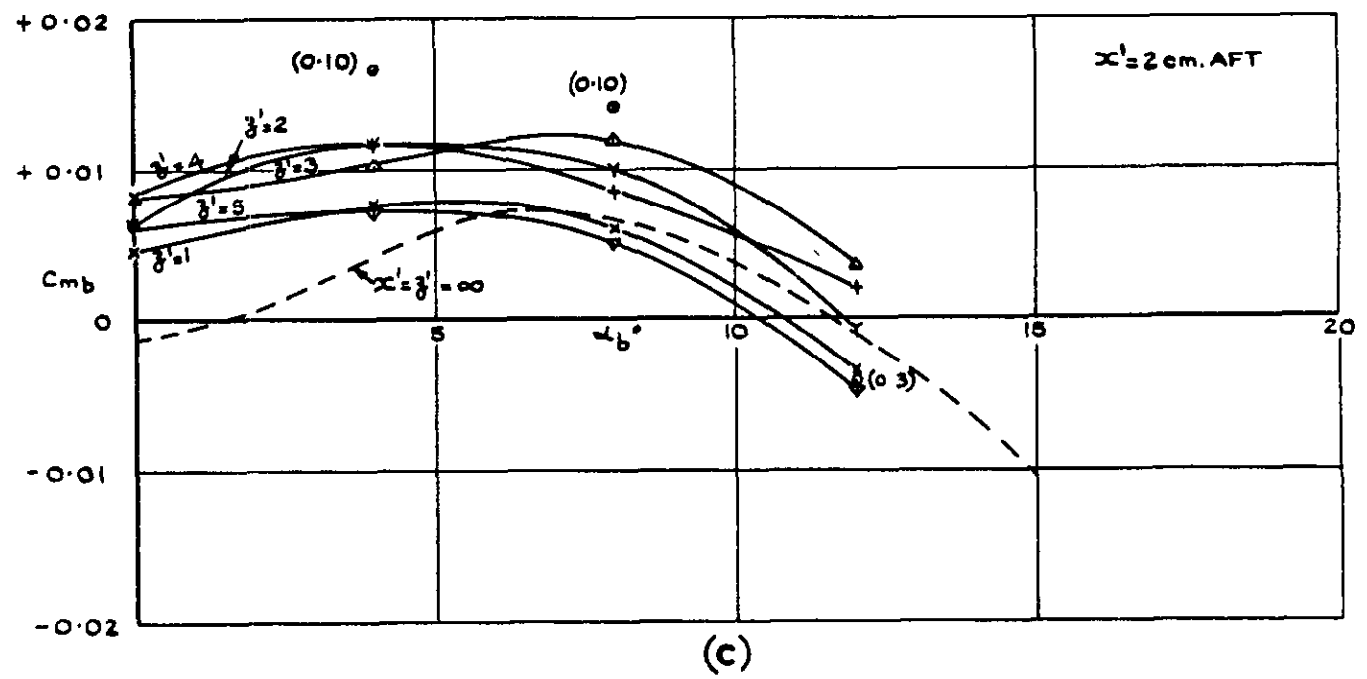

(c)

FIG.17. C_{mb} vs. α_b AT VARIOUS x' AND y' STATIONS FOR THE TWIN BOOST UNIT WITH THE 0·70"c REAR AEROFOIL, IN THE PRESENCE OF THE BOMB AT ZERO INCIDENCE, M = 2·47.

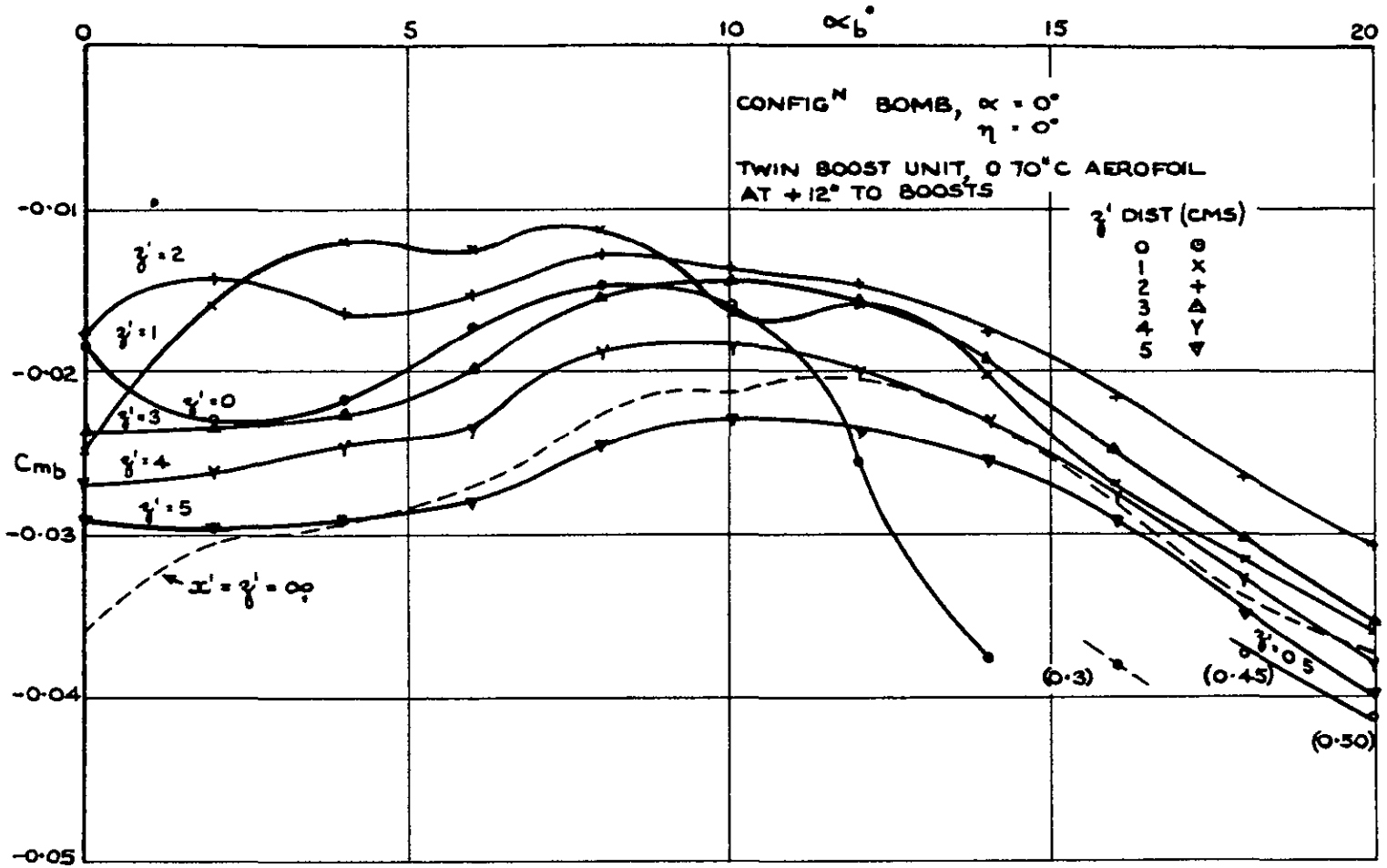

FIG. 18. C_{m_b} vs α_b AT $x' = 0$ AND VARIOUS ζ' STATIONS FOR THE TWIN BOOST UNIT WITH THE 0·70"C REAR AEROFOIL SET AT 12° TO THE BOOSTS, IN THE PRESENCE OF THE BOMB AT ZERO INCIDENCE, M = 2·47.

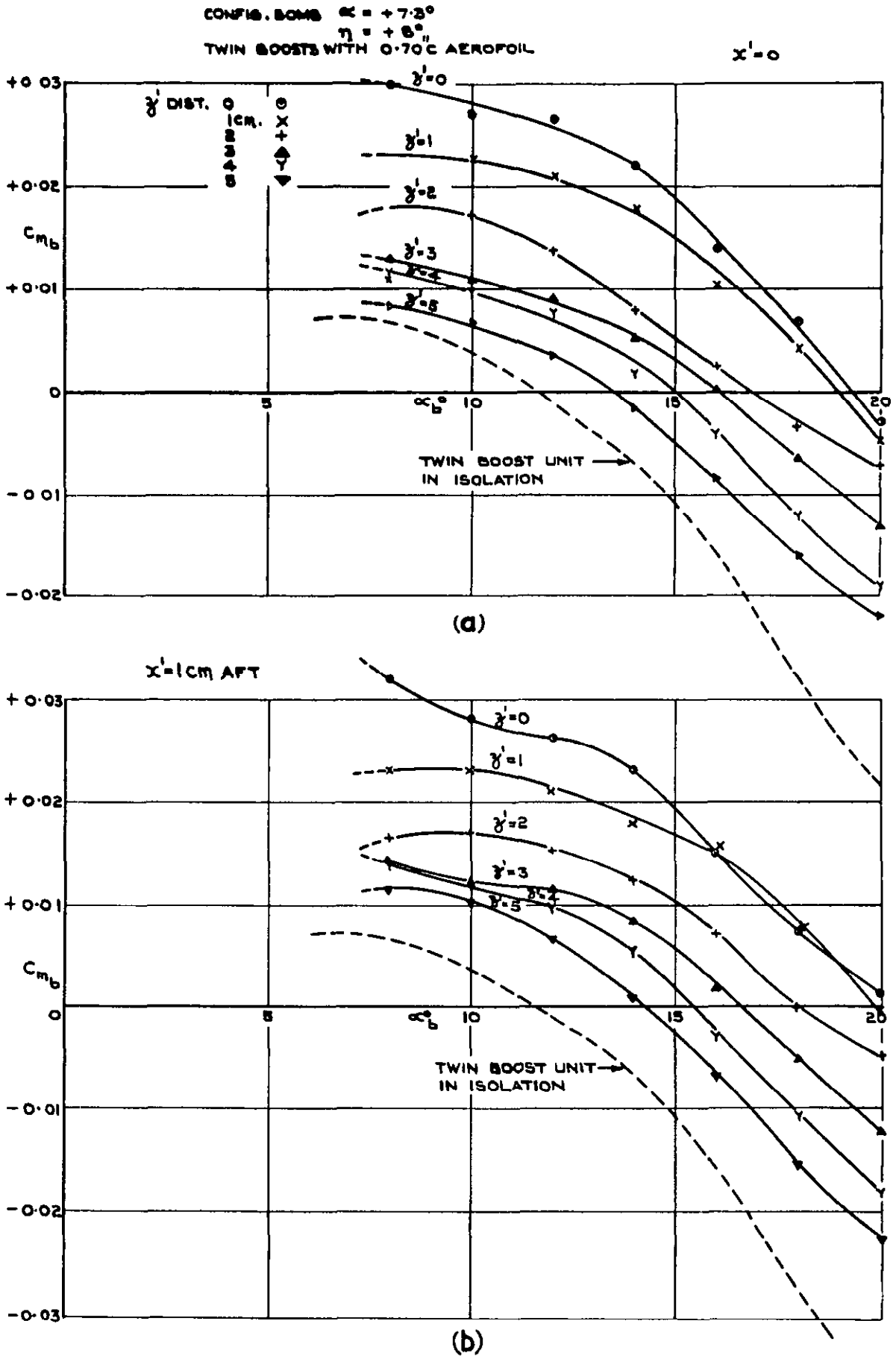

FIG.19. Cm_b vs α_b AT VARIOUS x' AND y' STATIONS FOR THE TWIN BOOST UNIT WITH THE 0·70c REAR AEROFOIL, IN THE PRESENCE OF THE BOMB AT CRUISING INCIDENCE, M = 2·47

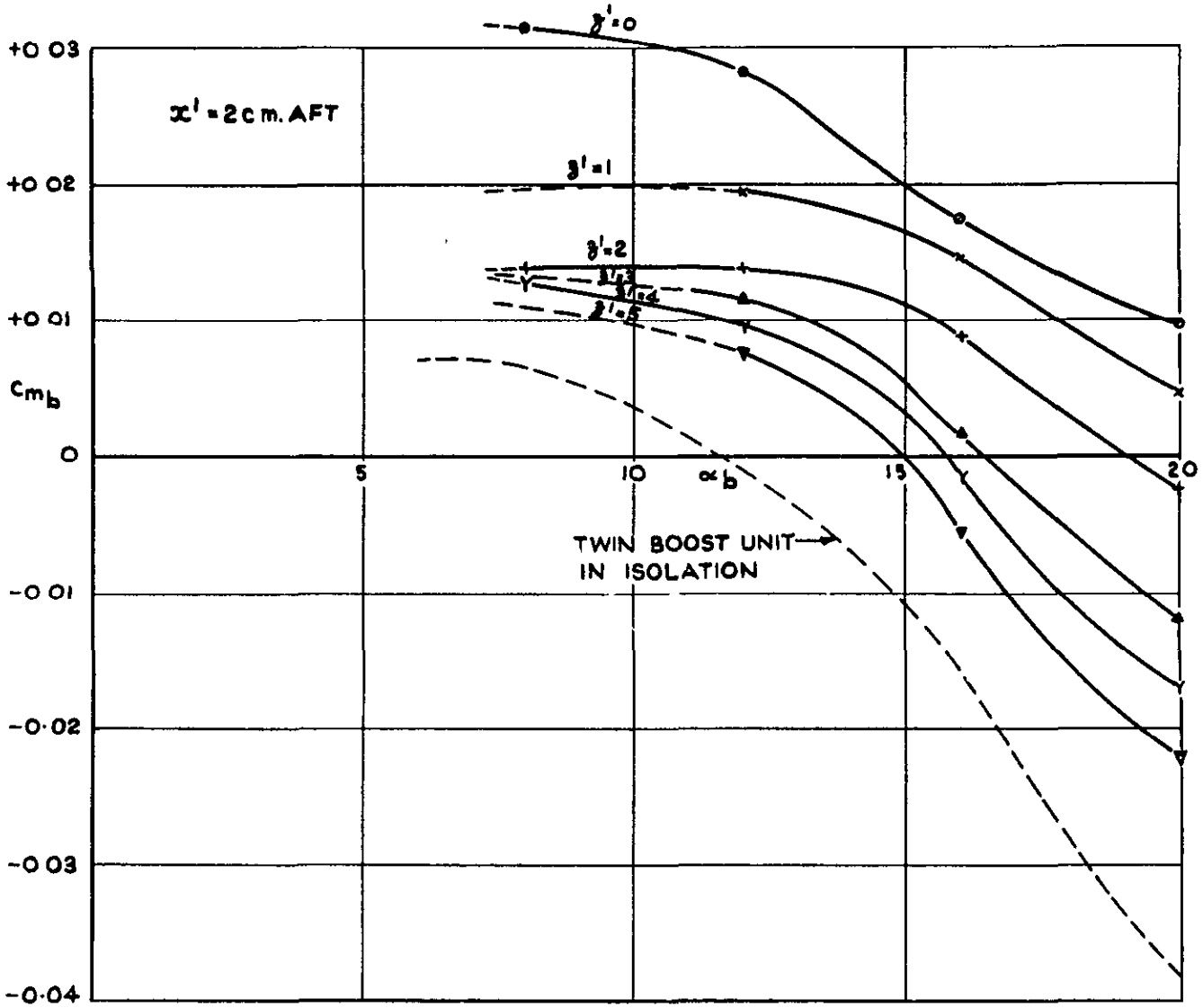

(c)

FIG. 19. C_{m_b} vs. α_b AT VARIOUS x^1 AND z^1 STATIONS FOR THE TWIN BOOST UNIT WITH THE 0·70c. REAR AEROFOIL, IN THE PRESENCE OF THE BOMB, AT CRUISING INCIDENCE, M = 2·47.

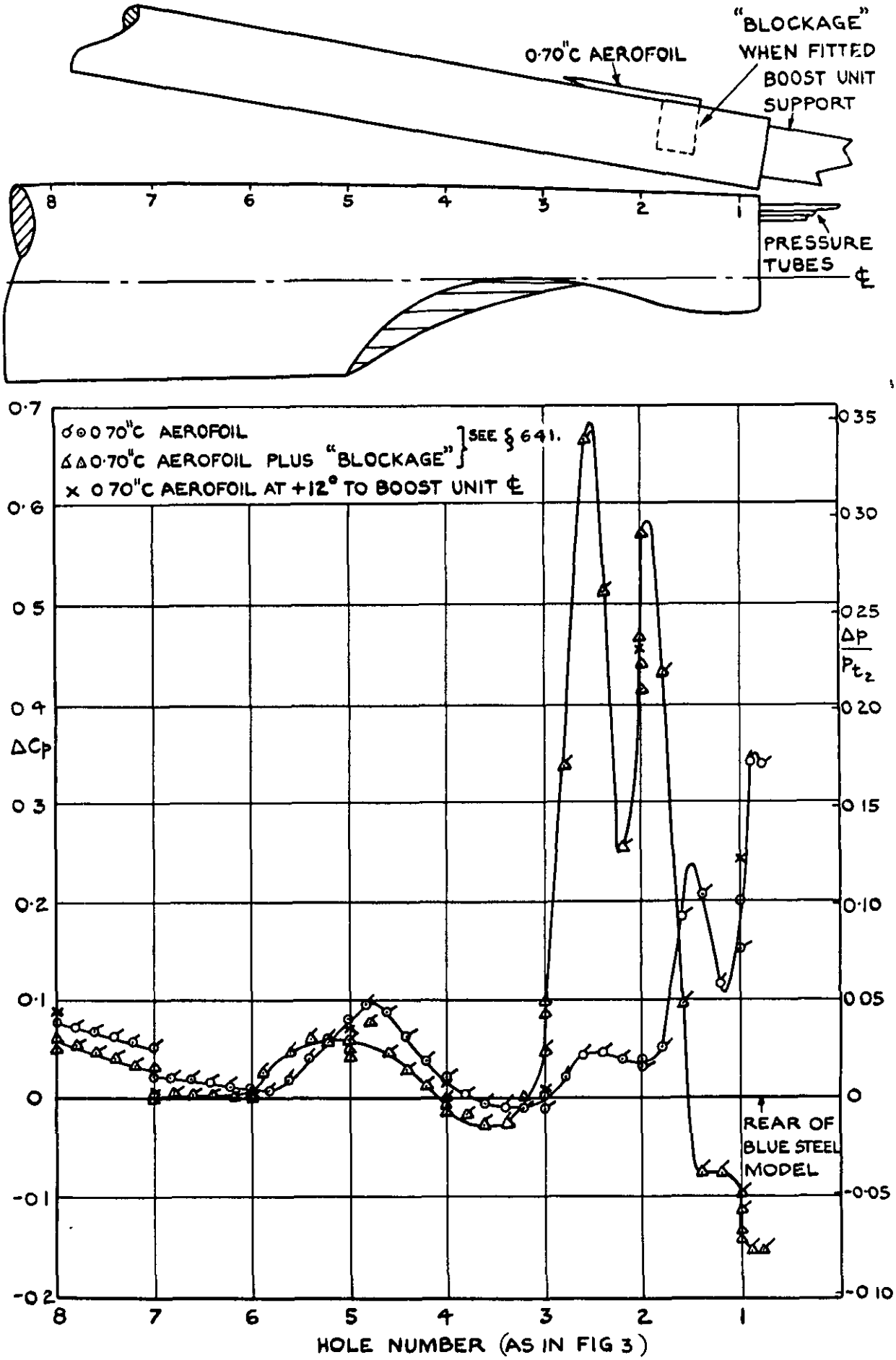

FIG. 20. INCREMENTAL STATIC PRESSURE COEFFICIENT ON THE BOMB DUE TO PRESENCE OF TWIN BOOST UNIT AT 10° INCIDENCE.

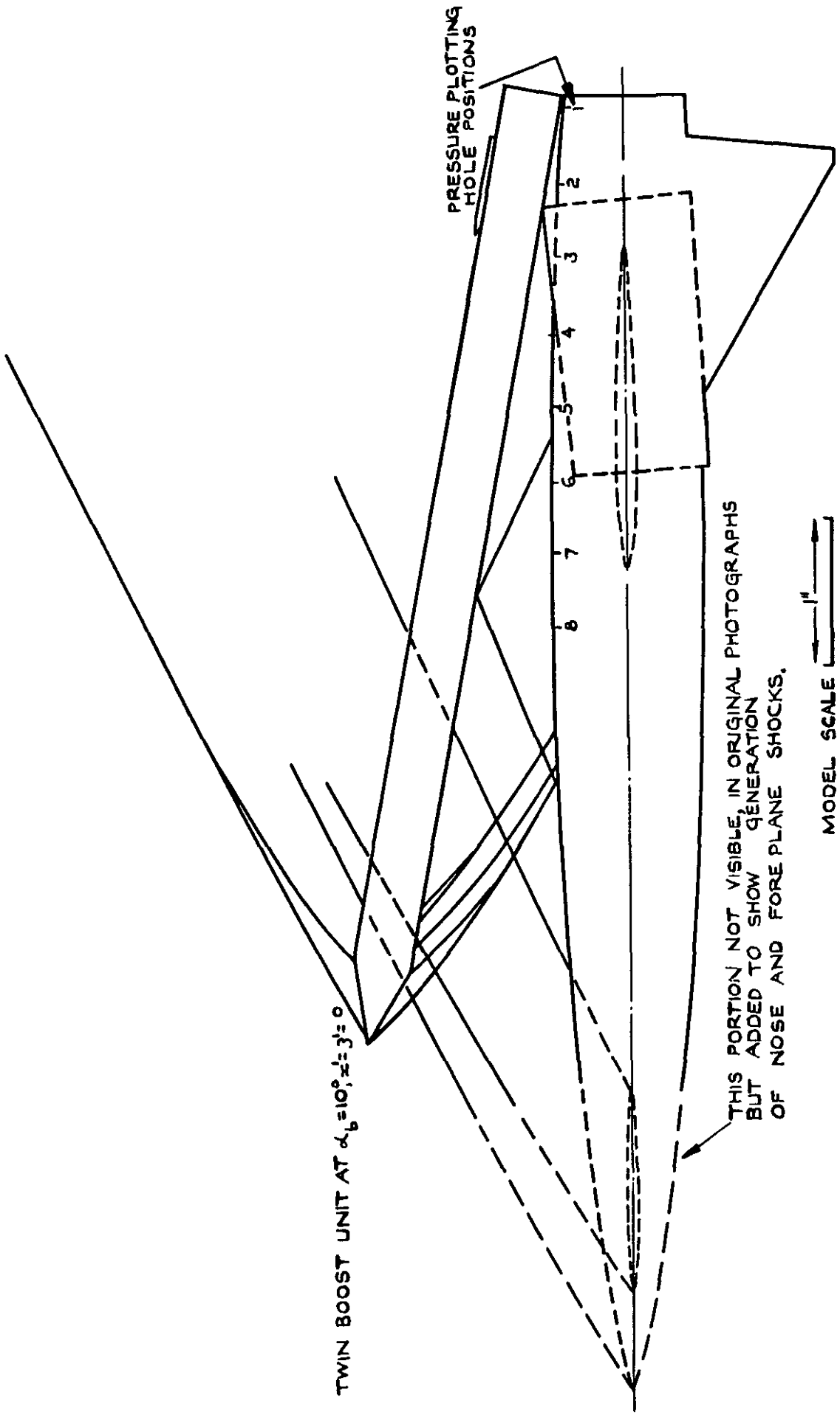

FIG.21. INTERFERENCE & ASSOCIATED SHOCK SYSTEM (REPRODUCED FROM A SCHLIEREN PHOTOGRAPH) TWIN BOOST UNIT AT 10°

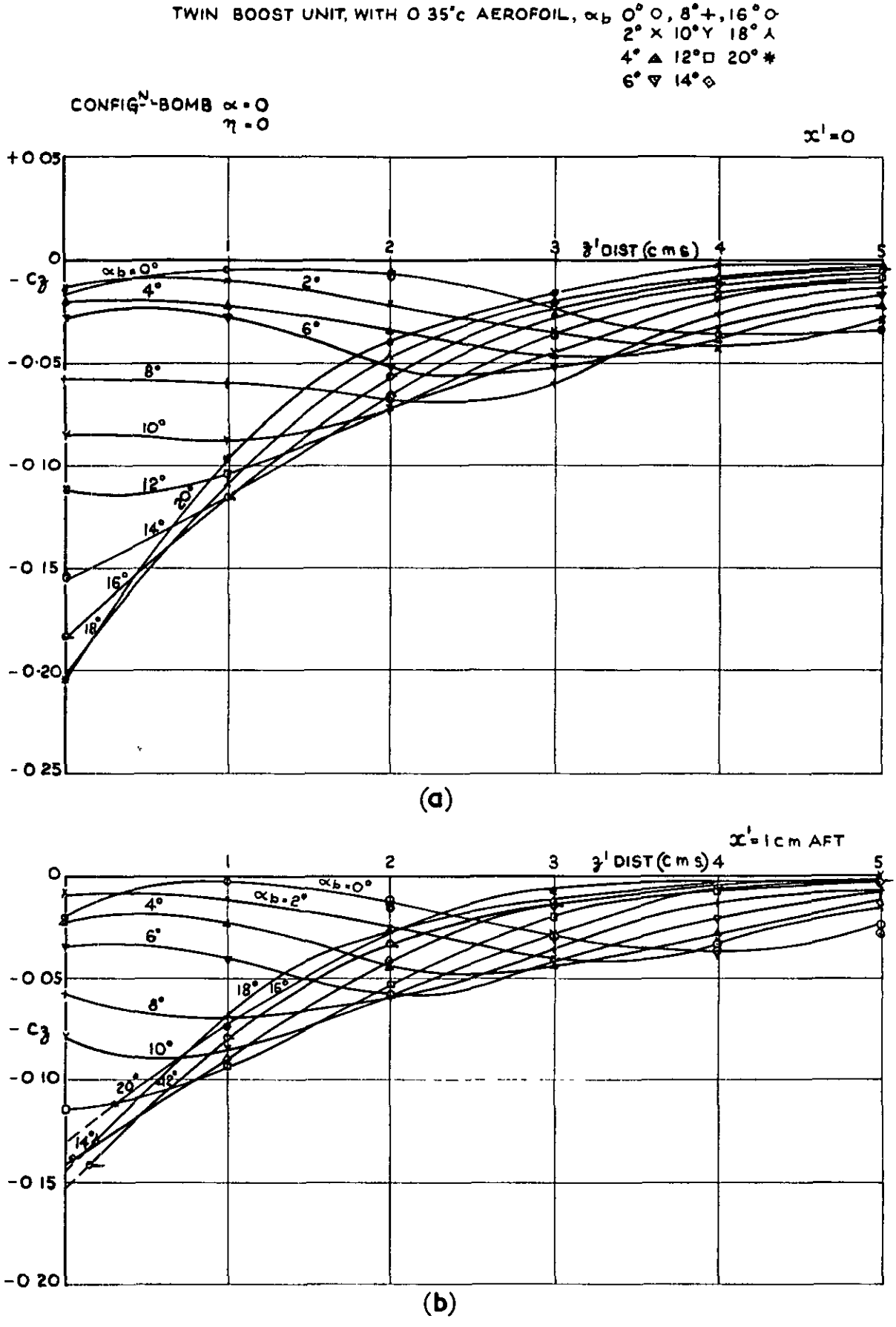

FIG. 22.-C_{ζ} vs. ζ' DISTANCE AND α_b, AT VARIOUS x' STATIONS, FOR THE BOMB AT ZERO INCIDENCE, IN THE PRESENCE OF THE TWIN BOOST UNIT WITH THE 0·35"c. REAR AEROFOIL, (M = 2·47.)

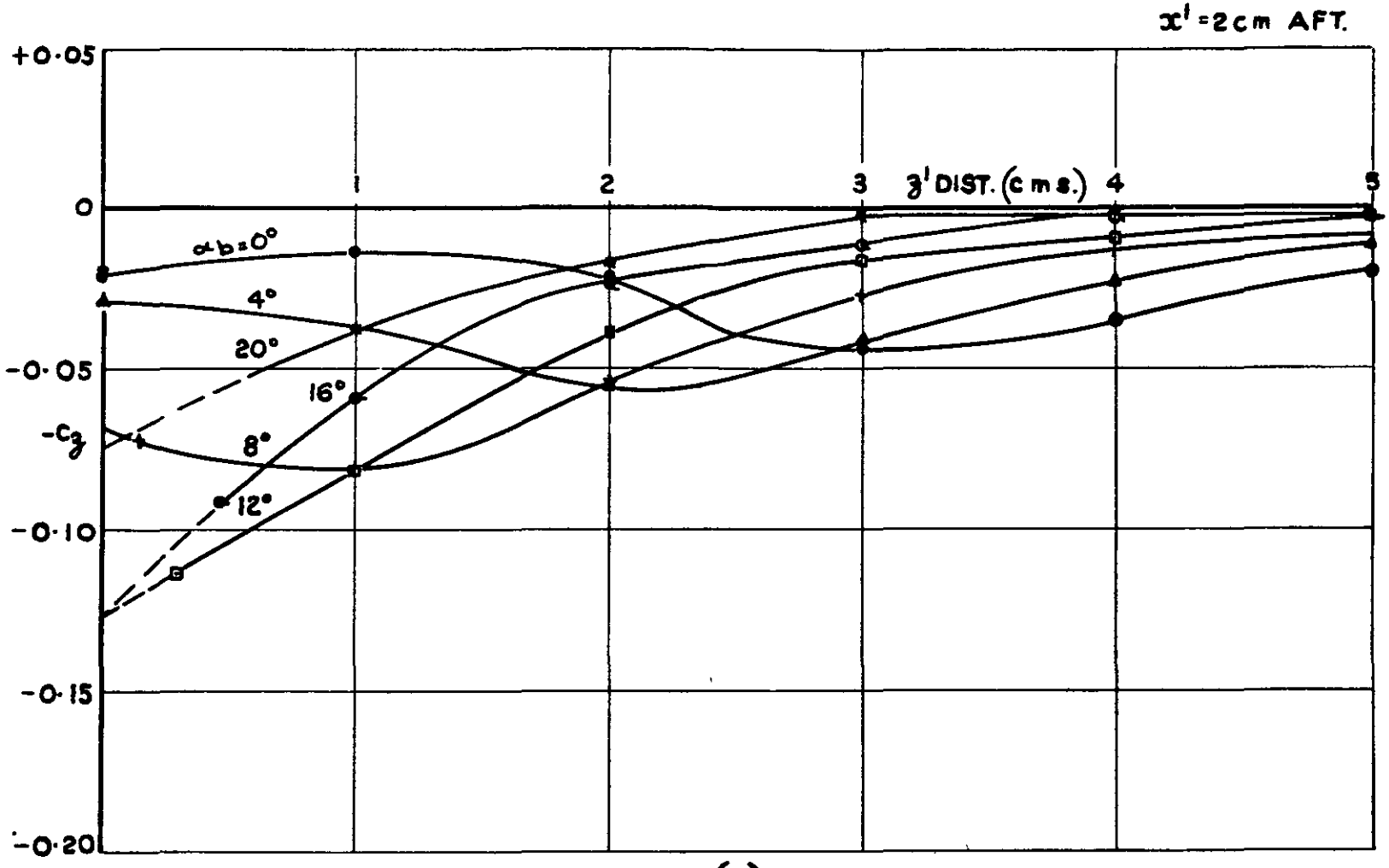

(c)

FIG. 22.-C_z vs. z' DISTANCE AND α_b, AT VARIOUS x' STATIONS, FOR THE BOMB AT ZERO INCIDENCE, IN THE PRESENCE OF THE TWIN BOOST UNIT WITH THE 0·35"c. REAR AEROFOIL, (M = 2·47.)

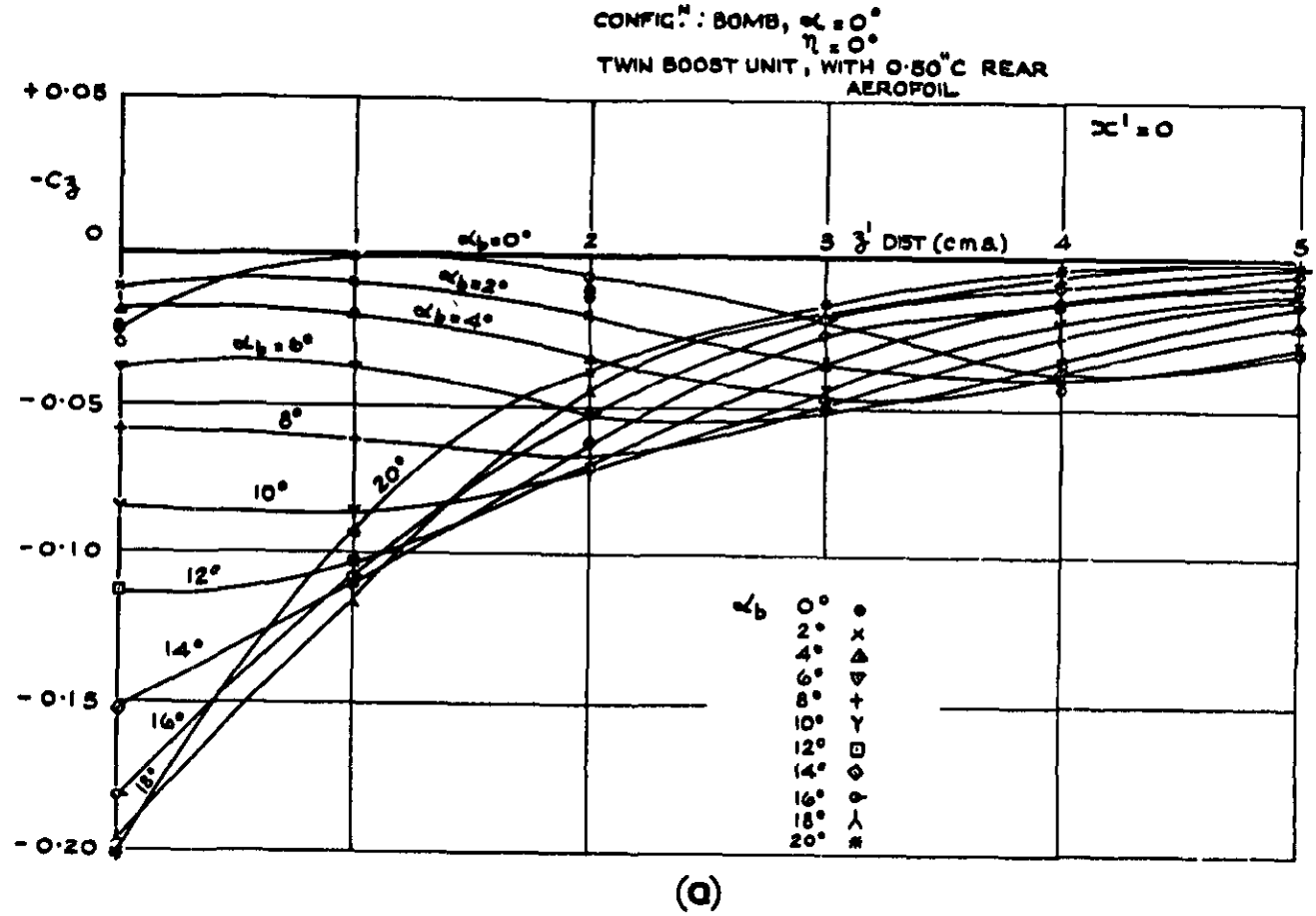

(a)

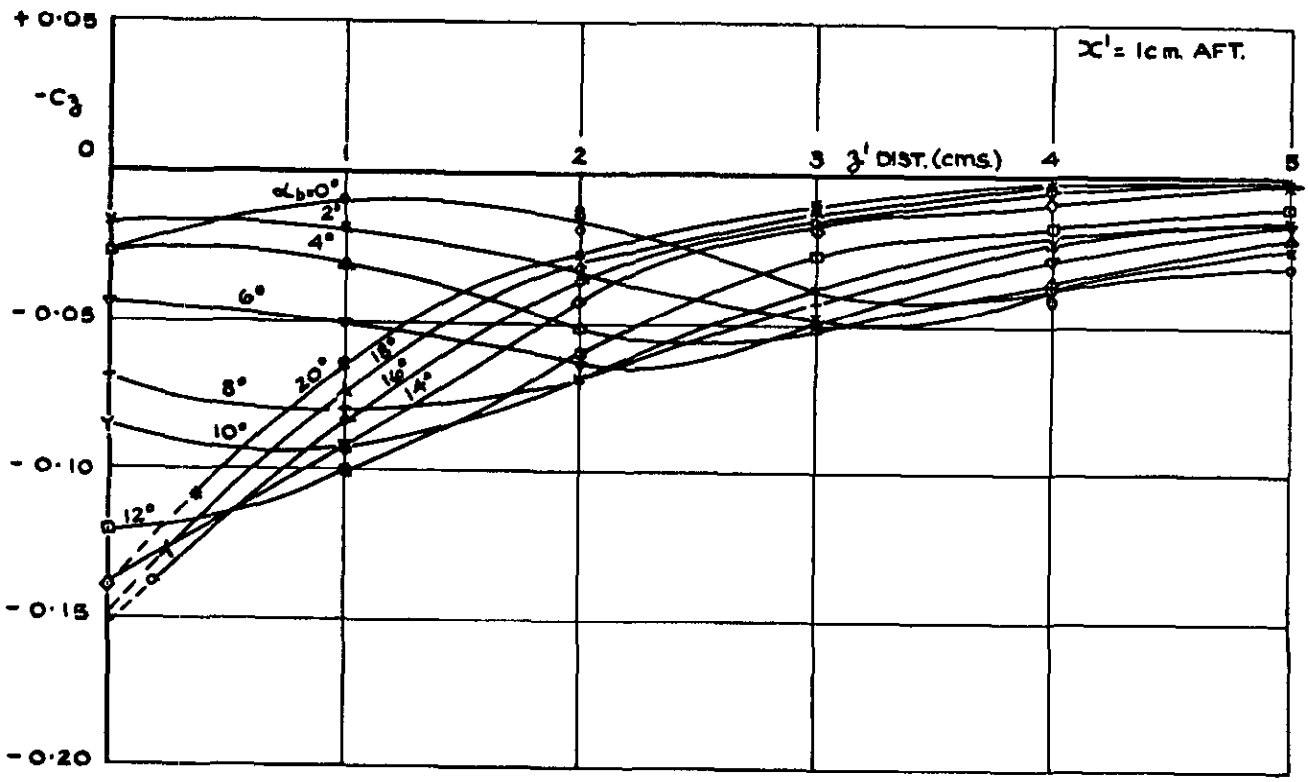

(b)

FIG.23. $-C_z$ vs. z' DISTANCE AND α_b, AT VARIOUS x' STATIONS, FOR THE BOMB AT ZERO INCIDENCE, IN THE PRESENCE OF THE TWIN BOOST UNIT WITH THE 0·50"c. REAR AEROFOIL, M = 2·47

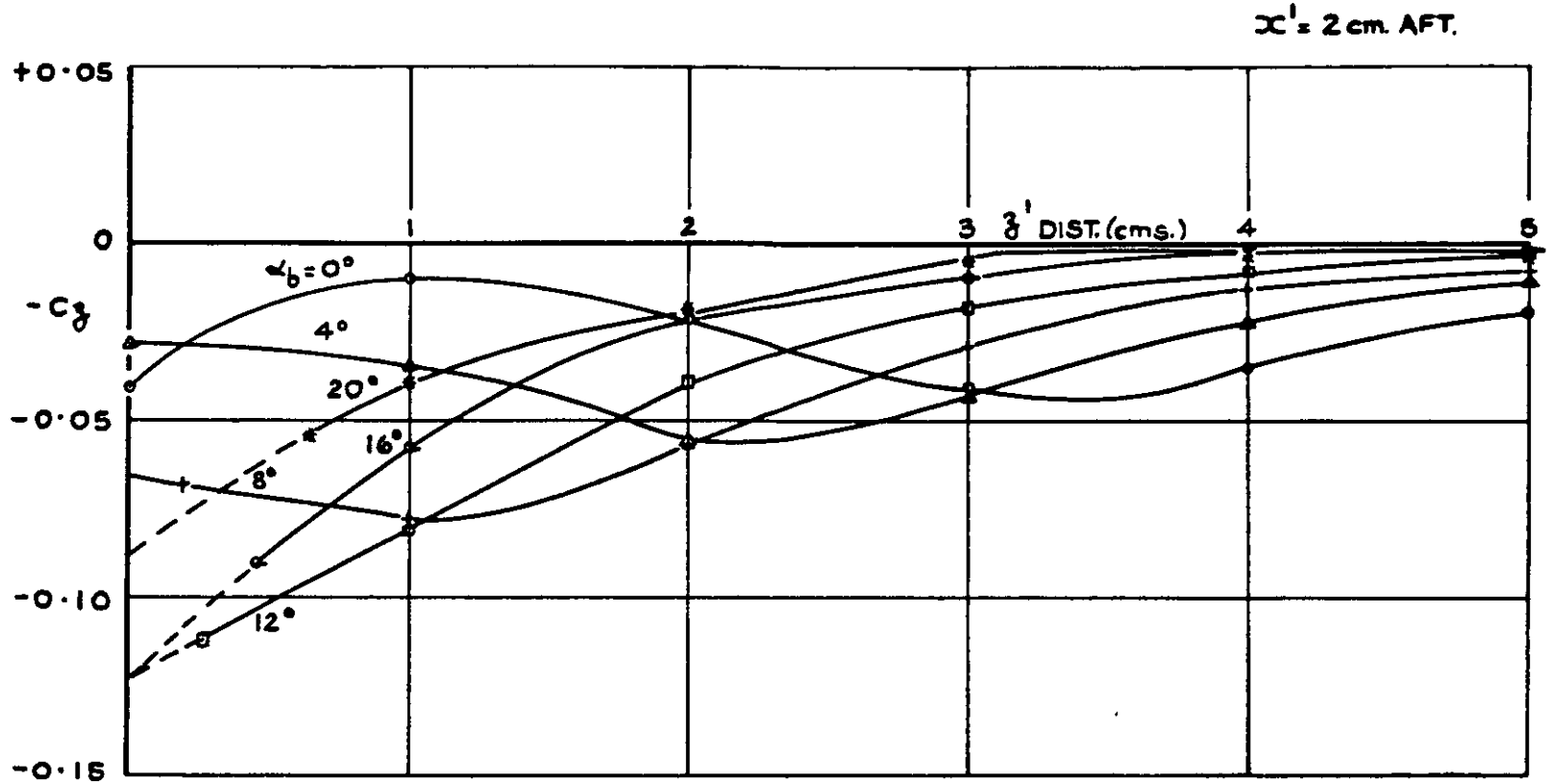

FIG. 23. $-C_z$ vs. z' DISTANCE AND α_b, AT VARIOUS x' STATIONS, FOR THE BOMB AT ZERO INCIDENCE, IN THE PRESENCE OF THE TWIN BOOST UNIT WITH THE 0·50"c. REAR AEROFOIL, M = 2·47

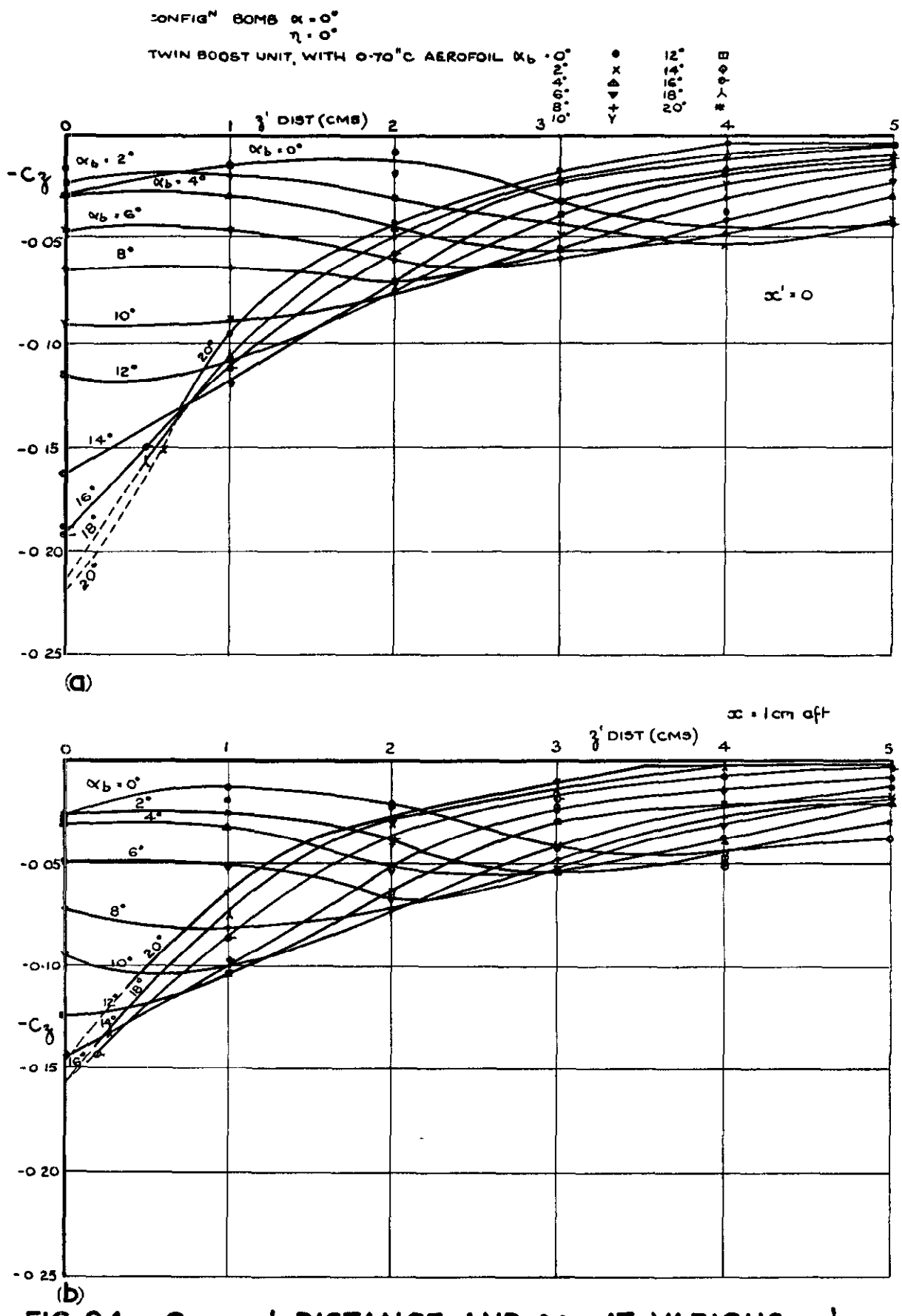

FIG. 24. $-C_y$ vs y' DISTANCE AND α_b, AT VARIOUS x' STATIONS, FOR THE BOMB AT ZERO INCIDENCE, IN THE PRESENCE OF THE TWIN BOOST UNIT WITH THE 0·70°C REAR AEROFOIL, M = 2·47.

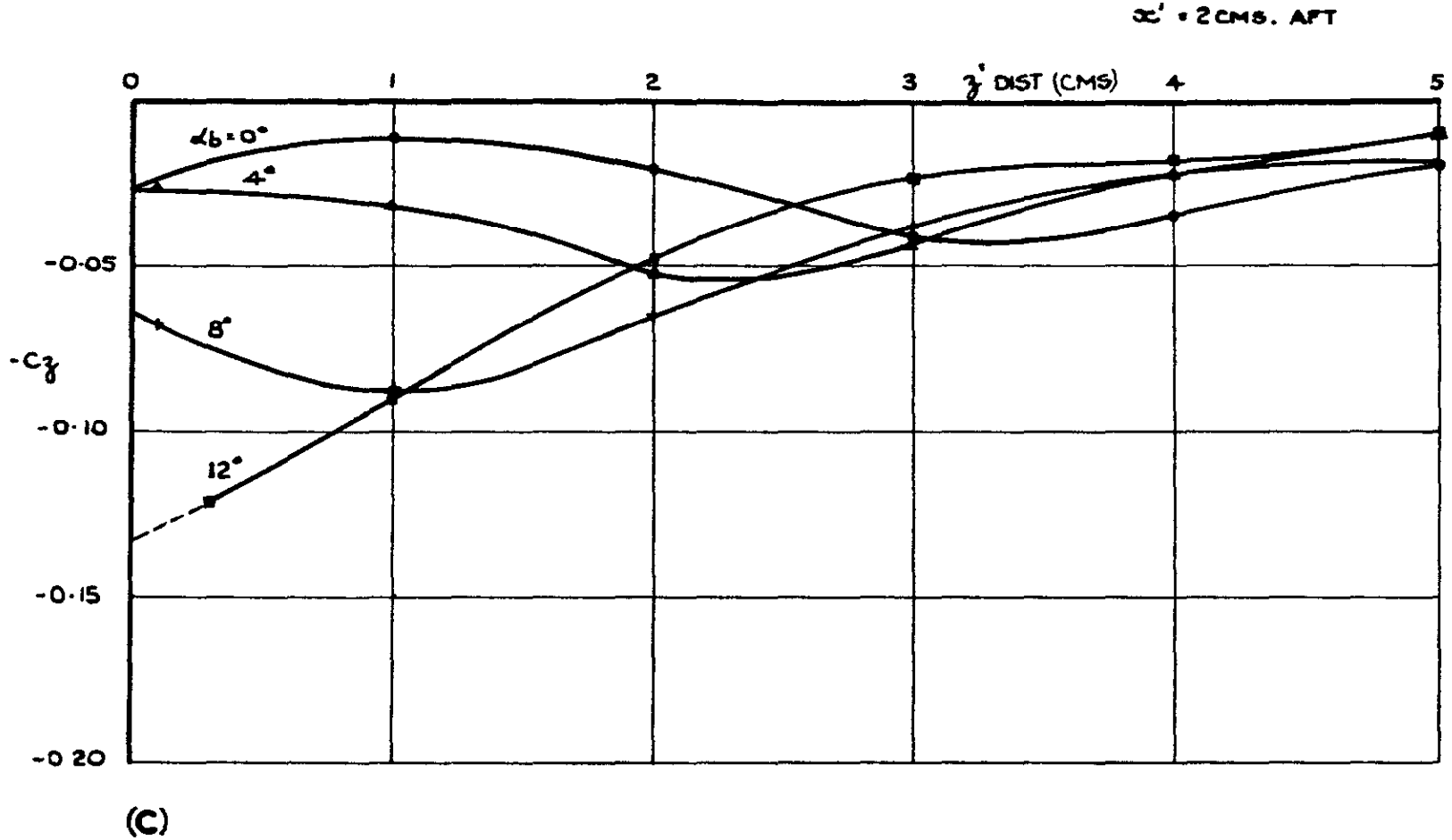

FIG. 24. $-C_z$ vs z' DISTANCE AND α_b, AT VARIOUS x' STATIONS, FOR THE BOMB AT ZERO INCIDENCE, IN THE PRESENCE OF THE TWIN BOOST UNIT WITH THE 0·70"C REAR AEROFOIL, M = 2·47.

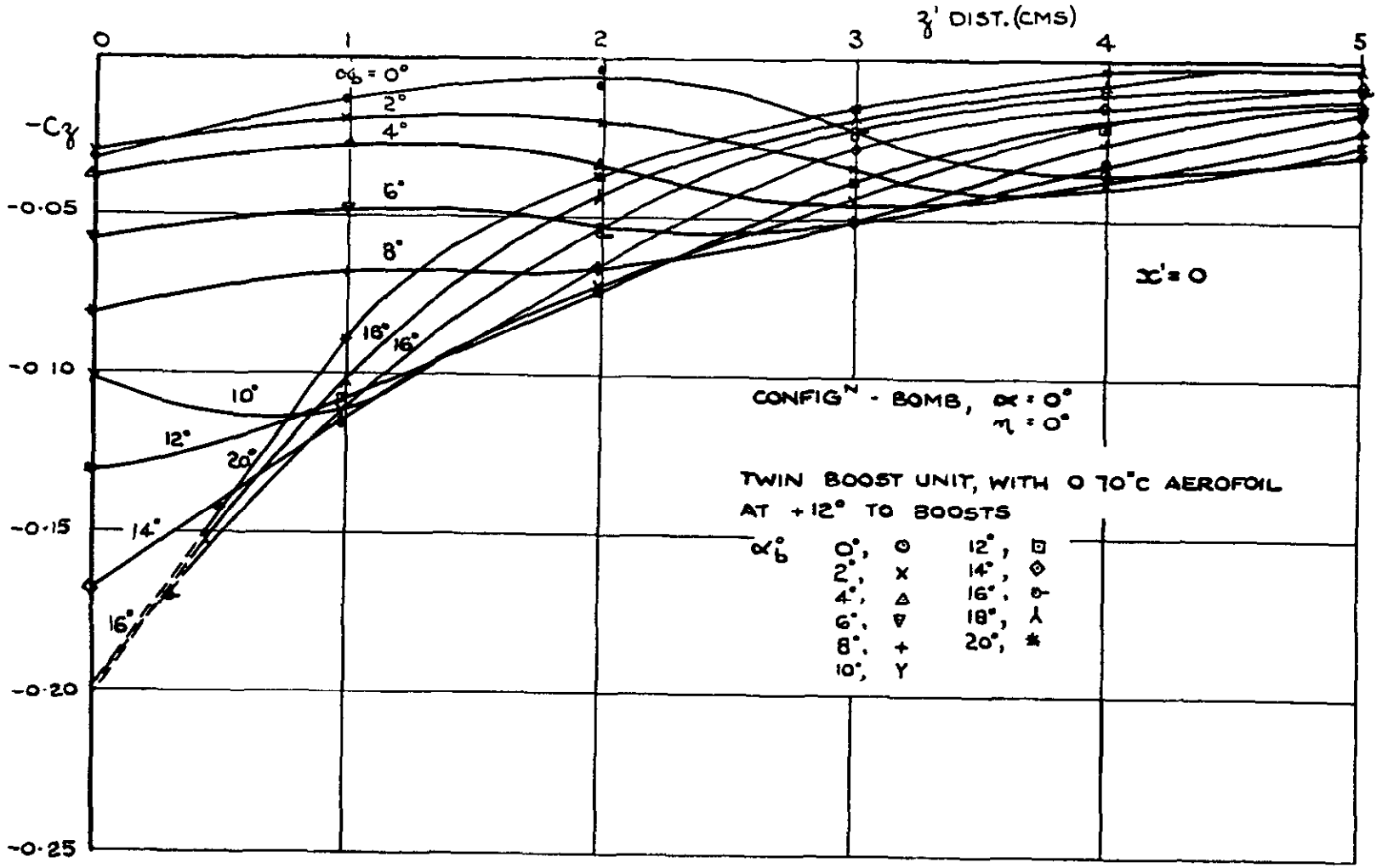

FIG. 25.-C_ζ vs ζ' DISTANCE AND α_b AT $x' = 0$ FOR THE BOMB AT ZERO INCIDENCE, IN THE PRESENCE OF THE TWIN BOOST UNIT WITH THE 0·70°C. REAR AEROFOIL SET AT 12° TO THE BOOSTS, M = 2·47.

CONFIG^{N} BOMB, α = +7·3°
η = +8°

TWIN BOOSTS, WITH 0·70"C. AEROFOIL, α_b = 8° + 16° ●
10° Y 18° ⅄
12° ⊡ 20° ✱
14° ⊕

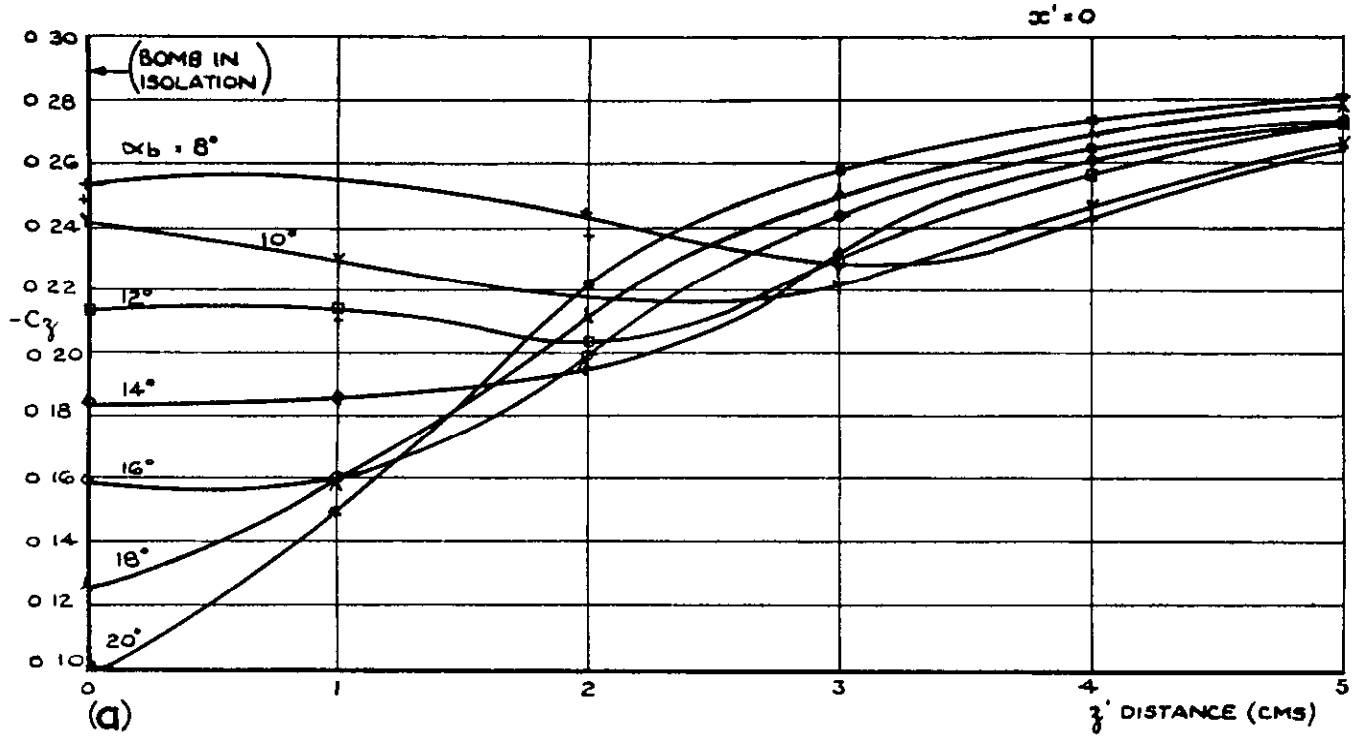

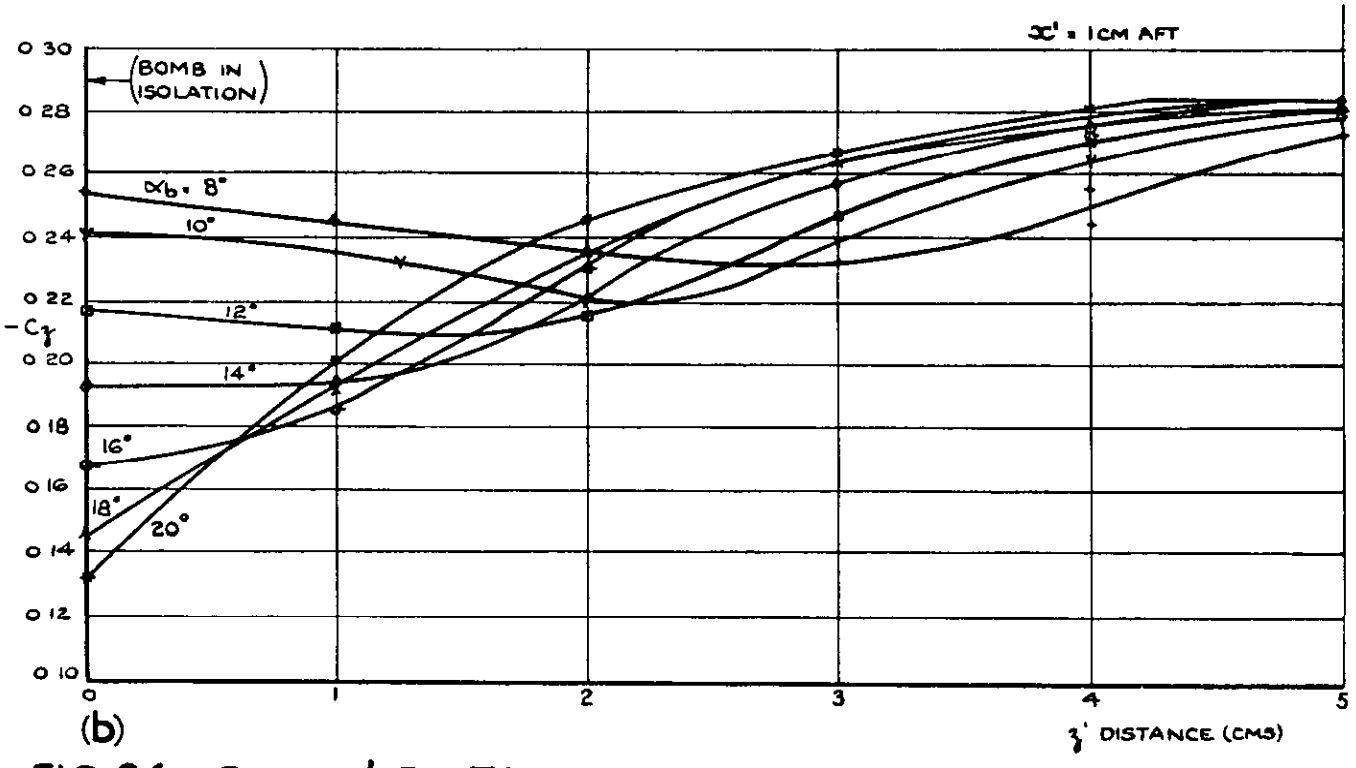

FIG. 26. $-C_z$ vs z' DISTANCE AND α_b, AT VARIOUS x' STATIONS, FOR THE BOMB AT CRUISING INCIDENCE, IN THE PRESENCE OF THE TWIN BOOST UNIT WITH THE 0·70"C REAR AEROFOIL, M = 2·47.

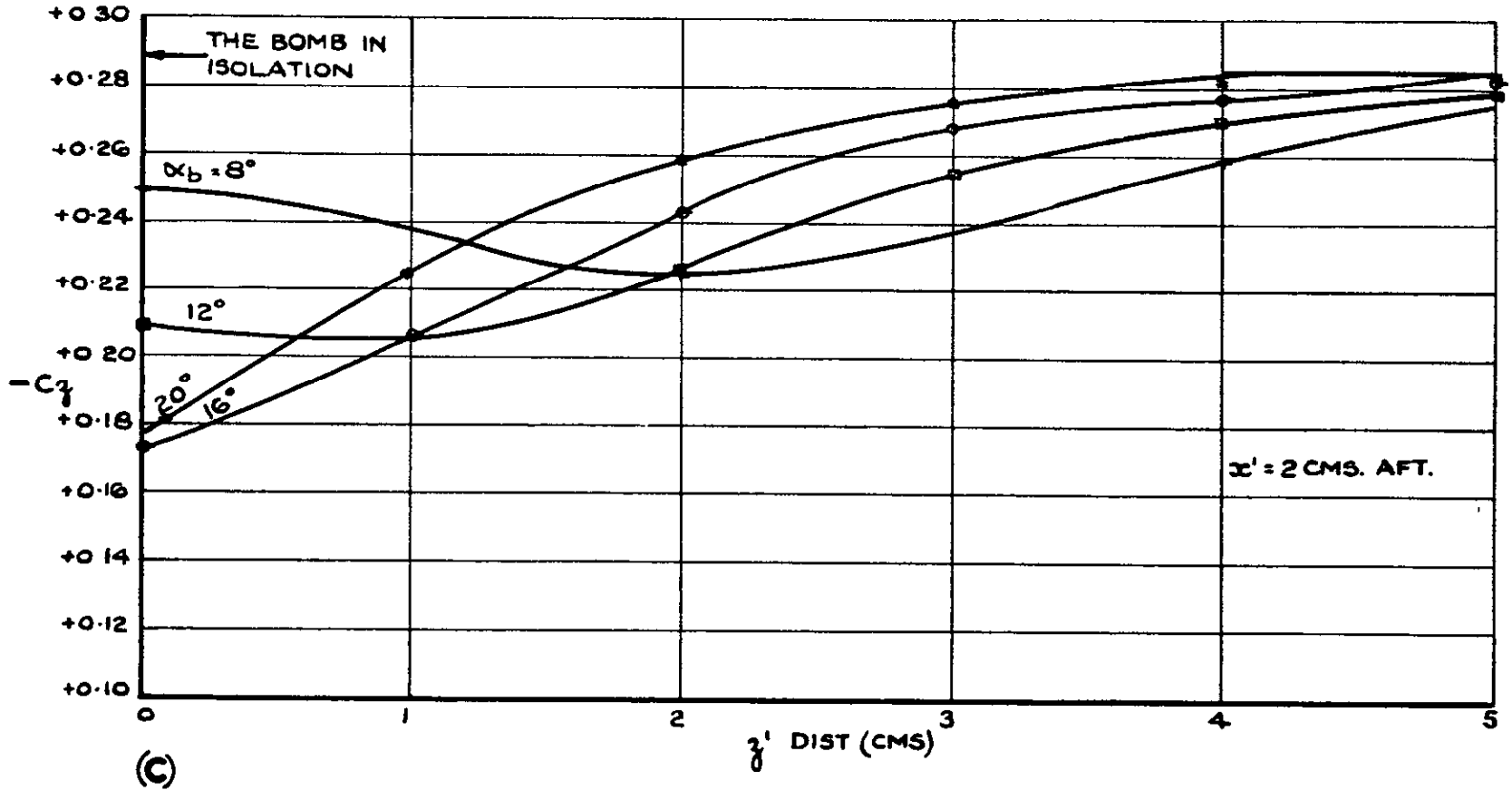

FIG. 26. $-C_z$ vs z' DISTANCE AND α_b, AT VARIOUS x' STATIONS, FOR THE BOMB AT CRUISING INCIDENCE, IN THE PRESENCE OF THE TWIN BOOST UNIT WITH THE 0·70"C REAR AEROFOIL, M=2·47.

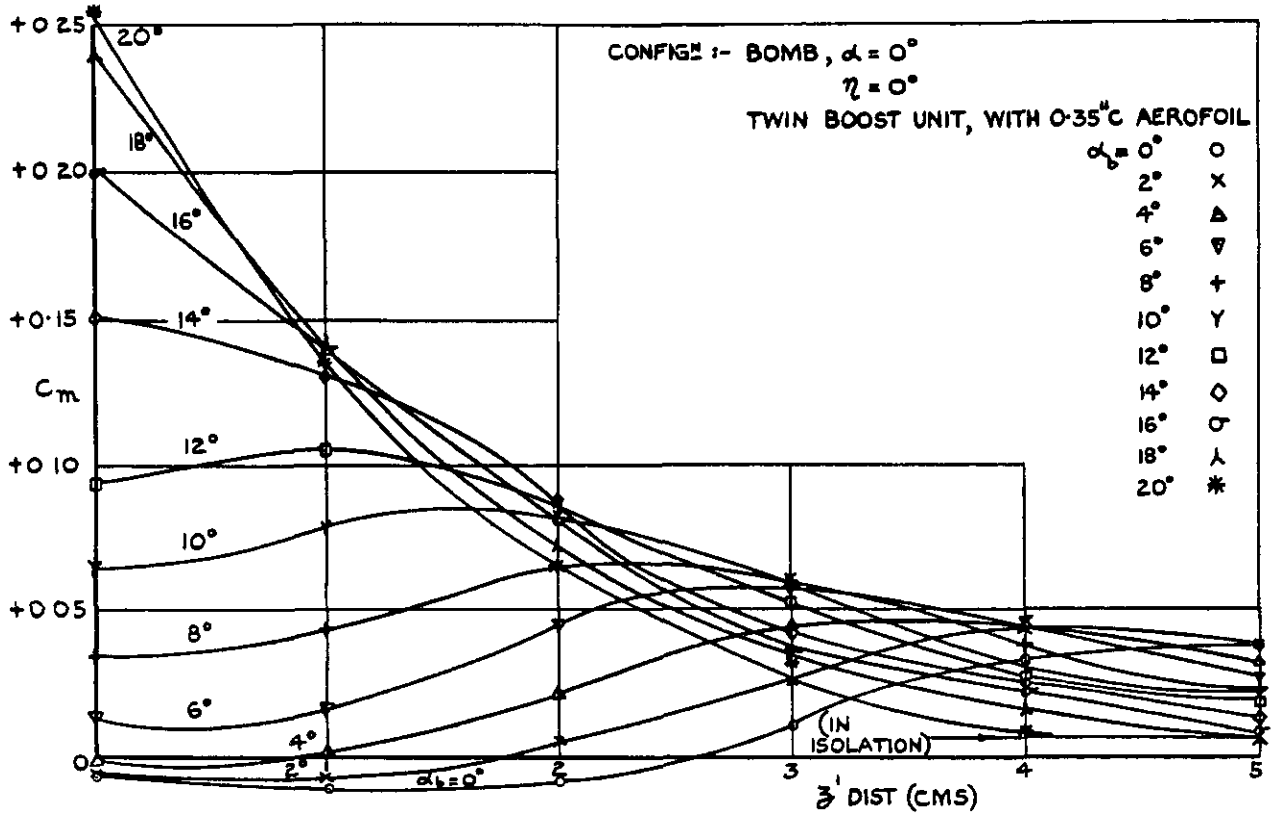

(a) x' = 0

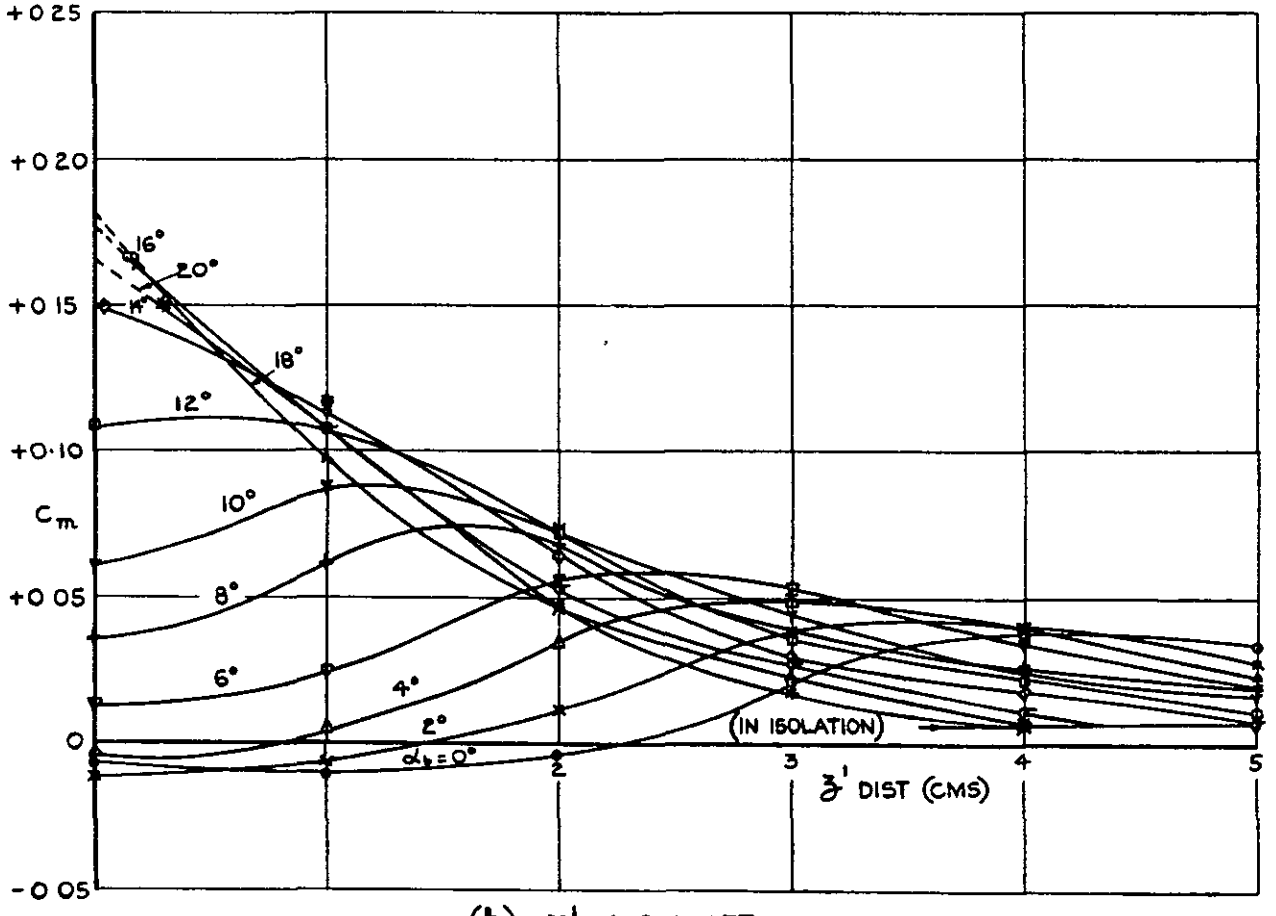

(b) x' = 1 CM. AFT.

FIG.27. C_m vs ȝ' DISTANCE AND α_b, AT VARIOUS x' STATIONS, FOR THE BOMB AT ZERO INCIDENCE, IN THE PRESENCE OF THE TWIN BOOST UNIT WITH THE 0·35"C. REAR AEROFOIL, M = 2·47.

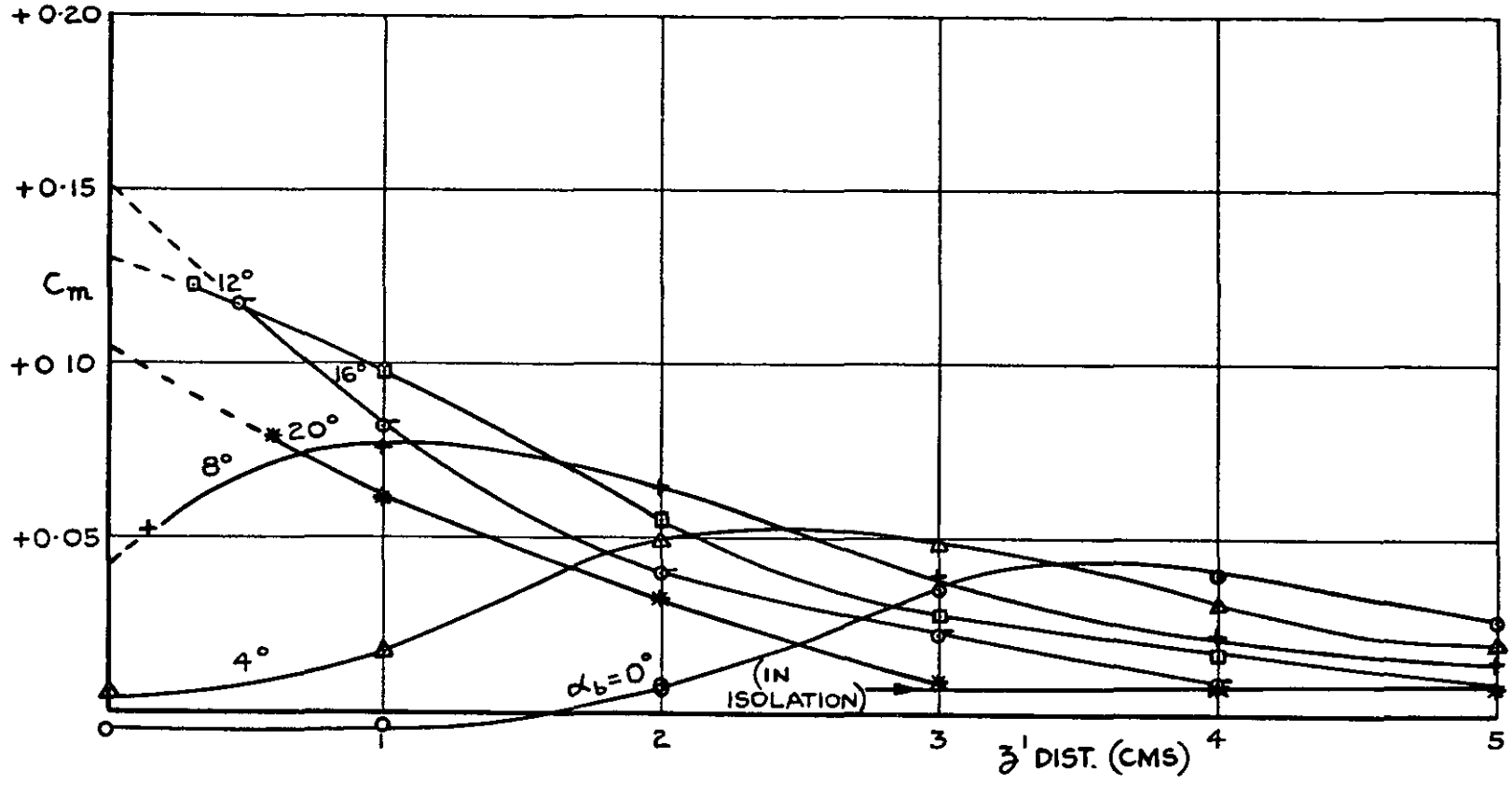

(c) x' = 2 CMS. AFT.

FIG.27. C_m vs $\mathfrak{z}'$ DISTANCE AND α_b, AT VARIOUS x' STATIONS, FOR THE BOMB AT ZERO INCIDENCE, IN THE PRESENCE OF THE TWIN BOOST UNIT WITH THE 0·35"C. REAR AEROFOIL, M= 2·47.

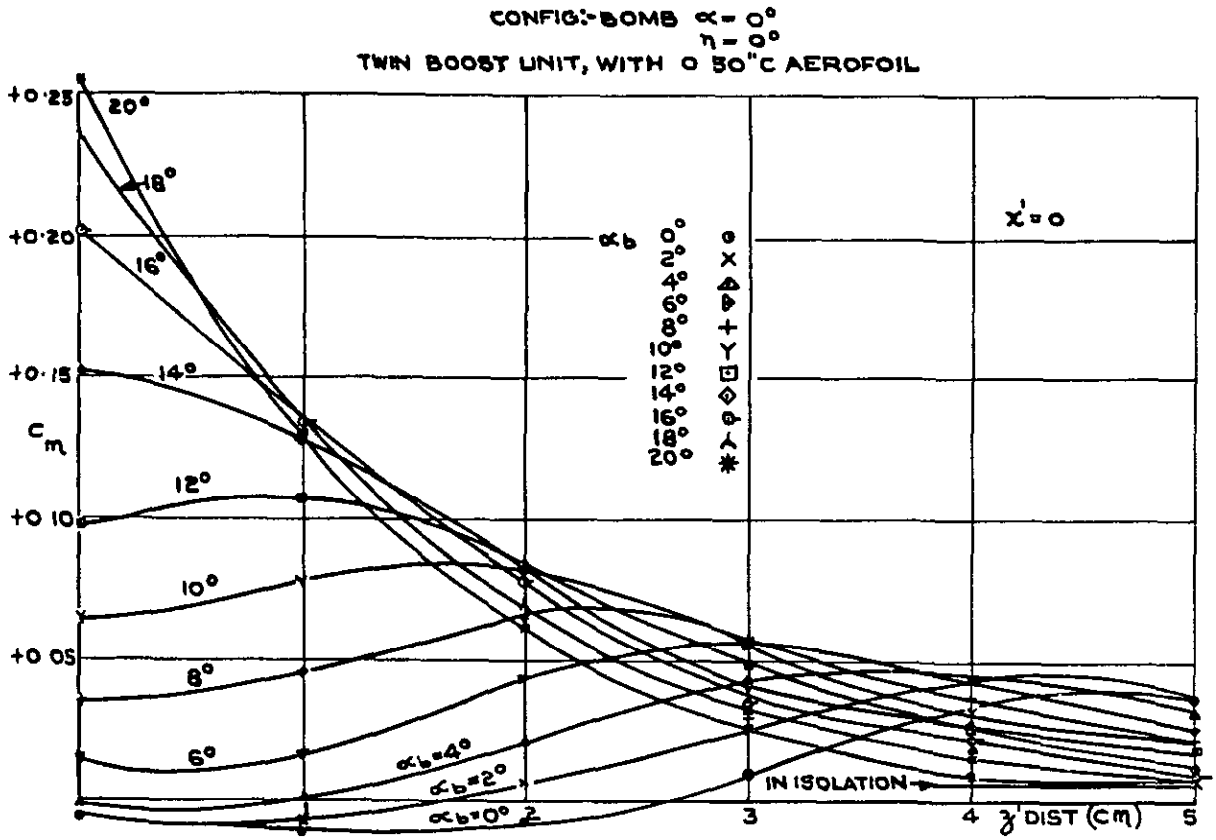

(a)

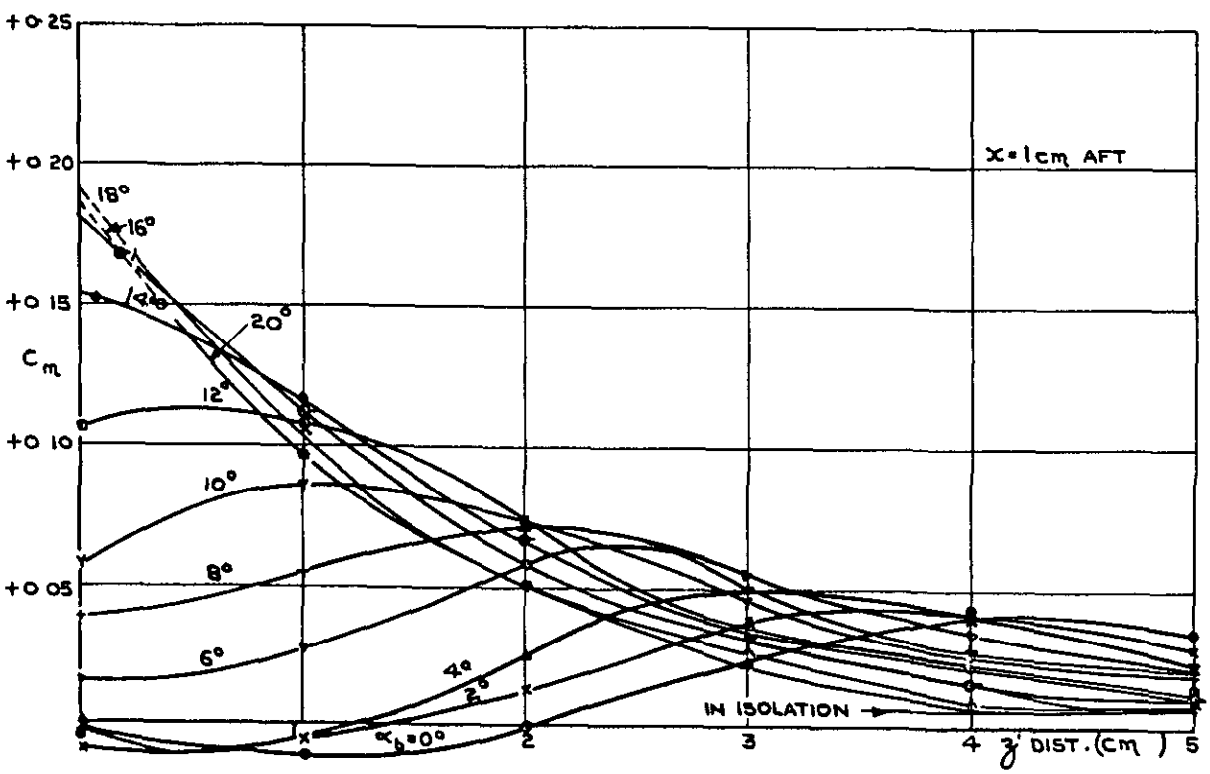

(b)

FIG.28. C_m vs y' DISTANCE AND α_b, AT VARIOUS x' STATIONS, FOR THE BOMB AT ZERO INCIDENCE, IN THE PRESENCE OF THE TWIN BOOST UNIT WITH THE 0·50"c REAR AEROFOIL, M-2·47

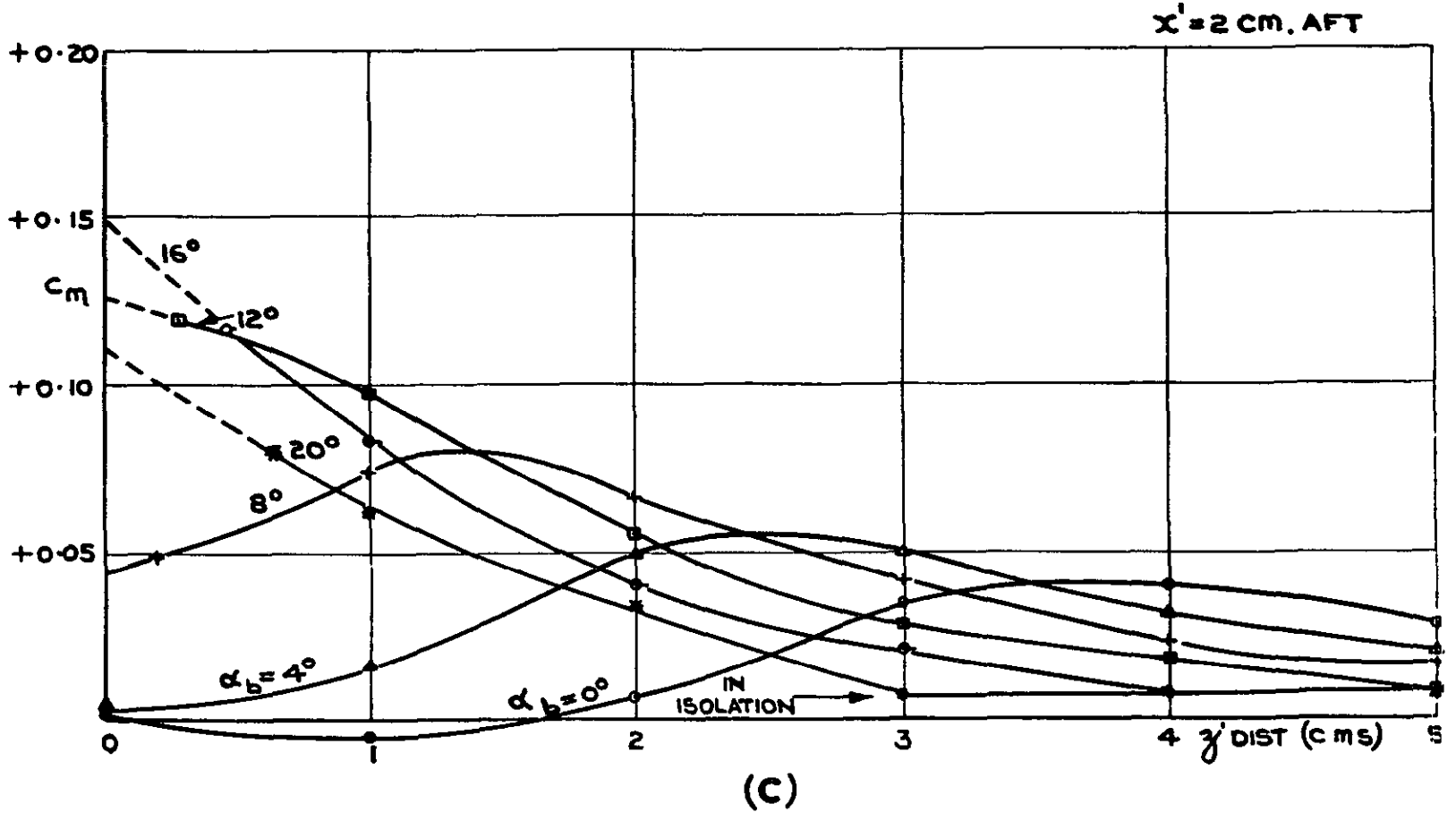

FIG. 28. C_m vs y' DISTANCE AND α_b, AT VARIOUS x' STATIONS, FOR THE BOMB AT ZERO INCIDENCE, IN THE PRESENCE OF THE TWIN BOOST UNIT WITH THE 0·50"c REAR AEROFOIL, M = 2·47

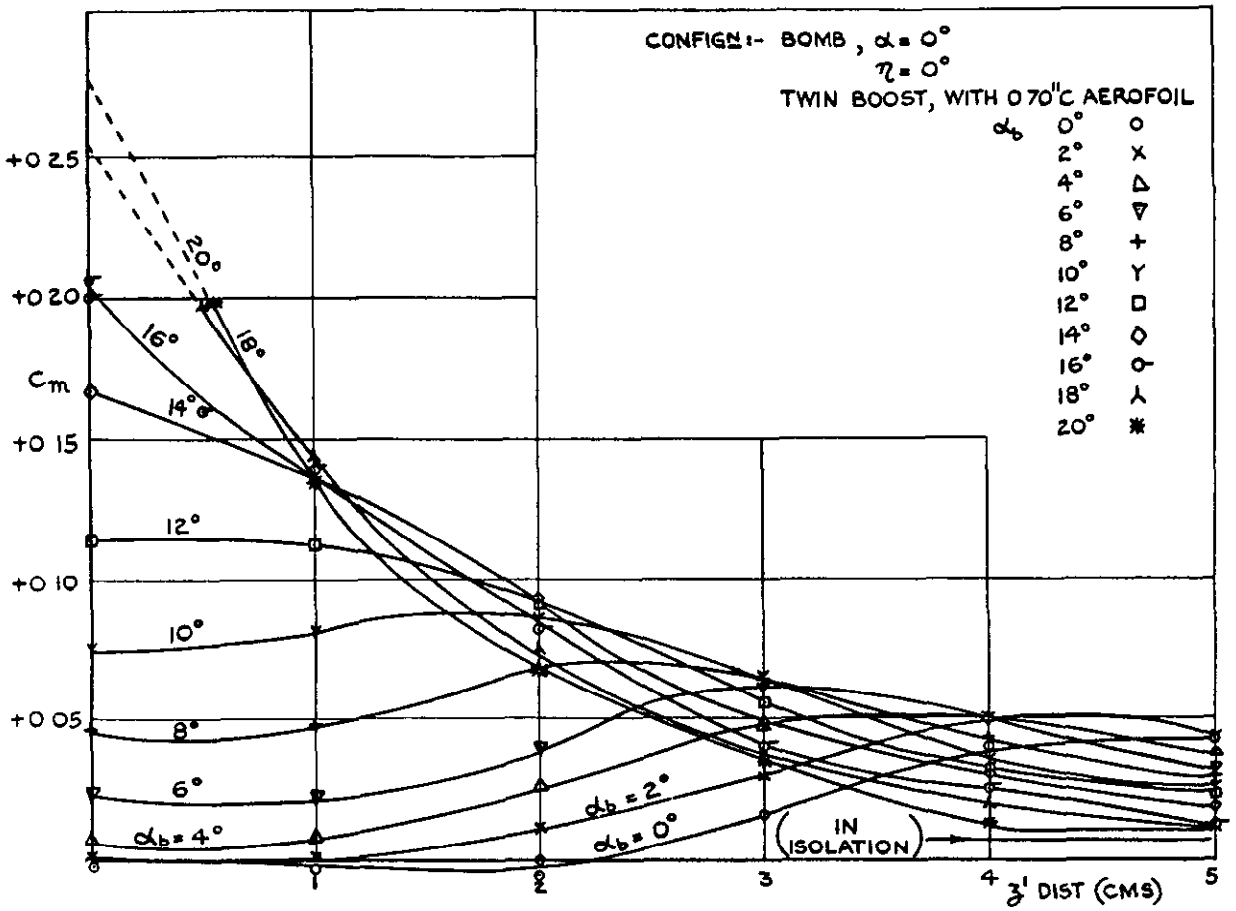

(a) $x' = 0$

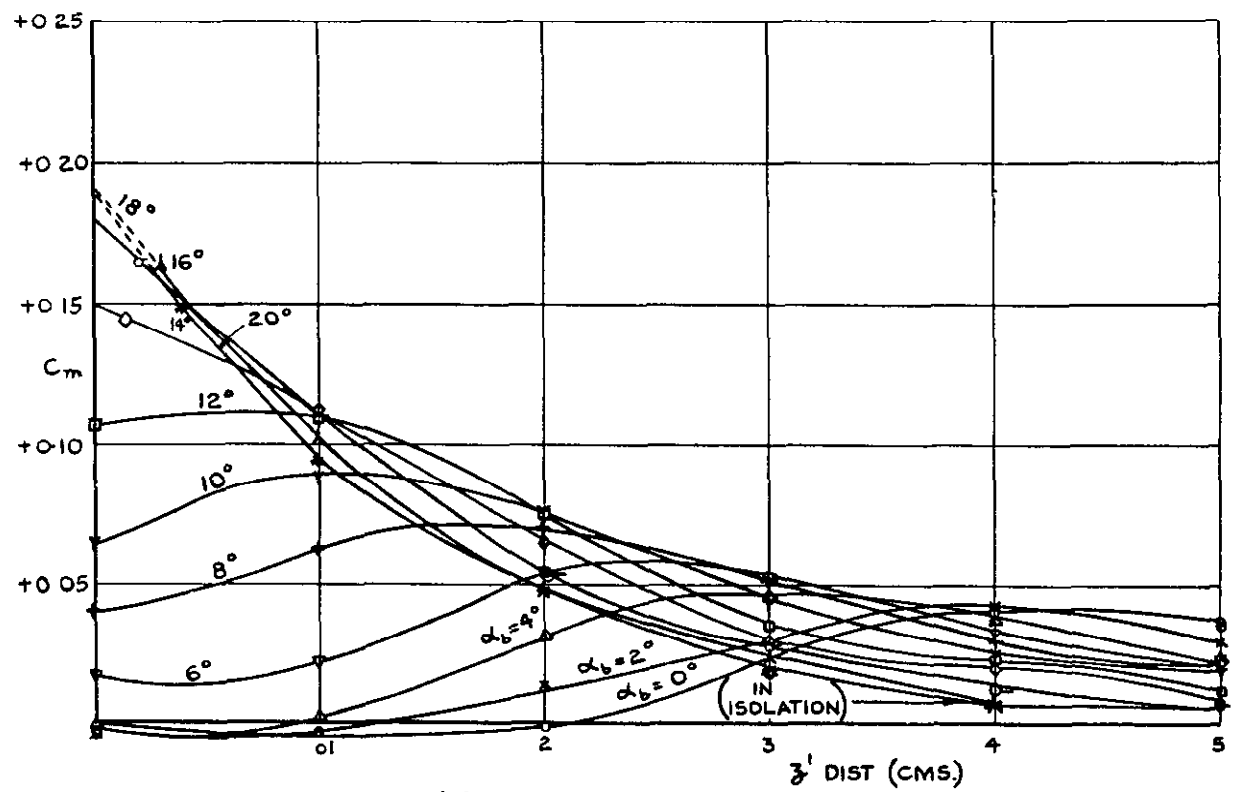

(b) $x' = 1$ CM AFT.

FIG. 29. C_m vs. ζ' DISTANCE AND α_b, AT VARIOUS x' STATIONS, FOR THE BOMB AT ZERO INCIDENCE, IN THE PRESENCE OF THE TWIN BOOST UNIT. WITH THE 0·70"C. REAR AEROFOIL, M = 2·47.

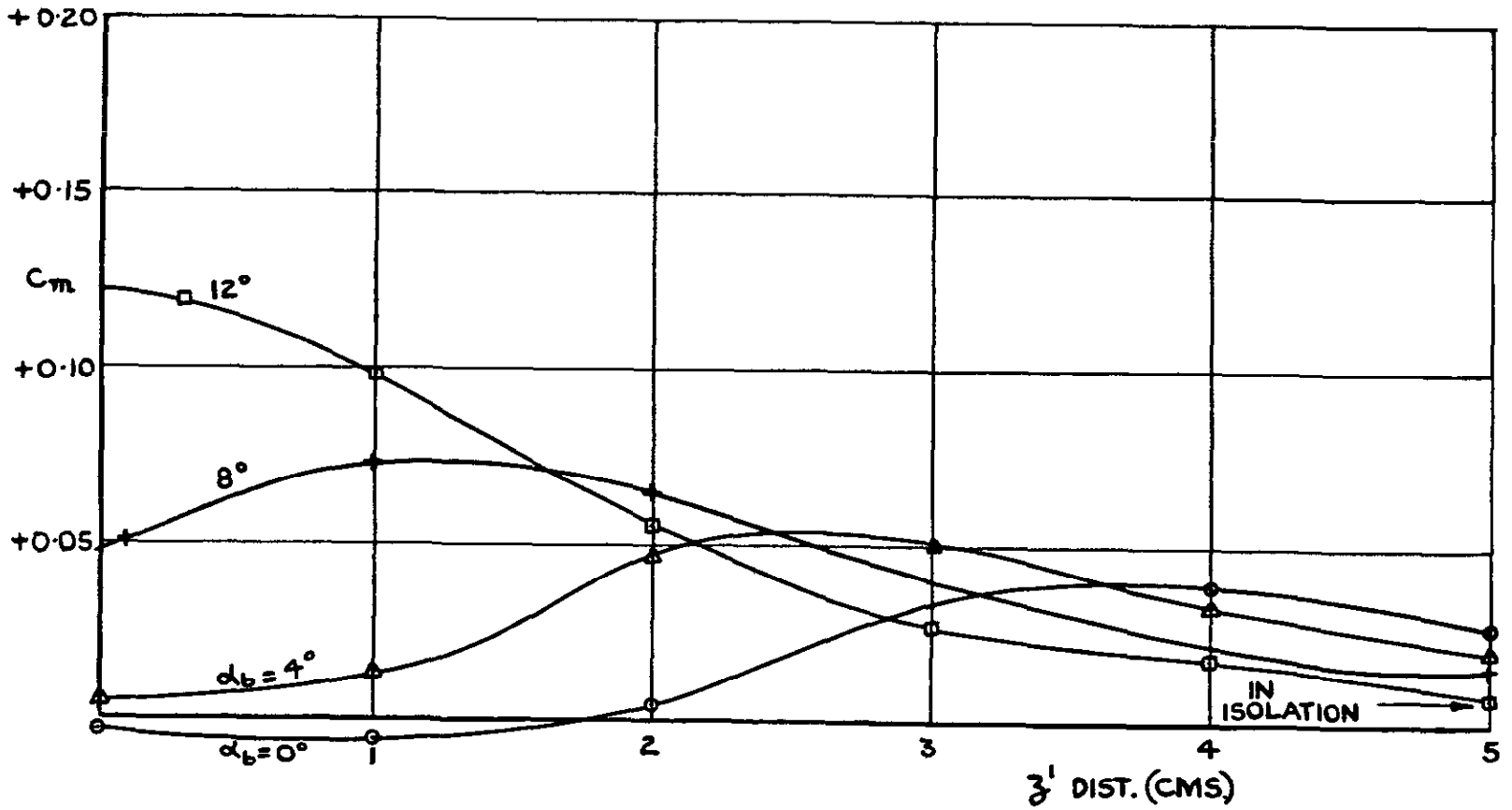

(c) $x' = 2$ CM. AFT.

FIG. 29. C_m vs. $3'$ DISTANCE AND α_b, AT VARIOUS x' STATIONS, FOR THE BOMB AT ZERO INCIDENCE, IN THE PRESENCE OF THE TWIN BOOST UNIT. WITH THE 0·70" C. REAR AEROFOIL, M = 2·47.

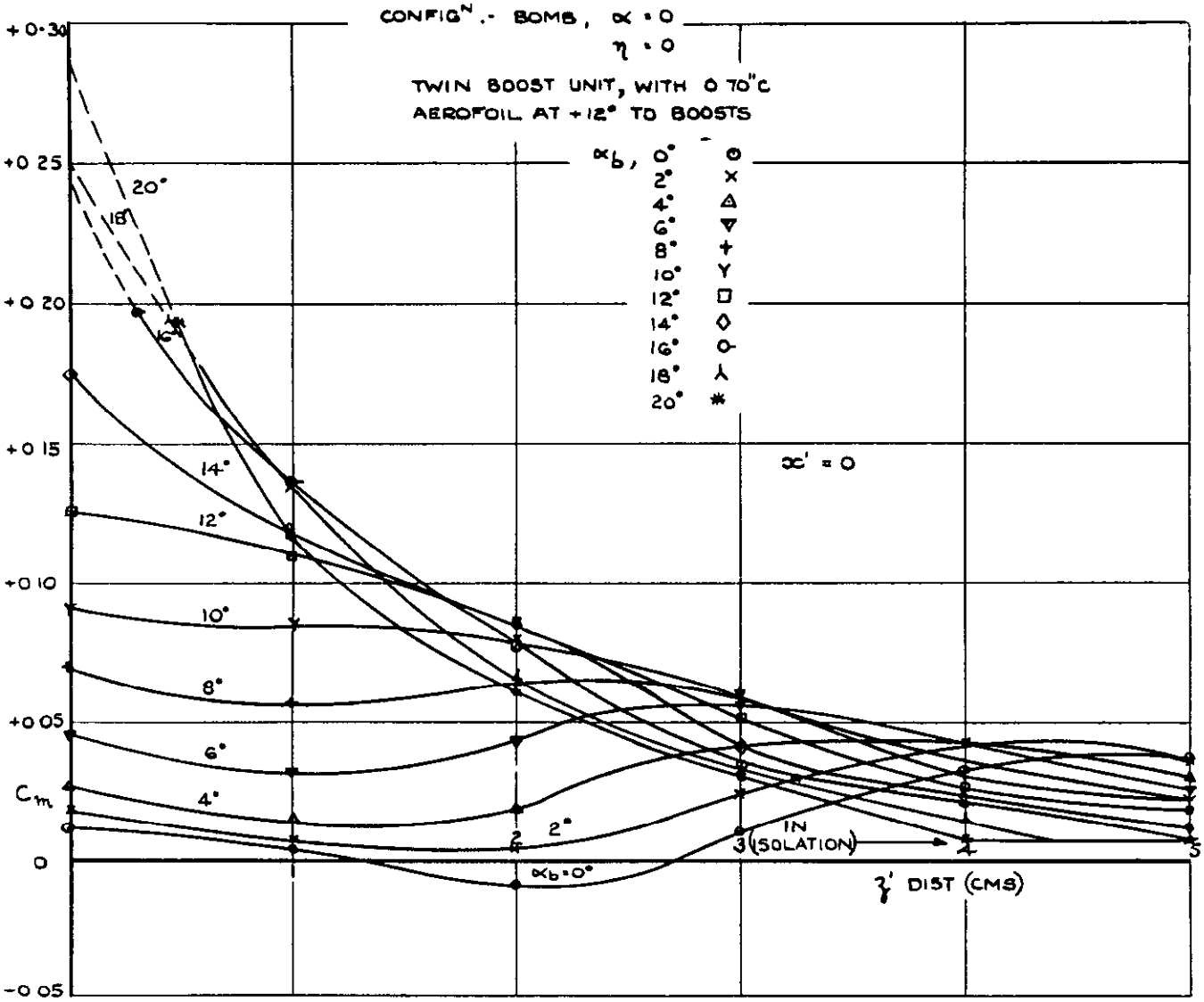

FIG. 30. C_m vs x' DISTANCE AND α_b AT $x'=0$ FOR THE BOMB AT ZERO INCIDENCE, IN THE PRESENCE OF THE TWIN BOOST UNIT WITH THE 0·70"C REAR AEROFOIL SET AT 12° TO THE BOOSTS, M = 2·47.

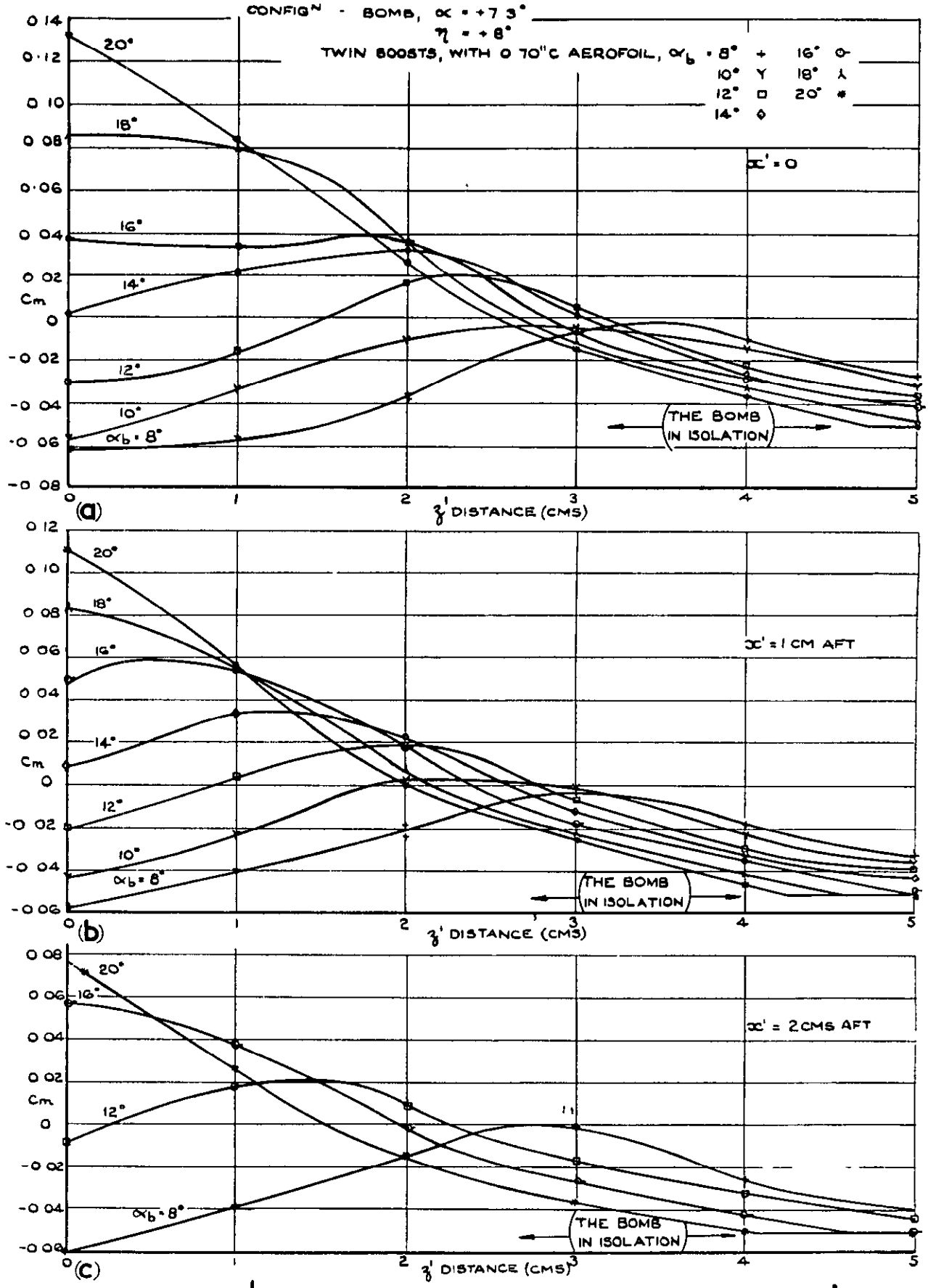

FIG. 31. C_m vs z' DISTANCE AND α_b AT VARIOUS x' STATIONS, FOR THE BOMB AT CRUISING INCIDENCE, IN THE PRESENCE OF THE TWIN BOOST UNIT WITH THE 0·70"C REAR AEROFOIL, M = 2·47.

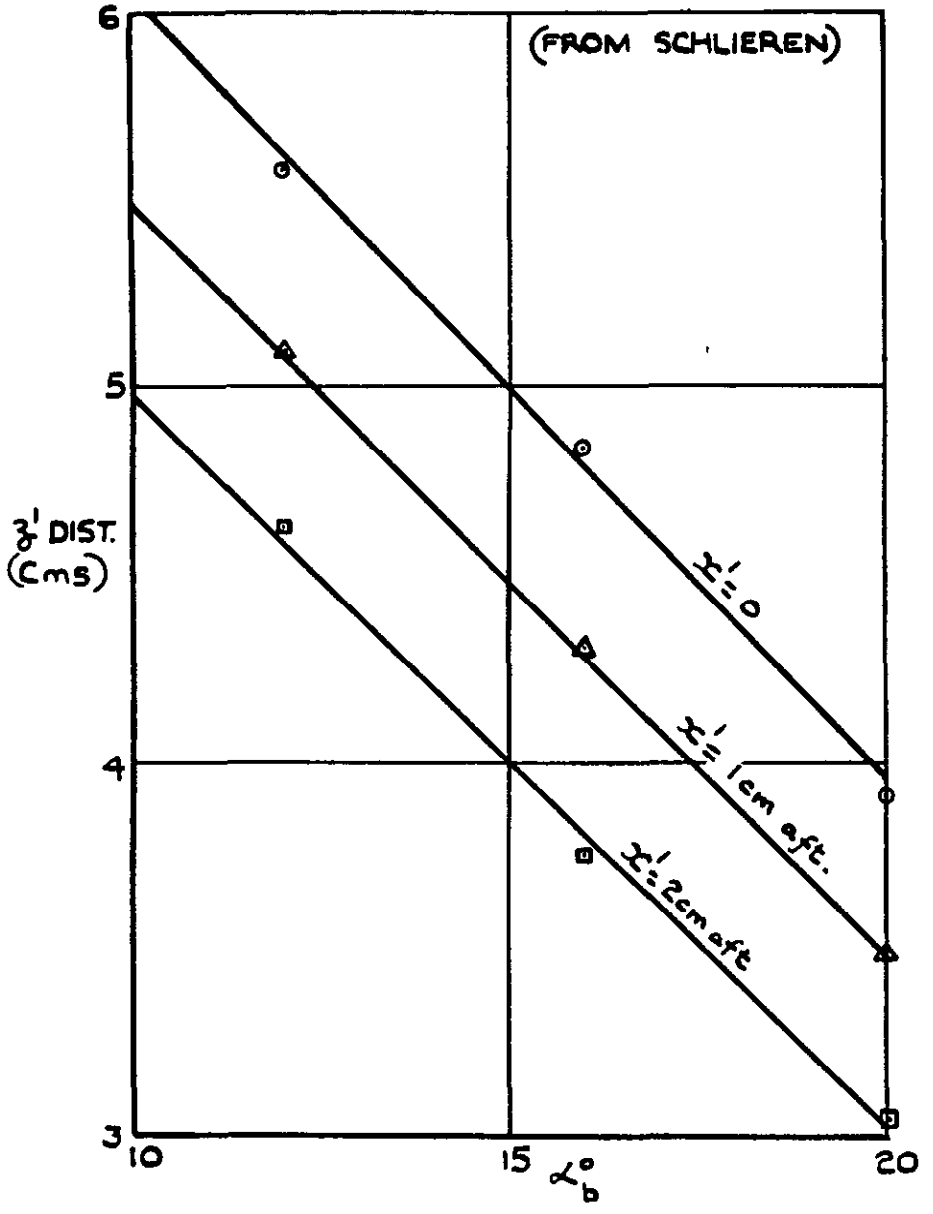

FIG.32. LOCUS OF TWIN BOOST UNIT POSITIONS FOR IMPINGEMENT OF ITS BOW SHOCK ON THE REAR EDGE OF THE BOMB AT ZERO INCIDENCE.

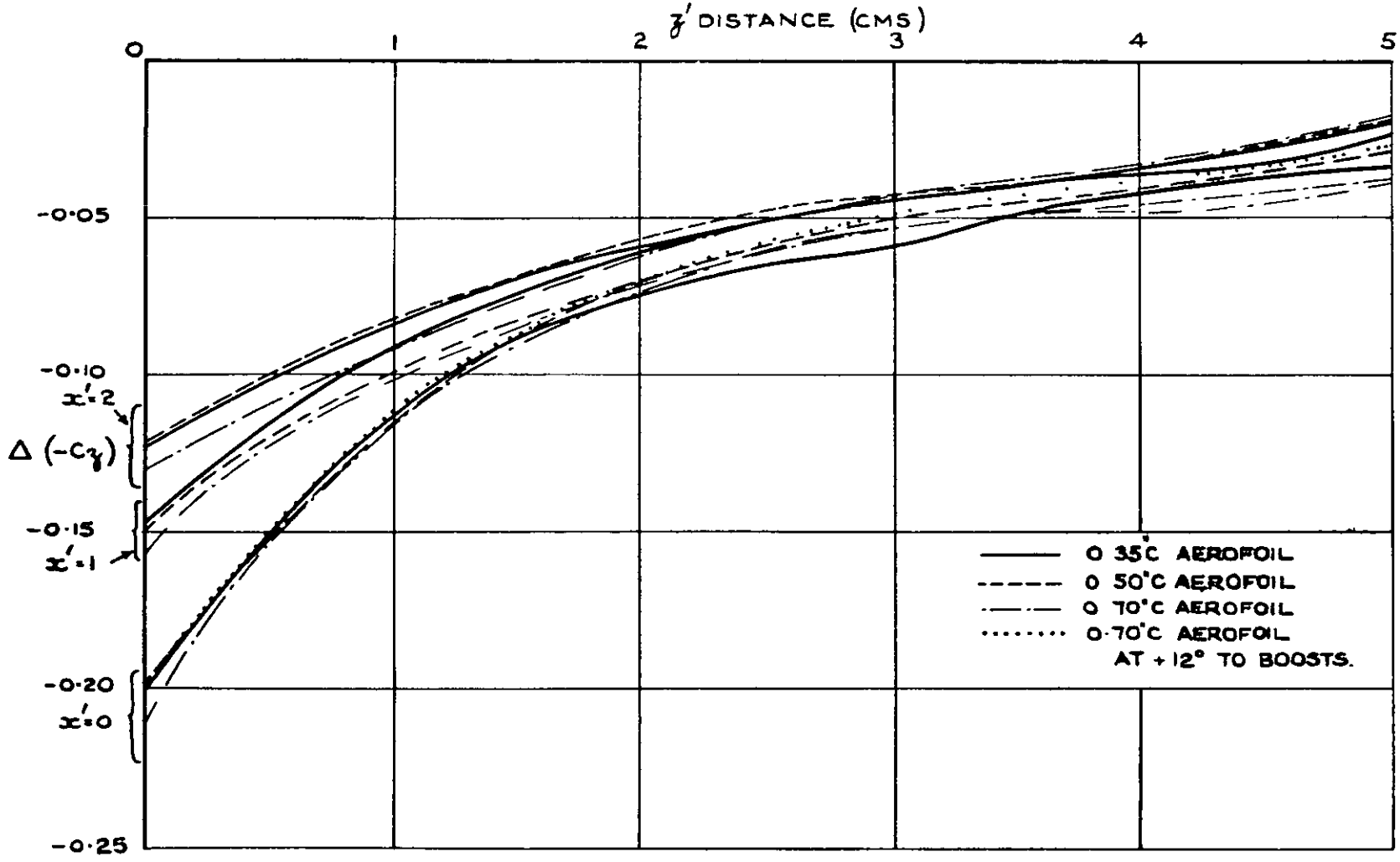

FIG. 33. 'ENVELOPE' VALUES OF NORMAL FORCE INCREMENT ON THE BOMB (WHEN AT ZERO INCIDENCE) DUE TO PRESENCE OF THE TWIN BOOST UNIT, ALL CONFIGURATIONS, M = 2·47.

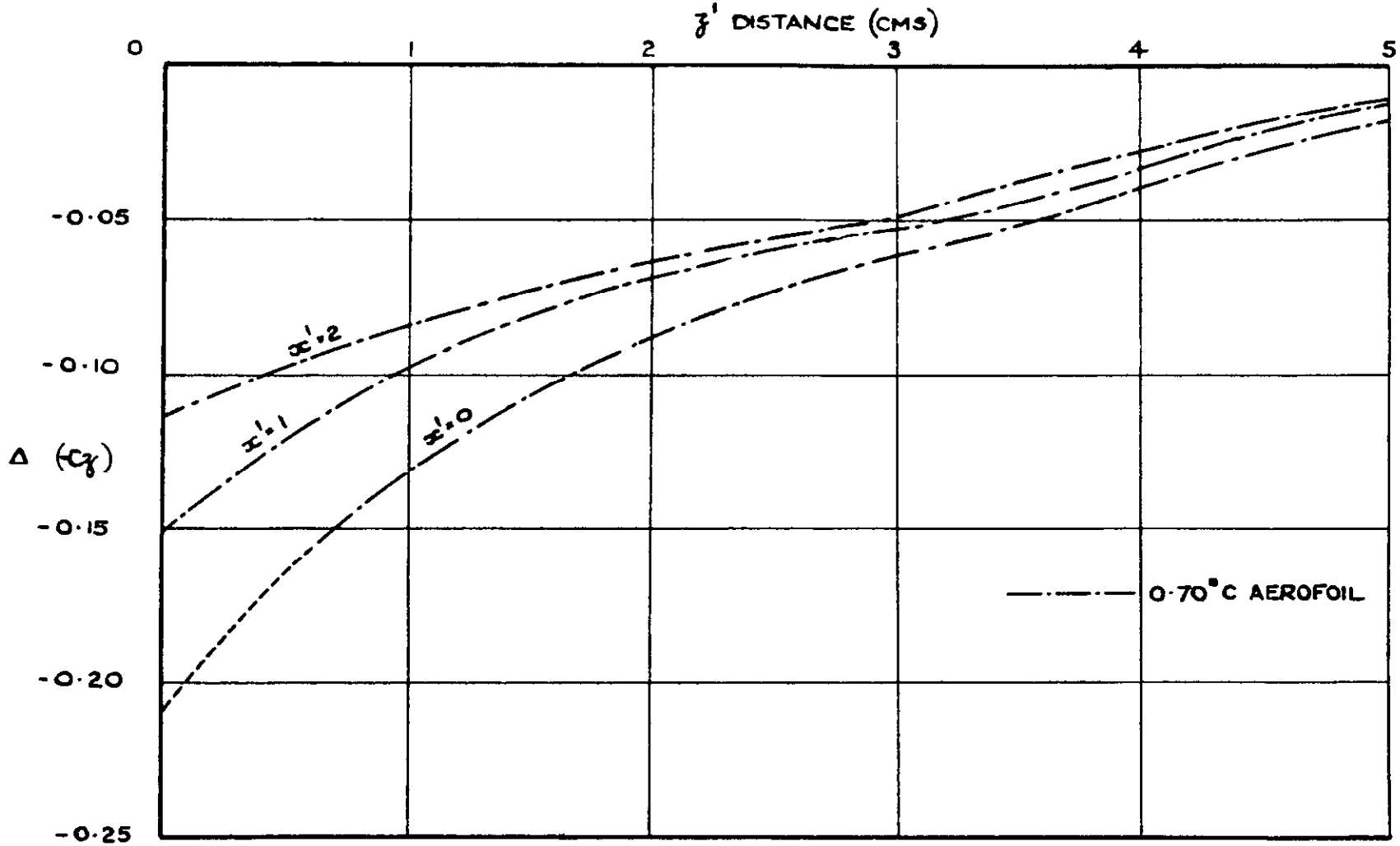

FIG. 34. ENVELOPE VALUES OF NORMAL FORCE INCREMENT ON THE BOMB (WHEN AT 7·3° INCIDENCE) DUE TO PRESENCE OF THE TWIN BOOST UNIT WITH THE 0·70°C REAR AEROFOIL, M = 2·47.

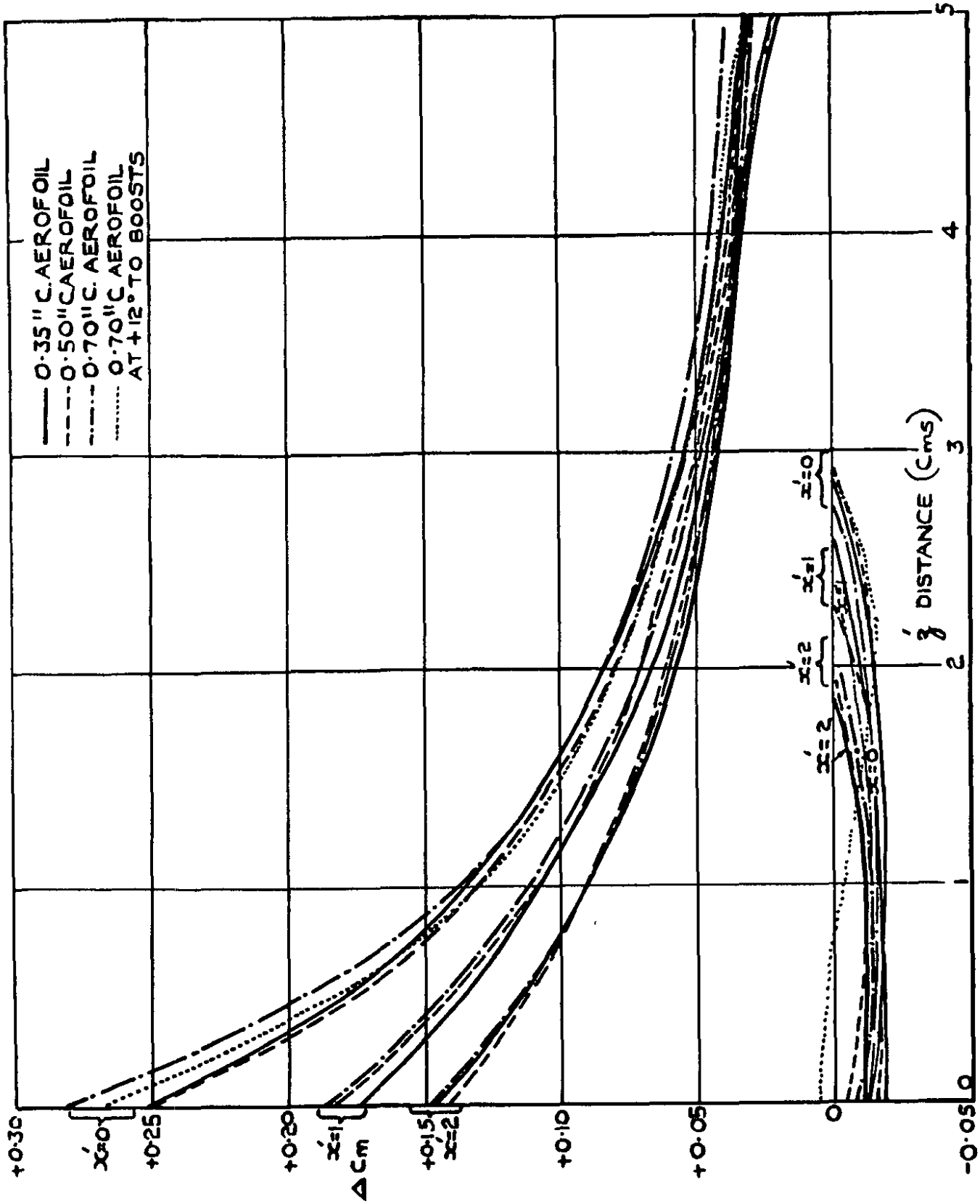

FIG. 35 'ENVELOPE' VALUES OF PITCHING MOMENT INCREMENT ON THE BOMB (WHEN AT ZERO INCIDENCE) DUE TO PRESENCE OF THE TWIN BOOST UNIT, ALL CONFIGURATIONS, M=2·47.

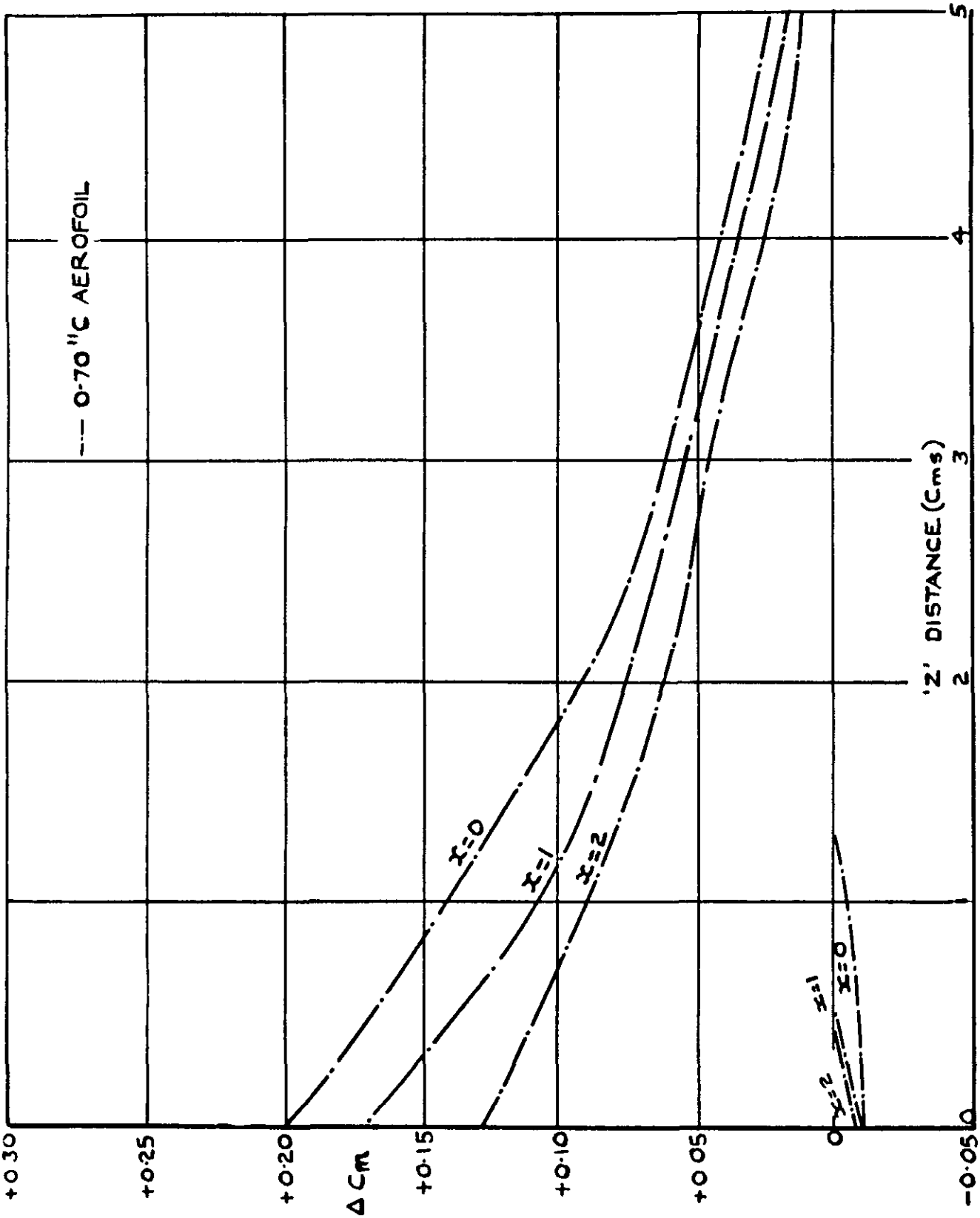

FIG. 36. 'ENVELOPE' VALUES OF PITCHING MOMENT INCREMENT ON THE BOMB (WHEN AT 7·3° INCIDENCE) DUE TO PRESENCE OF THE TWIN BOOST UNIT WITH THE 0·70"C REAR AEROFOIL, M = 2·47.

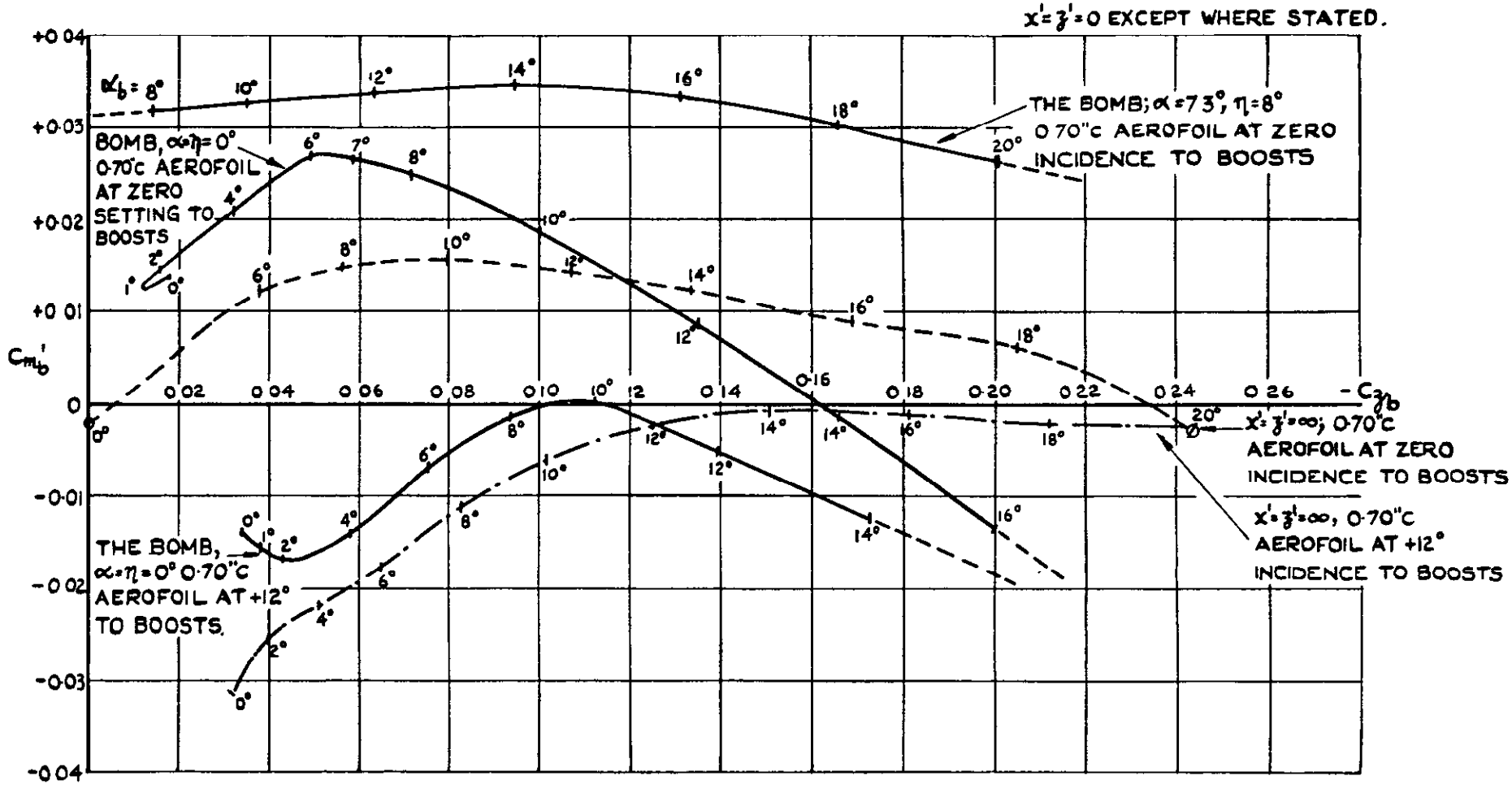

FIG. 37. C'_{mb} vs $-C_{zb}$ FOR THE TWIN BOOST UNIT, TAKEN ABOUT AN AXIS 51·2% AFT OF TWIN BOOST UNIT NOSE, (SEE §6·3·1a) WITH AND WITHOUT THE PRESENCE OF THE BOMB AT M=2·47.

Printed in England for Her Majesty's Stationery Office by the Royal Aircraft Establishment, Farnborough Dd 502109 K 4

DETACHABLE ABSTRACT CARD

A.R.C. C.P. 1161
May 1962

Lang, J. A.

WIND TUNNEL MEASUREMENTS AT M = 2.47 OF THE MUTUAL AERODYNAMIC INTERFERENCE BETWEEN A GUIDED BOMB AND ITS BOOST UNIT DURING THE SEPARATION PHASE

Loads on boost motors in the vicinity of a guided bomb have been measured over a range of positions and incidences likely to occur during separation in order to provide data from which the trajectory may be determined. The loadings and local pressures induced on the bomb by the aerodynamic interference from the boosts have also been measured

The influence of deflected rear surfaces on the boosts has been investigated as a means of limiting the boost incidence, attained through the angular momentum acquired after release of the forward constraint.

A.R.C. C.P. 1161
May 1962

Lang, J A

WIND TUNNEL MEASUREMENTS AT M = 2 47 OF THE MUTUAL AERODYNAMIC INTERFERENCE BETWEEN A GUIDED BOMB AND ITS BOOST UNIT DURING THE SEPARATION PHASE

Loads on boost motors in the vicinity of a guided bomb have been measured over a range of positions and incidences likely to occur during separation in order to provide data from which the trajectory may be determined. The loadings and local pressures induced on the bomb by the aerodynamic interference from the boosts have also been measured

The influence of deflected rear surfaces on the boosts has been investigated as a means of limiting the boost incidence, attained through the angular momentum acquired after release of the forward constraint.

Published by
HER MAJESTY'S STATIONERY OFFICE

To be purchased from
49 High Holborn, London WC1 V 6HB
13a Castle Street, Edinburgh EH2 3AR
109 St Mary Street, Cardiff CF1 1JW
Brazennose Street, Manchester M60 8AS
50 Fairfax Street, Bristol BS1 3DE
258 Broad Street, Birmingham B1 2HE
80 Chichester Street, Belfast BT1 4JY
or through booksellers

C.P. No. 1161

SBN 11 470429 5